BALTEX

Baltic Sea Experiment

World Climate Research Programme / Global Energy and Water Cycle Experiment
WCRP GEWEX

Hydrological, Oceanic and Atmospheric Experience from BALTEX

Extended Abstracts
of the
XXII EGS Assembly

Vienna, Austria
April 21 - 25, 1997

Editors : Mikko Alestalo, Hans-Jörg Isemer

International BALTEX Secretariat
Publication No. 8
August 1997

International BALTEX Secretariat
GKSS Research Center
Max Planck Straße
D-21502 Geesthacht
Germany
Phone : + 49 4152 87 1536
Fax : + 49 4152 87 2020
e-mail : isemer@gkss.de

Hydrological, Oceanic and Atmospheric Experience from BALTEX

Extended Abstracts of the XXII EGS Assembly

Vienna, Austria
April 21 - 25, 1997

Editors : Mikko Alestalo, Hans-Jörg Isemer

Contents:

FOREWORD

The 22nd Assembly of the European Geophysical Society was held April 21-25, 1997 in Vienna, Austria. The Assembly included a session "Hydrological, oceanic and atmospheric processes governing heat and mass balances at northern latitudes: experience from NOPEX and BALTEX". The session was a joint one under two main subprograms Hydrological Sciences and Oceans and Atmosphere.

The BALTEX (Baltic Sea Experiment) program is one of five Continental-Scale Experiments in the frame of GEWEX (the Global Energy and Water Cycle Experiment), and as such a part of the WMO World Climate Research Program. BALTEX is a multi-year research program that is intended to be continued well beyond the year 2000. It covers meteorological, hydrological and oceanographic aspects related to the energy and moisture balance of the Baltic Sea and its drainage basin. The scientific objectives include the determination of the energy and water cycle in that region by a combined data and modelling exercise as well as the development of coupled advanced high-resolution forecasting systems for better weather and climate services. The participants come from meteorological and hydrological institutes as well as from several research institutions in more than 10 countries in the Baltic Sea drainage area and elsewhere in Europe.

Most of the BALTEX-related contributions presented in the EGS Assembly have been collected into the present publication in the form of extended abstracts. They are examples of the most recent progress done in the field by several research groups. They include observational and model-based investigations, many using satellite data. It should be noted that the abstracts reproduced in this volume have not been reviewed. Permission to use any scientific material published in this volume should be obtained from the authors. Addresses of the leading authors are given at the end of the report.

The editors wish to thank the authors for the submission of their papers. We thank Wiebke Jansen and Rüdiger Brandt at the BALTEX Secretariat, who did an excellent job compiling the papers from various formats into one manuscript for this BALTEX Secretariat report.
Financial support for the printing of the abstracts through GKSS Research Centre Geesthacht, Germany, is gratefully acknowledged.

Mikko Alestalo
Finnish Meteorological Institute, Helsinki, Finland

Hans-Jörg Isemer
GKSS Forschungszentrum Geesthacht, Germany

Can Similarity Theory be Applied in the Atmospheric Marine Boundary Layer over the Baltic Sea ?

A. Rutgersson and A. Smedman
Department of Meteorology, University of Uppsala
Uppsala, Sweden

ABSTRACT

In this investigation the turbulence structure in the unstable and near-neutral atmospheric boundary layer is focused. Data from a marine experiment over the Baltic Sea have been analysed. Turbulence measurements together with buoy measurements from a six-day period with gale winds decreasing to low wind speeds at the end have been used. It is found that the state of the sea will affect the vertical exchange of momentum. Two flow regimes have been identified, a regular type of flow, similar to the situation over land, and a situation with decaying sea with very low exchange of momentum between air and sea. Monin-Obukhov similarity theory does not apply during the decaying sea situation and there is a frictional decoupling between the surface and levels above. The turbulence that still exists is probably imported from higher levels by pressure transport.

1 INTRODUCTION

One of the main interests of BALTEX is to determine the water and energy budgets over the Baltic Sea and its drainage basin, important parts of these budgets are the surface exchange of heat, water and energy. Measurements of surface fluxes as well as standard meteorological parameters are very sparse over sea and methods of calculating these fluxes are often developed for land areas. The structure of the Marine Atmospheric Boundary Layer (MABL) is different from that over land and further investigations are needed of the special phenomena occurring over sea. For example the turbulent exchange processes as well as the turbulent structure seem to depend on the state of the waves. In this study the structure of the MABL has been studied during one period with two distinct flow regimes. Increasing winds, young waves with a regular type of unstable flow and decreasing winds, decaying sea giving a situation different from what is expected.

The basic idea is that the total momentum flux over sea is determined by two parts, a turbulent part, t_t, which is the same as over land and one part due to the interaction between the wave perturbation and the mean velocity profile, t_w. The wave-induced part is most important close to the surface and its influence decreases upward. The depth of the layer influenced by this additional term can be defined as the height where the mean wind speed is equal to the phase speed of the dominant wave. Laboratory studies of Lai and Shemdin (1971) show that the layer affected by wave-induced energy transfer is much deeper for the case of decaying waves than for developing waves and field studies reported by Makova (1975) seem to indicate that wave energy can be traced to appreciable heights. If t_w is of the same size as t_t there are zero fluxes and a frictional decoupling from the surface. This super-smooth flow has been observed in other investigations as well, Kitaigorodskii (1973), Donelan (1990) and Smedman et al. (1994). If it is a common phenomenon it could be of considerable interest when climatological fluxes are calculated.

The measurements are taken on Östergarnsholm, a small island east of Gotland almost in the middle of the Baltic Sea. The measurements and the measuring period are described in Section 2, some results are shown in Section 3 and in Section 4 the findings are discussed and compared with earlier results.

2 MEASUREMENTS AND MEASURING SITUATION

The measuring site Östergarnsholm is a small very flat island, situated 4 kilometres east of Gotland. A 30 meter tower is situated at the southern tip of the island with the base of the tower about 1 meter above mean sea level. The sea floor outside of the island has optimum slope in terms of disturbances to incoming surface waves and the sector 60 - 220 degrees has more than 150 km undisturbed upwind fetch. The measuring site can for these wind directions be considered almost as close to marine conditions as possible when measuring on a land-based site. Wind speed and direction and turbulent fluctuations are recorded with sonic anemometers at the heights of 8, 16 and 24 meters above the tower base. Wave height and direction as well as water temperature are measured with a Directional Waverider Buoy (run and owned by the Finnish Marine Research Institute) moored 5 kilometres south-southeast of the tower. The instrumentation and measuring site is described more carefully in Smedman et al. (1997).

For the present analysis data have been chosen from one particular period of six days, 14-20 September 1995. The wind during this period increased from 7 m/s to a maximum of almost 16 m/s followed by a rather rapid decrease to around 4 m/s. The wind direction was steady around 90 degrees during the first part of the period, turning to about 150 degrees during the last two days.

Wave age, c_0/U_8, is used as characteristic wave parameter, c_0 is the phase speed of the dominant wave and U_8 the wind speed at the lowest level. The wave parameter is used to separate between young waves (increasing winds and waves building up) and old waves (decreasing winds and decaying sea). The approximate limit between these two regimes is $c_0/ U_8 \sim 1.2$. The wave age during the period varied between 0.7 and 3.5. The studied period was divided into two regimes, the first part with increasing or steady high winds and young waves and a second part with decreasing winds and older waves.

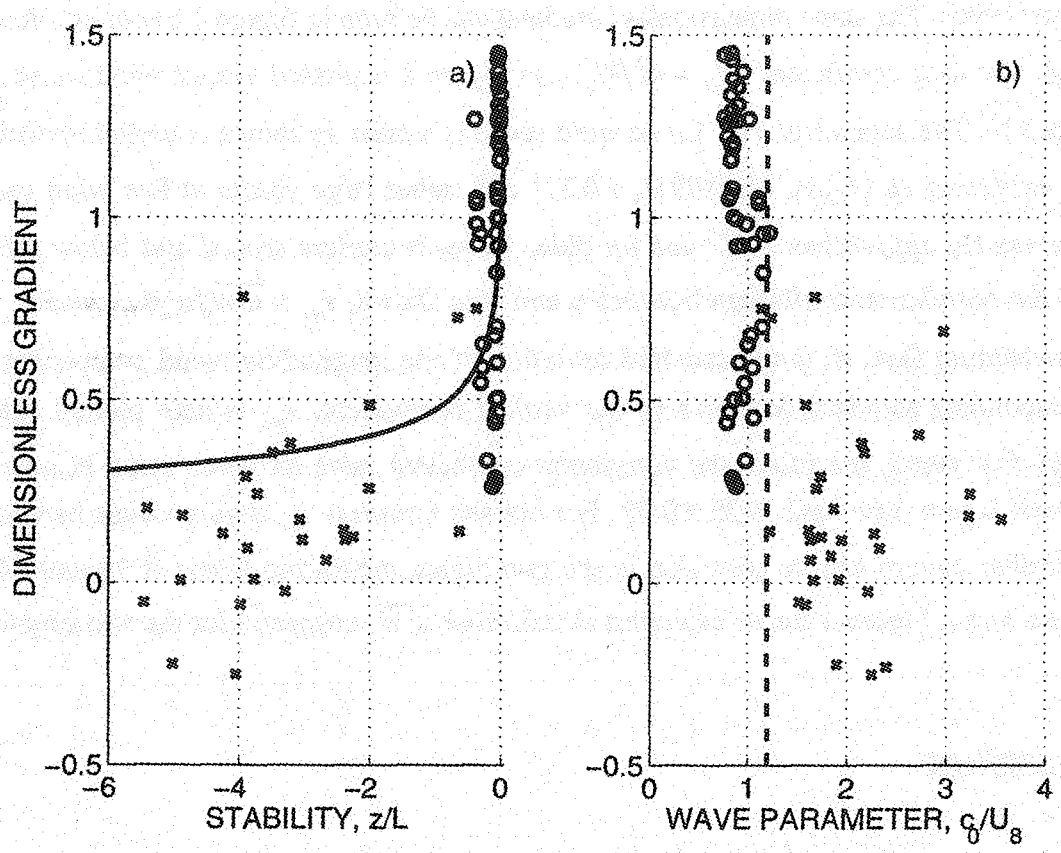

Figure 1: Dimensionless gradient ($\partial U/\partial z * zk/u_*$) versus a) stability parameter z/L , b) wave parameter c_0/ U_8

3. RESULTS

In order to examine the limits of Monin-Obukhov similarity theory the dimensionless gradient $\left(\frac{\partial U}{\partial z}\frac{z\kappa}{u_*}\right)$ is plotted versus stability parameter z/L in Figure 1 a). Here z is the measuring height, k the von Karmans constant and u_* the friction velocity. L is the Obukhov length $\left(L=-u_*^3 T_0/\left(\kappa\, g\overline{w'\theta'}\right)\right)$, T_0 is a reference surface temperature, g acceleration of gravity and $\overline{w'\theta'}$ the surface kinematic heat flux. The full line shows the expected behaviour over land, Högström (1996). The same dimensionless gradient can be seen in Figure 1 b) but as a function of wave age. The drag coefficient $\left(C_D=u_*^2/U_8^2\right)$ in Figure 2 is plotted against wind speed 2 a) and wave age 2 b). The dependence of C_D on wind speed is similar as shown in earlier investigations, linearly increasing as $\left(C_D 10^{-3}=0.09U_8+0.27\right)$ and rather large scatter at low wind speed. For young waves C_D approaches $2\cdot10^{-3}$ and for older waves it scatters around and below $0.5\cdot10^{-3}$. In Figure 3 the correlation coefficient between u and w is shown, $r_{uw}=\overline{u'w'}/\sigma_u\sigma_w$, where $-\rho\,\overline{u'w'}$ is the momentum flux, σ_u is the standard deviation of the longitudinal wind component and σ_w the corresponding standard deviation of the vertical component, r_{uw} is here plotted against the wave age. For young sea (dots) the correlation coefficient have its usual value in near neutral atmospheric layers over land, 0.35 ± 0.05. For old sea (crosses) r_{uw} attains values between -0.15 and 0. Similar pattern can be seen also in the two higher measuring levels at 16 and 24 meters (not shown here). Figure 4 shows examples of half-hour $\overline{u'w'}$-cospectra for the two situations.

4 DISCUSSION

During the young sea situation the turbulent structure more or less behaves as expected. The dimensionless gradient does not exactly follow the expected curve and the reason for this needs further investigation, but the correlation coefficients obtains normal values and so do other parameters as σ_u/u_* and σ_w/u_* (not shown here). For the decaying sea the situation is different. The total momentum flux is very low and sometimes even positive. This makes the friction velocity inappropriate as a characteristic length scale and as can be seen the dimensionless gradient does not follow the expected curve at all, the values of the dimensionless gradient are

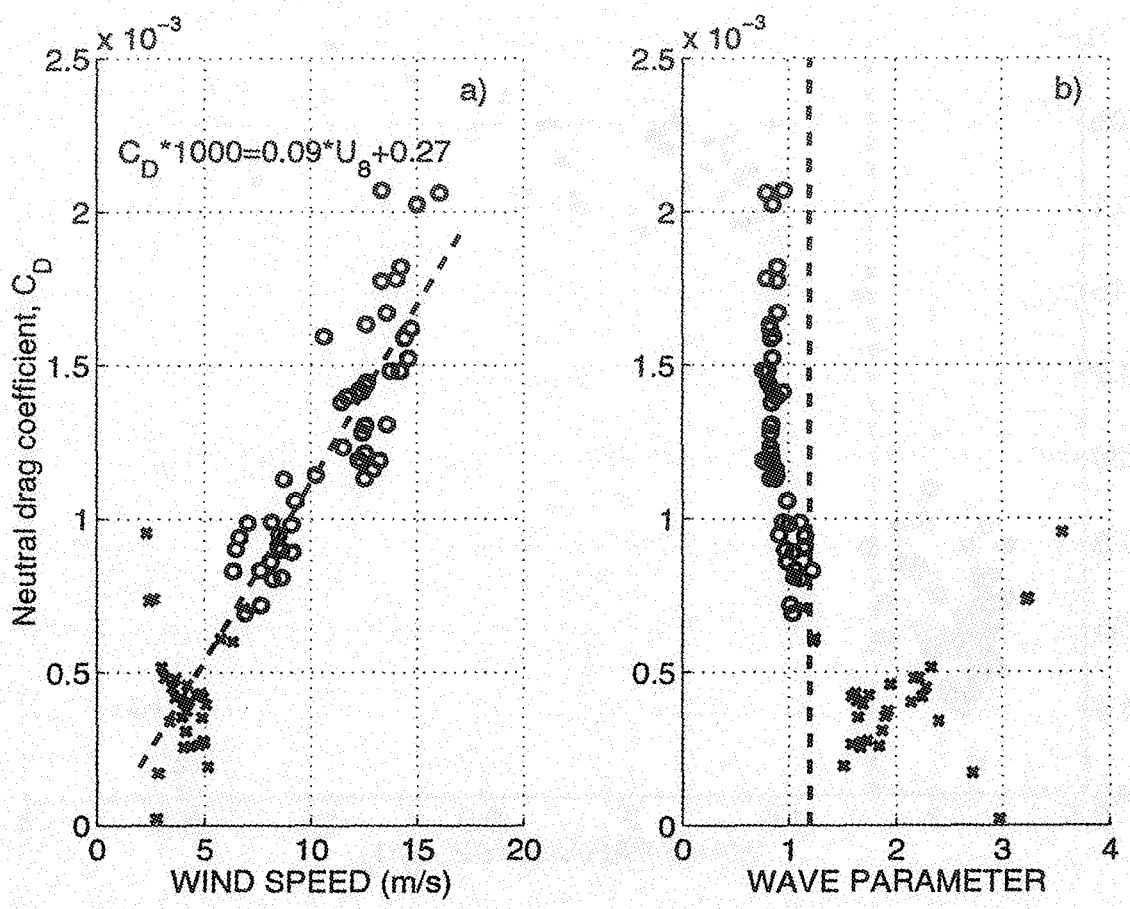

Figure 2: Drag coefficient against a) wind speed, b) wave age

scattered for old waves. The drag coefficient increases more or less linearly with wind speed as is seen in a number of investigations, see e.g. Smith et al. (1992) and others. C_D scatters below $0.5 \cdot 10^{-3}$ for old waves and perhaps some of the scatter often seen in C_D plots for light wind could be explained by the decaying sea phenomenon. The turbulent intensities remain high when the fluxes decrease during old waves so the correlation coefficient in Figure 3 approaches zero. This means that there exists developed turbulence in the layer not coupled to the momentum flux. From Figure 4 it is obvious that the cospectra are much lower for the old sea situation than for young sea in a spectral band between $3 \cdot 10^{-3}$ and 3 Hz. This frequency band is similar to the frequency where the wave energy has its maximum. The missing energy transport in the decaying sea case could thus be explained by wave influence.

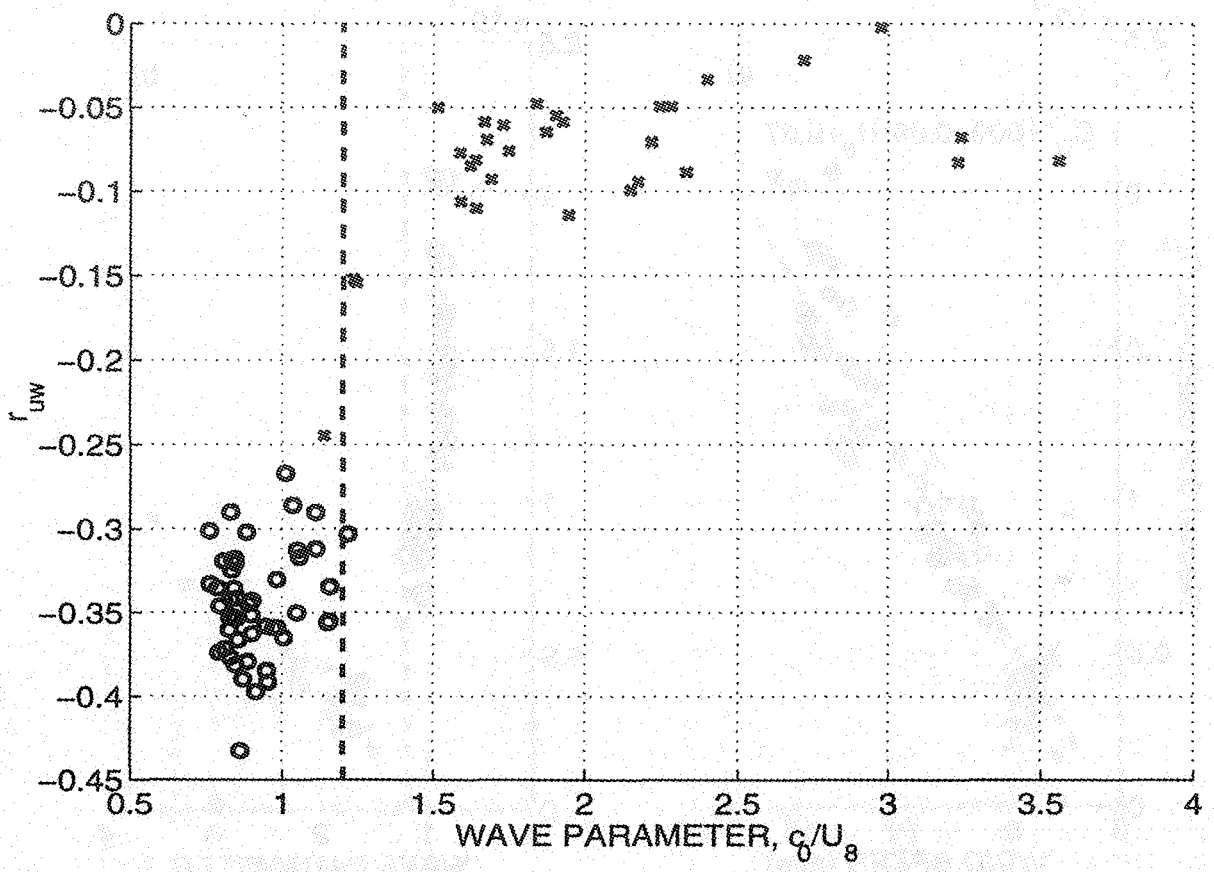

Figure 3: The correlation coefficient $r_{uw} = \overline{u' w'}/\sigma_u \sigma_w$ of u and w as a function of wave age.

A similar situation to the present one was studied in Smedman et al (1994) with simultaneous airborne and tower measurements. There a period with low winds after a gale situation was studied and the turbulence intensities were constantly high in a 700 meter thick layer and there were practically no shearing stress at the surface. The main conclusions drawn from that study was that the surface shearing stress was close to zero and the existing turbulence was so-called inactive turbulence, (Högström, 1990), imported from above by pressure transport. It is plausible to assume that a similar feature to what is observed in Smedman et al. (1994) also occurs in this study. The frictional decoupling from the surface results in almost no actively developed turbulence at the surface and small fluxes of momentum. The observed high turbulence levels originates from levels of high shear in the upper part of the boundary layer brought down to the surface by pressure transport. Almost zero fluxes implies in this study as well as in Smedman et al. (1994) that the turbulence is of the inactive kind. A furhter discussion and comparison of this situation and earlier studies can be found in Smedman et al. (1997).

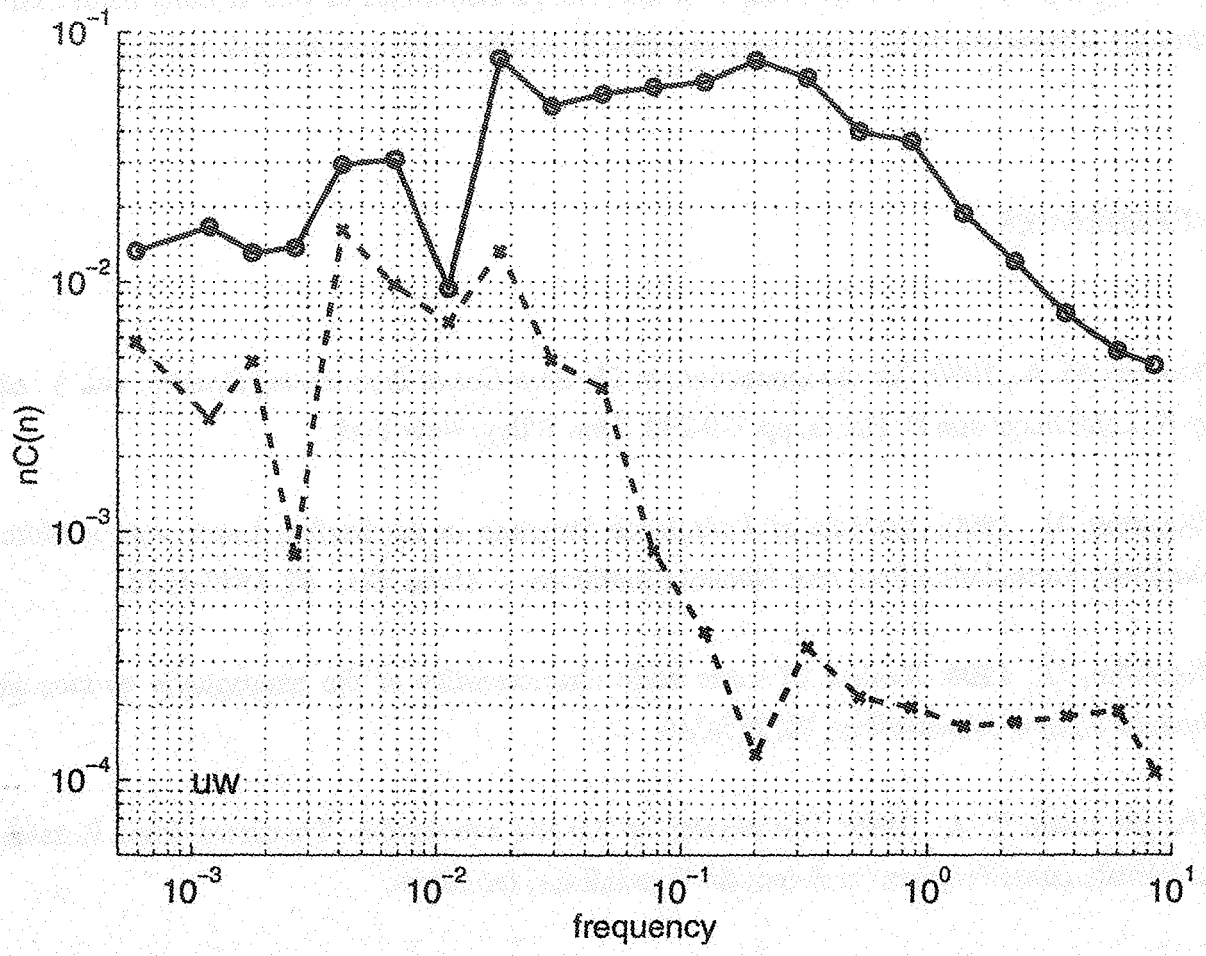

Figure 4: The cospectrum of vertical transport of momentum as a function of frequency.

For a situation like this to occur there must be a frictional decoupling from the surface. An inner surface layer close to the surface directly influenced by the waves must develop together with a net momentum transport close to zero between this inner and the outer surface layer. Decaying sea and the additional upward transport of momentum is an important requirement for this situation to develop. But the exact conditions and how often it occurs is not very well studied. How large decrease in the wind is needed, what is the timescale and what happens when omni-directional waves are present are other factors of interest.

5 CONCLUSIONS

It has been shown from a case study with measurements over the Baltic Sea that Monin-Obukhov similarity theory is not always valid over sea. The surface fluxes as well as other parameters are strongly suppressed during high wave-age conditions (decaying sea after gale winds).

REFERENCES

Donelan, M. A., 1990: Air sea interaction, in *The Sea: Ocean Engineering Science*, **vol. 9.**, edited by B. LeMehaute and D. Hanes, pp 239-292, John Wiley, New York.

Högström, U., 1990: Analysis of Turbulence Structure in the Surface Layer with a Modified Similarity Formulation from near Neutral Conditions. *J. Atmos. Sci.*, **47**, 1949-1972.

Högström, U., 1996: Review of some basic characteristics of the atmospheric surface layer. *Boundary-Layer Meteorology*, **78**, 215-246.

Kitaigorodskii, S. A., 1973: *The physics of Air-Sea Interaction.* Translated from Russian by A. Barush, Israel Program for Scientific Translations, Jerusalem.

Lai, R. J. and O.H. Shemdin, 1971: Laboratory investigations of air turbulence above simpler water waves, *J. Geophys. Res.*, **76**, 7334-7350.

Makova, V. I., 1975: Features of the dynamics of turbulence in the marine atmospheric surface layer at various stages in the development of waves. *Atmos. Ocean. Phys.*, **11**, 177-182.

Smedman, A., M. Tjernström, U. Högström, 1994: The near-neutral marine atmospheric boundary layer with no surface shearing stress: a case study. *J. Atmos. Sci.*, **51**, 3399-3411.

Smedman, A., U. Högström, H. Bergström, A. Rutgersson, K. Kahma, and H. Pettersson, 1997: A case-study of air-sea interaction during swell conditions. Submitted to *J. Geoph.. Res.*

Smith S. D., R.J. Andersson, W.A. Oost, C. Kraan, N. Maat, J. DeCosmo, K.B. Katsaros, K.L. Davidson, K. Bumke, L. Hasse, and H.M. Chadwick, 1992: Sea surface wind stress and drag coefficients: The HEXOS results. *Boundary-Layer Meteorology*, **60**, 109-142.

SOLAR RADIATION FLUXES AT THE BALTIC SEA SURFACE

Anna Rozwadowska
Institute of Oceanology, Polish Academy of Sciences, Sopot, Poland

Hans-Jörg Isemer
Institute for Atmospheric Physics, GKSS Forschungszentrum Geesthacht, Germany

ABSTRACT

Solar fluxes at the surface of the Baltic Proper are computed using a semi-empirical model applied to ship meteorological observations of the COADS (Comprehensive Ocean-Atmosphere Data Set) from the period 1980 to 1992. Spatial distribution of the fluxes as well as their seasonal and interannual variability are presented. The impact of both meteorological and astronomical factors is analysed.

1 INTRODUCTION

The implementation of BALTEX foresees the analysis of historical data sets in order to e.g. establish climatological statistics as background information for studies of actual events. An important source for climatological information from the open Baltic Sea, covering time periods on time scales of years to decades, are the meteorological reports made onboard of Voluntary Observing Ships (VOS).

The basic aim of this study is to calculate monthly and annual estimates of incident solar radiation fluxes at the surface of the Baltic Proper, using a semi-empirical model applied to ship meteorological observations of the COADS (Comprehensive Ocean - Atmosphere Data Set, see *Woodruff et al., 1987*). Spatial distribution of the fluxes, their seasonal and interannual variability, as well as impact of both meteorological and astronomical factors on the monthly and annual means of the fluxes are analysed.

2 METHODS AND DATA

The model used is based on works by *Atwater and Brown (1974), Atwater and Ball (1978)* and *Krêzel (1985)* . A short description is given here, for details see the paper by *Rozwadowska (1991).*

The input parameters to the model are the geographical coordinates of the area under investigation (ϕ, λ), day number of the year d, UTC time t , and the following surface meteorological observations: air pressure p, air temperature T_a, dew point temperature T_d, total cloud amount c , low cloud amount cl, low-, middle- and high-level cloud class as well as sea ice cover information.

The algorithm used includes the parameterizations of the following processes:

- irradiance transmittance for an ideal (dry) atmosphere (molecular scattering, absorption by ozone and other gases),
- absorption by water vapour,
- irradiance transmittance for atmospheric aerosols,
- irradiance transmittance for clouds, and
- multiple reflection between the sea surface and the atmosphere.

The modelled downward irradiance at the sea surface is expressed by the relation:

$$E(c,cc,\vartheta) = \frac{S \cdot f \cdot (T_i - A_{wa}) T_{aer} \cdot T_{cl} \cdot \cos\vartheta}{1 - A_{sk} \cdot A_s}$$

where:

S - the solar constant (1368 W/m^{-2}, *Wilson, 1993*)

$f(d)$ - the factor describing seasonal changes in S due to changes in the Sun - Earth distance (*Spencer, 1971*)

$\vartheta(t,d,\phi,\lambda)$ - solar zenith angle

$T_i(\vartheta,p)$ - transmittance for an ideal (dry) atmosphere (*Atwater & Brown, 1974, Kastrov, 1956*)

$A_{wa}(e_o,\vartheta)$ - absorbance of water vapour (*McDonald, 1960*)

$e_o(T_a,T_d)$ - water vapour pressure

$T_{aer}(\vartheta, month, \varphi, \lambda)$ - aerosol transmittance

$T_{cl}(c,cc,\vartheta)$ - cloud transmittance function

$A_{sk}(c,cc)$ - sky albedo

$A_s(T_{atm},\vartheta,ice)$ - sea surface albedo.

The cloud transmittance function was calculated using standard meteorological observations and time series of instantaneous values of irradiance, which were collected at Sopot and during research cruises to the Baltic Sea in the period 1984-1989. For calculation of this function three cloud classes (*cc*) are distinguished in the model (*Rozwadowska, 1991*):

- cloud class L - predominantly cumulus (Cu, Cb), low-level (St, Ns, Sc) or middle level layer clouds (As, Ac) covering a considerable part of the sky (c(As, Ac) > 5/8); when c=8/8 this class includes situations when the clouds are opaque,
- cloud class M - predominantly middle-level or low-level clouds and c = 8/8; clouds at least partially semi-transparent,
- cloud class H - predominantly high-level clouds (Ci, Cs, Cc) or middle-level cloud cover with c(As, Ac) <=5/8.

Cloud class H combines high-level clouds with middle-level clouds because the latter type when appearing in a small amount is usually optically thin and often accompanies high level clouds. The cloud class M comprises cases when the layer of mainly middle or low clouds cover the sky entirely, but reveals a relatively high transmittance due to small optical thickness. According to *Dobson and Smith (1988)* thick fog obscuring the sky (ww=43,45,47,49 and c=9) was treated like stratus clouds with c=cl=8.

The cloud classification used is based on the cloud information which is available in the COADS.

The effective albedo of the sky is calculated as a weighted sum of the clear sky albedo (from *Kamada and Flocchini, 1986)* and the cloud albedo (from *Kondratev and Binenko, 1984*), taking into account the percentage of sky covered by clouds from the COADS observations. The effective albedo of the sea surface is a weighted sum of the albedo of the ice-free sea surface (from *Payne, 1979*) and the sea ice, according to the percentage of the surface covered by ice (*ice*). Because no information about the state of the ice surface is available, the ice albedo is assumed constant and equal to 0.4. Sea-ice coverage data have been digitized from bi-weekly ice-charts published by the Swedish Meteorological and Hydrological Institute (SMHI).

Since the COADS does not contain any information about aerosols, the aerosol transmittances based on the data given by *Krêzel (1985)* are adopted in the model. They are computed from solar

radiation measurements and meteorological observations made on cloudless days at Gdynia, Helsinki, Stockholm (1965-74) and Copenhagen (1965-70), and are extrapolated to the Baltic Sea.

Air pressure p, air temperature T_a, dew point temperature T_d, total cloud amount c, low cloud amount cl, low-, middle- and high-level cloud categories are taken from the VOS meteorological reports of the COADS. The period 1980-1992 was chosen because of the high number of suitable ship observations (118 777) containing the necessary model input data.

Cloudiness data were analysed to look for a diurnal cycle in cloud type and cloudiness. Because the existence of such cycles could not be ruled out, only daylight observations were used in the model computations (73 013 observations).

All the computations and further analysis were confined to the Baltic Proper area, which was divided into 3 subregions:

- Northern Baltic Proper - north of 57° N,
- Southern Baltic Proper - south of 57° N and east of 15° E,
- Western Baltic Proper - west of 15° E.

Atmospheric transmittances for daily and monthly totals of solar radiation and incident solar radiation fluxes at the Baltic Proper surface were computed using the model. Spatial distribution of the mean cloudiness, transmittances and irradiances and their seasonal and interannual variability were estimated. The relative estimation error for the monthly mean irradiance and transmittance for an individual month depends mainly on the number of observations available and the season of the year. Its typical values vary from ± 2-3 % for late spring and summer to ± 12-110 % for winter. This is ± 4-7 W/m^{-2} and ± 8-12W/m^{-2}, respectively, in terms of the absolute errors of the monthly mean irradiance.

3 RESULTS AND CONCLUSIONS

- The annual mean downward irradiance at the sea surface averaged over the period 1980 - 1992, computed using the semi-empirical model applied to ship meteorological observations, is 119 Wm^{-2} (± 4 Wm^{-2}) for the Southern Baltic Proper, 118 Wm^{-2} (± 4 Wm^{-2}) for the Northern, and 114 Wm^{-2} (± 5 Wm^{-2}) for the Western Baltic Proper. The annual mean irradiance for the entire Baltic Proper is estimated to 118 (± 4) Wm^{-2}. During the whole period under analysis the highest values were found for the Southern, whereas the lowest for the

Western Baltic (Figure 1). Standard deviations of the individual annual means are given in parenthesis.

- Modelled monthly mean downward irradiance at the surface of the Baltic Proper varies from 251 (± 23), 241 (± 21) and 225 (± 32) Wm^{-2} in June to 10 (± 2), 14 (± 2) and 15 (± 2) Wm^{-2} in December for the northern, southern and western parts respectively (Figures 2 and 3). Standard deviations of the individual monthly means are given in parenthesis.

- From September to March the spatial distribution of radiation fluxes is under strong influence of astronomical factors, i.e. day length and solar elevation, which results in lower fluxes in the northern than in the southern and the western parts of the Baltic Proper. In June and July, when the latitudinal gradient of the solar radiation flux at the top of the atmosphere is weakest, the spatial distribution of the flux is controlled by the atmospheric transmittance, i.e. meteorological factors (the maximum flux at the Northern, the minimum at the Western Baltic Proper; compare Figures 2, 4, and 5).

- Modelled mean transmittance for monthly sums of incident solar radiation varies from 0.55 (± 0.05), 0.54 (± 0.05) and 0.51 (± 0.06) in May to 0.29 (± 0.05), 0.27 (± 0.04) and 0.26 (± 0.03) in December for the Northern, the Southern and the Western Baltic Proper, respectively (Figure 5).

- Cloudiness is the crucial factor influencing atmospheric transmittance (compare Figures 5 and 6). However, the impact of spatial distribution of aerosol transmittance is also significant (the highest aerosol transmittance is found for the Northern Baltic Proper thoughout the whole year except in the period from March to June - see *Krêzel, 1985*, *Rozwadowska,1991*).

REFERENCES

Atwater M. A., J.T. Ball, 1978: *A numerical solar radiation model based on standard meteorological observations*. Solar Energy, 21, 163-170

Atwater M. A., Ph. S. Jr. Brown, 1974: *Numerical computations of the latitiudinal variation of solar radiation for an atmosphere of varying opacity*. J. Appl. Meteorol., 13, 289-297

International Cloud Atlas. 1956: Warszawa

Dobson F. W, S. D. Smith, 1988: *Bulk models of solar radiation at sea*. Q. J. R. Meteorol. Soc., 114, 165-182

Kamada R. F., Flocchini, 1986: *Gaussian solar flux model*. Solar Energy, 36, 73-87

Kastrov V. G., 1956: *Solnechnaya radyatsya v troposfere v sluchaye absolutno chistogo i sukhogo vozdukha*. Trudy CAO, 16, 26

Kondratev K. Ya., V.I. Binenko, 1984: *Vliyanye oblachnosti na radyatsyu i klimat*. Gidrometeoizdat, Leningrad, 240 pp.

Krêzel A., 1985: *Solar radiation at the Baltic Sea surface*. Oceanologia, 21, 5-21

McDonald J. E., 1960: *Direct absorption of solar radiation by atmospheric water vapour*. J. Meteor., 17, 319-328

Payne R. E., 1979: *Albedo of the sea surface*. J. Atmos. Sci., 29, 959-970

Rozwadowska A., 1991: *A model of solar energy input into the Baltic Sea*. Studia i Mater. Oceanol., 59, Marine Physics 6, 223-242

Spencer J. W., 1971: *Fourier series representation of the position of the Sun*. Search, 2, 172

Willson R. C., 1993: *Solar irradiance*, [in:] *Atlas of satellite observations related to global change*, R. J. Gurey, J. L. Foster, C. L. Parkinson (eds.), Cambridge Univ. Press, Cambridge.

Woodruff, S.D., R.J. Slutz, R.L.Jenne, und P.M.Steurer, 1987: A comprehensive ocean-atmosphere data set. Bull. Amer. Meteor.Soc., 68, 521-527.

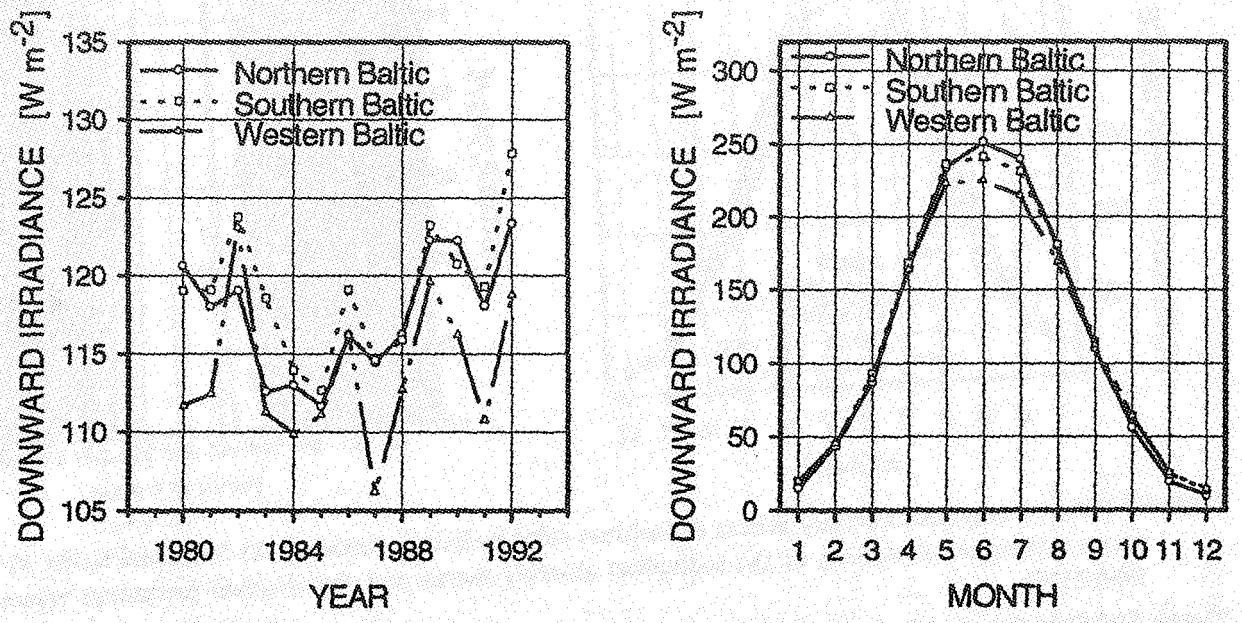

Figure 1 (left): Interannual variations in the annual mean solar radiation fluxes at the Northern, the Southern and the Western Baltic Proper during 1980 to 1992.

Figure 2 (right): Monthly mean incident solar radiation fluxes at the Northern, the Southern and the Western Baltic Proper surface for the period 1980 to 1992.

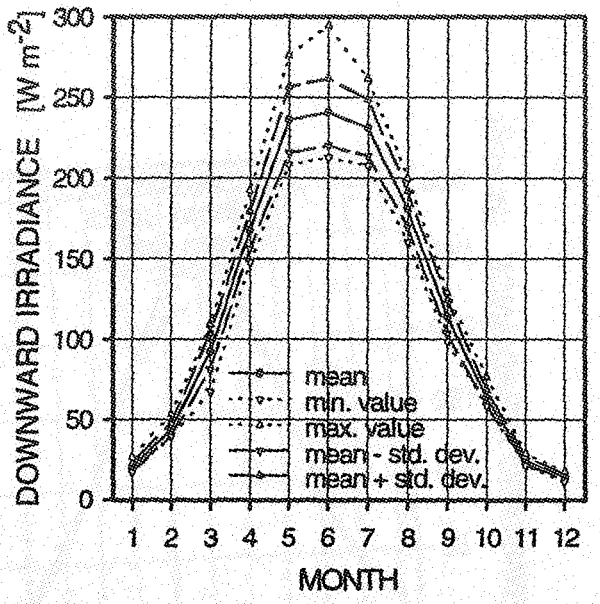

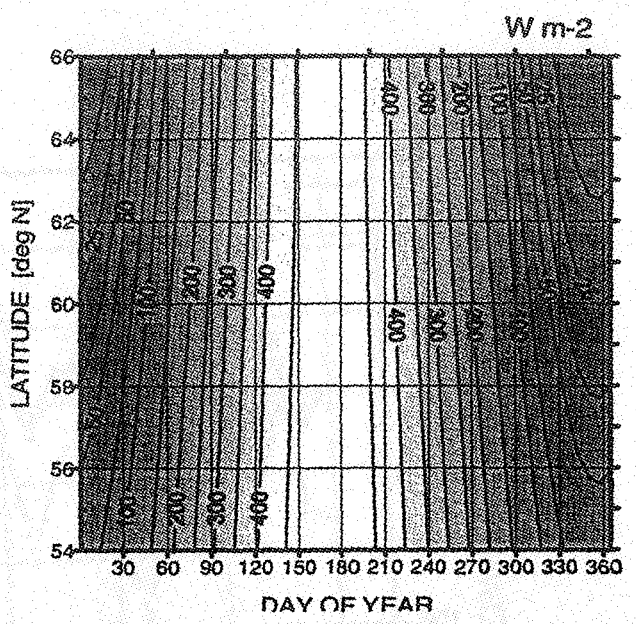

Figure 3 (left): Long-term monthly means of incident solar radiation fluxes at the Southern Baltic Proper surface, standard deviations of the individual monthly means and the absolute extremum values for 1980-1992.

Figure 4 (right): Solar radiation daily mean fluxes at the top of the atmosphere in the Baltic Sea region.

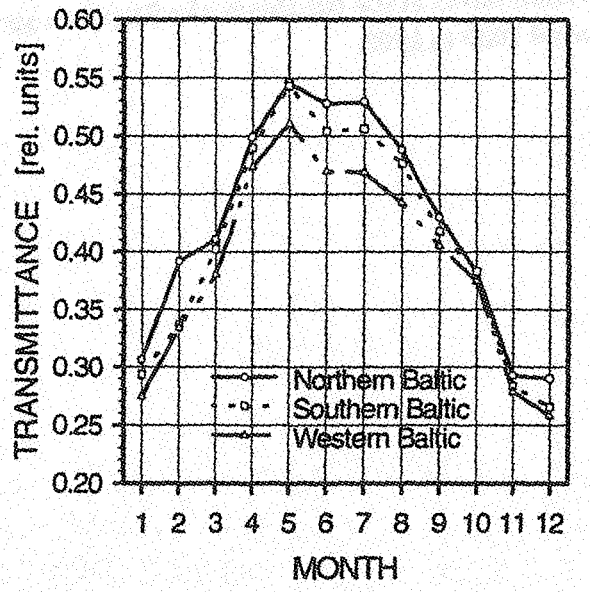

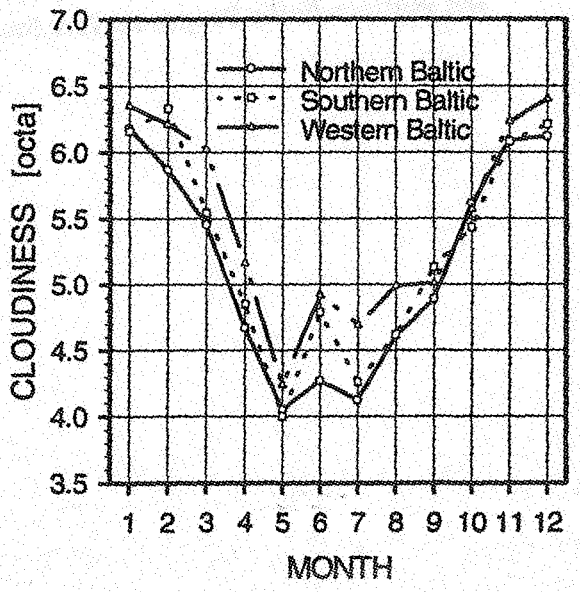

Figure 5 (left): Mean atmospheric transmittance of solar radiation monthly sums for the Northern, the Southern and the Western Baltic Proper for 1980-1992.

Figure 6 (right): Mean cloudiness for the Northern, the Southern and the Western Baltic Proper, based on daylight observations of the COADS during 1980-1992.

BALTIC AIR-SEA-ICE STUDY (BALTEX-BASIS) - A field experiment of BALTEX

Jouko Launiainen, Finnish Institute of Marine Research
Burghard Brümmer, Universität Hamburg, Meteorologisches Institut
Bertil Hakansson, Swedish Meteorological and Hydrological Institute
Rainer Roth, Institut für Meteorologie und Klimatologie der Universität Hannover
Ann-Sofi Smedman, Department of Meteorology, University of Uppsala
Timo Vihma, Department of Geophysics, University of Helsinki

Baltic Air-Sea-Ice Study (BASIS) aims at an improved understanding and modelling of energy and water cycles during winter conditions by conducting a winter field experiment in the ice edge zone of the Baltic Sea in February-March 1998 (Figure 1). The study is carried out as a co-operation of five institutes from Finland, Sweden and Germany. BASIS will be the first field experiment in the Baltic Sea covering the various branches of physical oceanography, sea ice research, marine meteorology and remote sensing. We will collect data particularly of

1) exchange of heat, moisture and momentum between the air, ice and sea

2) structure of atmospheric and oceanic boundary layers and their interaction with the exchange processes

3) ice motion and the atmospheric and oceanic driving forces, and

4) interaction between thermodynamic and dynamic processes in the air, sea and ice.

Research vessels, research aircraft and helicopters, meteorological balloon stations and a good set of automatic weather stations, turbulence equipments, and drifting buoys will be used (Figure 1, Table 1). Analyses of the data sets will result in improved remote sensing algorithms and, in particular, better parameterizations of air-ice-ocean interaction processes for development, validation, and optimization of the coupled atmosphere-ice-ocean models.
The duration of the project is 1997-2000 and the first milestone is a meeting with the modellists in Norrköping, Sweden, in June 1997.

EU has granted the funding support applied for the project .

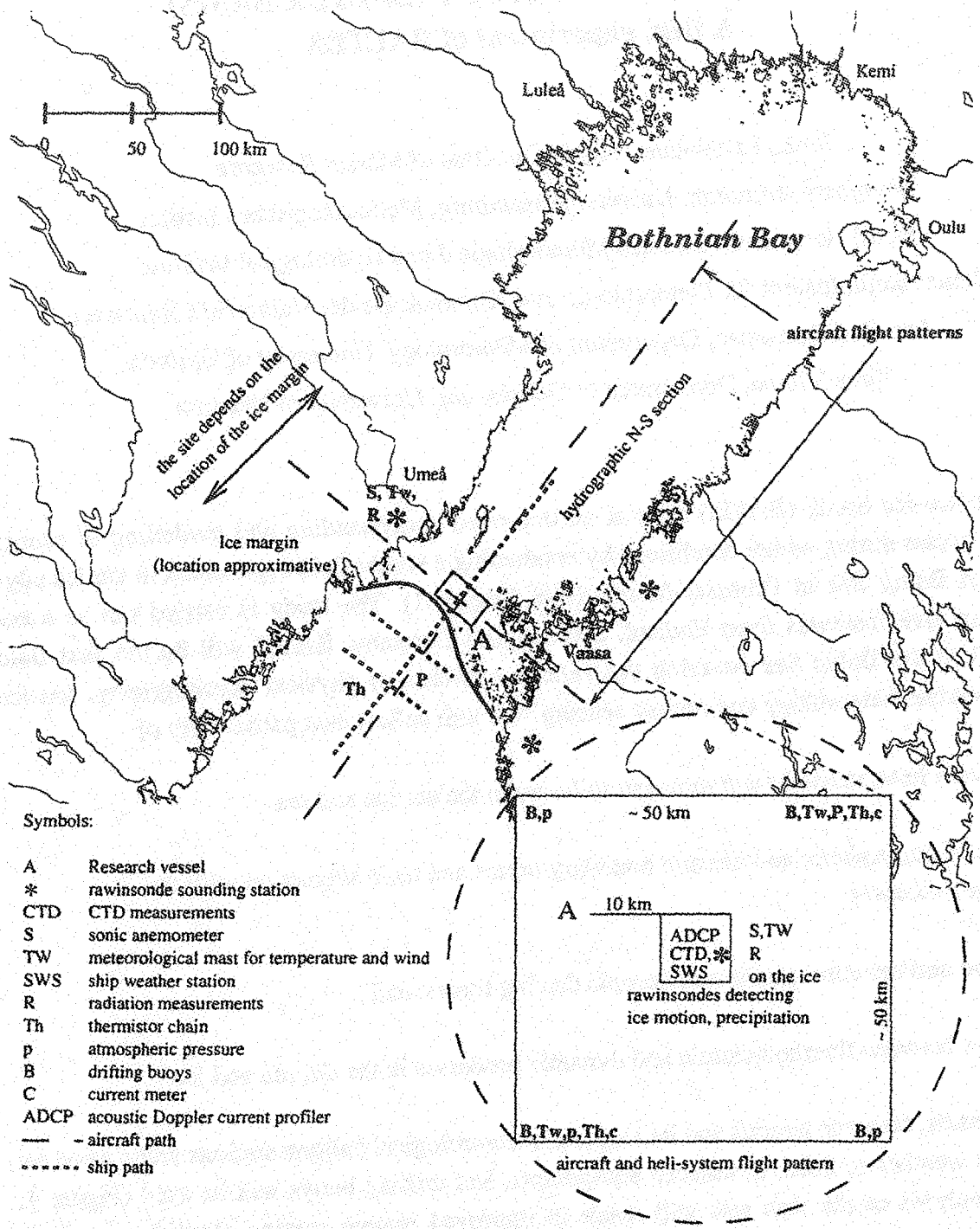

Figure 1: Map of the research area. The measurement activities at the main experiment site are shown in the lower right-hand corner. The experiment data will be completed by meteorological synoptic and sounding station data. The airborne measurements are listed in Table 1.

Table 1: Airborne measurements in BASIS.

measurement quantity	Helipod- system	research aircraft
Wind speed	- five-hole probe	- five-hole probe (100 Hz)
Air temperature	- sensor with long-time stability - fast sensor (100 Hz)	- sensor with long-time stability (10 Hz) - fast sensor (100 Hz)
Air Humidity	- dewpoint mirror - capacitive sensor - Lyman-Aplha sensor	- dewpoint mirror (10 Hz) - Humicap (10 Hz) - Lyman-Alpha sensor (100 Hz)
Surface temperature	- infrared thermometer	- infrared thermometer
Surface roughness	- laser profilometry	none
Turbulent fluxes	- eddy-correlation technique	- eddy-correlation technique
Radiative fluxes	none	- short- and longwave radiation (10 Hz)
Cloud droplets	none	- two particle size probes - liquid water sensor (10 Hz)
Navigation	- 3 x GPS - inertial platform	- GPS - Omega - inertial platform (100 Hz)

Results of the PILPS-2c Experiment

D. Lohmann, X. Liang, E.F. Wood, D.P. Lettenmaier
Princeton University, University of Washington

ABSTRACT

Todays weather prediction and climate models require land surface parameterization schemes which are able to model the large scale energy and water fluxes with the same spatial and temporal resolution as the atmospheric models. Within the Project for Intercomparison of Land Surface Parameterization Schemes (PILPS) 2c phase 16 of such models were tested in the Arkansas-Red-River basin (600 000 km^2) in the south-west of the USA.

1 INTRODUCTION

PILPS, the Project for Intercomparison of Land Surface Parameterization Schemes, is designed to improve the parameterization of processes at the continental surface, especially the hydrological, energy, and momentum exchanges, as represented in climate and numerical weather prediction models. Its approach is to facilitate comparisons between models, and between models and observations, that will help diagnose shortcomings, and motivate improvements in the model schemes. The PILPS philosophy is outlined in overview papers by Henderson-Sellers et al. (1993, 1995).

PILPS 2c is motivated by a desire to resolve the scale mismatch between the application of land surface parametrization schemes in numerical weather prediction and climate models and their testing against real data, to incorporate streamflow as an evaluation variable, and to compare the ability of the models to simulate land surface energy and moisture fluxes using a multi-year test period. The use of streamflow for model evaluation is attractive because it is a spatial integrator, and observations are fairly widely available. By moving to the scale of a continental river basin, the spatial scale is enlarged to the size of several grid cells in a typical land-atmosphere model application. The scale becomes large enough that it is possible to estimate evapotranspiration (in the water and energy budget) by atmospheric budget methods.

The general strategy was to provide the participants with radiative and meteorological forcings for six ISA catchments located throughout the Arkansas-Red River basin, and for each of the 61 one degree grid cells that make up the Arkansas-Red River basin (see Lettenmaier et al., 1997).

2 RESULTS

Figure 1 shows the spatial distribution of yearly total runoff (averaged from 1980-1988) for all models over the basin area. The model results can be compared to a runoff climatology (GGHYDRO, Cogley, 1991) obtained for the basin area in Figure 3. The observations show a general east-to-west gradient of total runoff with generally higher runoff rates in the eastern portion of the basin and lower rates in the west. This spatial pattern of observed runoff is consistent with the precipitation climatology. The model results are in qualitative agreement with the observed east-west gradient of total runoff. However, the models shown also depict a wide range in the magnitude of the total runoff over the basin and in the strength of the east-west gradient of total runoff. For some of the models, the performance of their simulated runoff varies among different climate regimes in the basin, with better performance in the humid areas than in the semi-humid and semi-arid regions.

Figure 5 shows how the different models partition their runoff into surface and subsurface runoff for the years 1980 - 1986. While some models produce only subsurface runoff, most of the models produce more surface runoff than subsurface runoff. Different runoff production processes result in different modeled streamflow patterns, as is shown in the PILPS-2c report (Lettenmaier et al., 1997).

Figure 6 compares naturalized streamflow data (provided by the Corps of Engineers) for the Arkansas River at Little Rock to model-generated streamflow for all of the models. The modeled streamflow was generated using daily total runoff at each grid-point, which was then routed using the method of Lohmann et al. (1996) through the channel network, then accumulated to monthly totals. The seasonal cycles were averaged over 7 years (1980-1986). The observed streamflow has a marked seasonality with a maximum in May and minimum in September. Most models are able to capture the observed seasonality. However, the magnitude of the seasonal cycle varies from model to model.

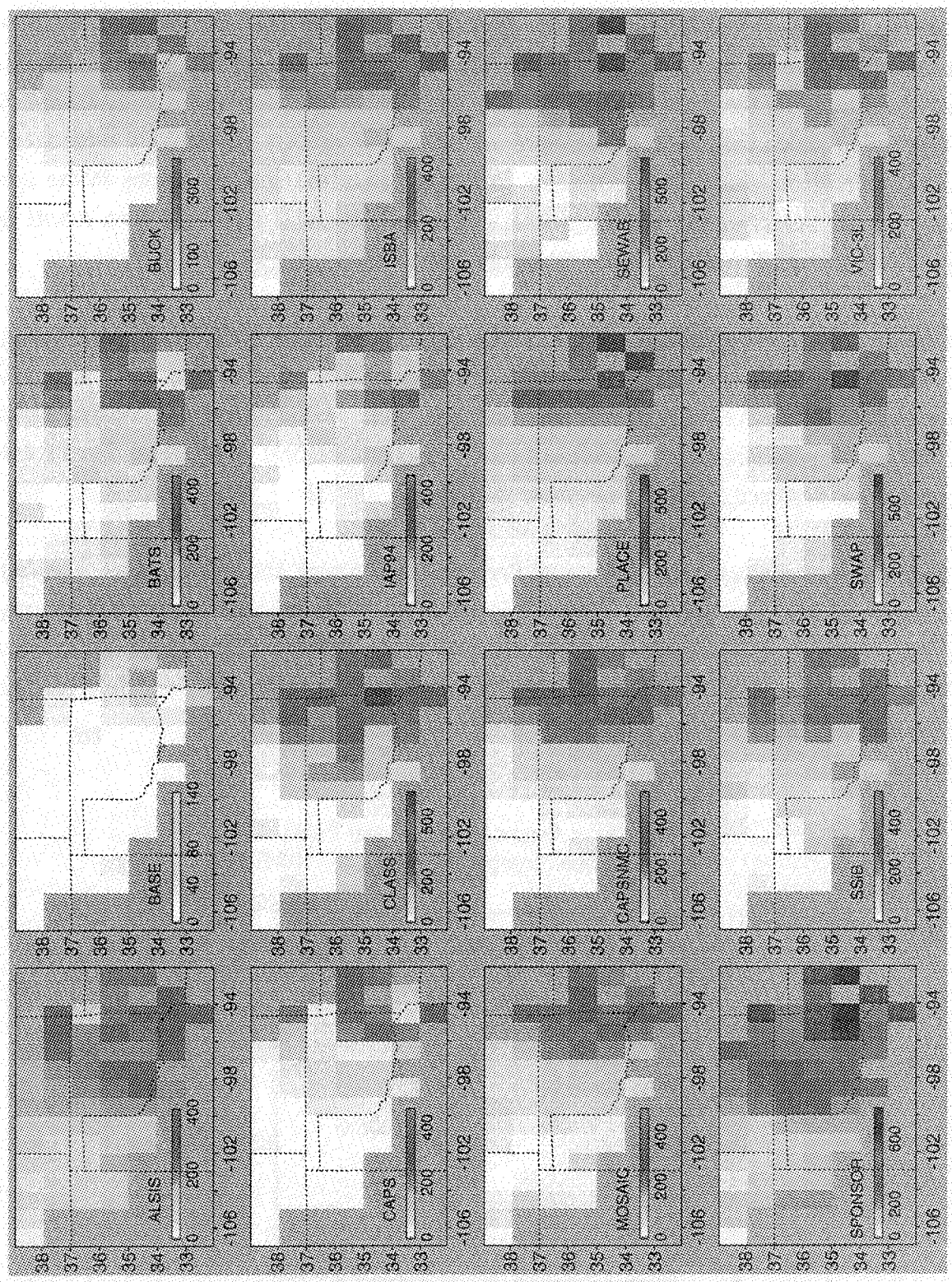

Figure 1: Spatial distribution of mean annual runoff (1980 - 1988) for all models

The seasonal cycles of model-simulated evaporation (1980-1986) averaged over the basin were compared. In Figure 2, the model simulations of evapotranspiration are compared to evapotranspiration estimated for the region using a water vapor budget based on radiosonde data, applied to a boxed region which roughly coincides with the basin. All models qualitatively reproduce the seasonal cycle of the evaporation estimates. However, small absolute deviations in the model evaporation can be associated with large relative changes in runoff due to the low runoff ratio (fraction of total runoff to precipitation) for the basin.

Model differences in surface temperature and albedo, together with the different partitioning of the latent and sensible heat fluxes, leads to a wide range of the predicted annual mean energy fluxes over the basin. Current LSP schemes used in weather prediction and climate models must be tested on temporal and spatial scales of the atmospheric models themselves. The PILPS-2c experiment was designed to resolve this scale mismatch.

The LSP schemes showed a large range of their modeled energy and water fluxes. The results shown here underline the need for more precise large-scale forcing and validation data sets, in order to compare the schemes across various climatic zones. Forthcoming papers will explore the PILPS-2c results in more detail, also giving implications about model sensitivities, model calibration and parameter transfer strategies.

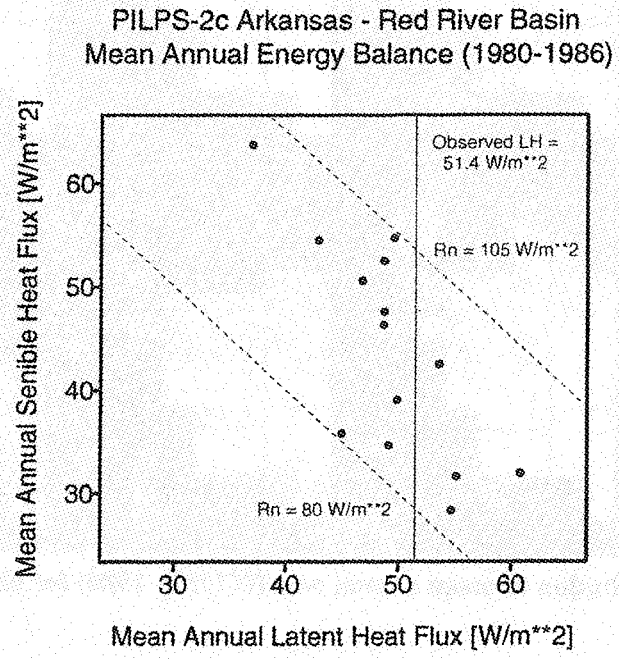

Figure 2: Model partitioning of net radiation into sensible and latent heat flux, averaged from 1980 - 1986.

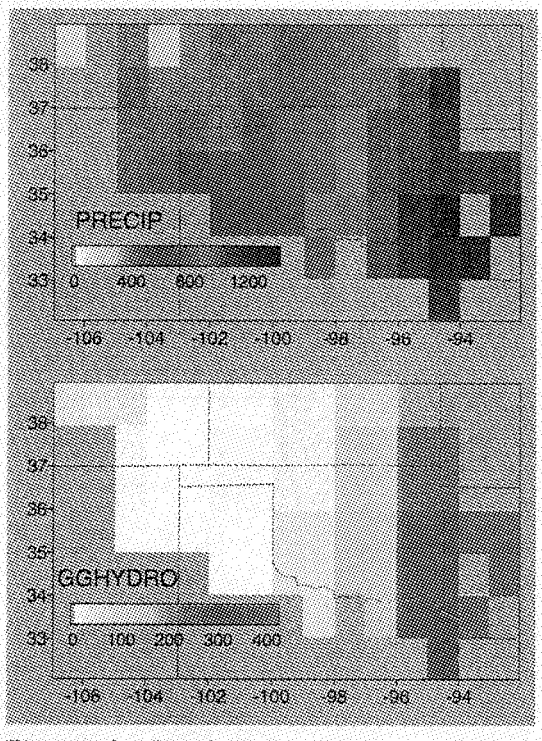

Figure 3: Spatial distribution of mean annual precipitation (1980 -1988) and runoff climatology (GGHYDRO, Cogley, 1991).

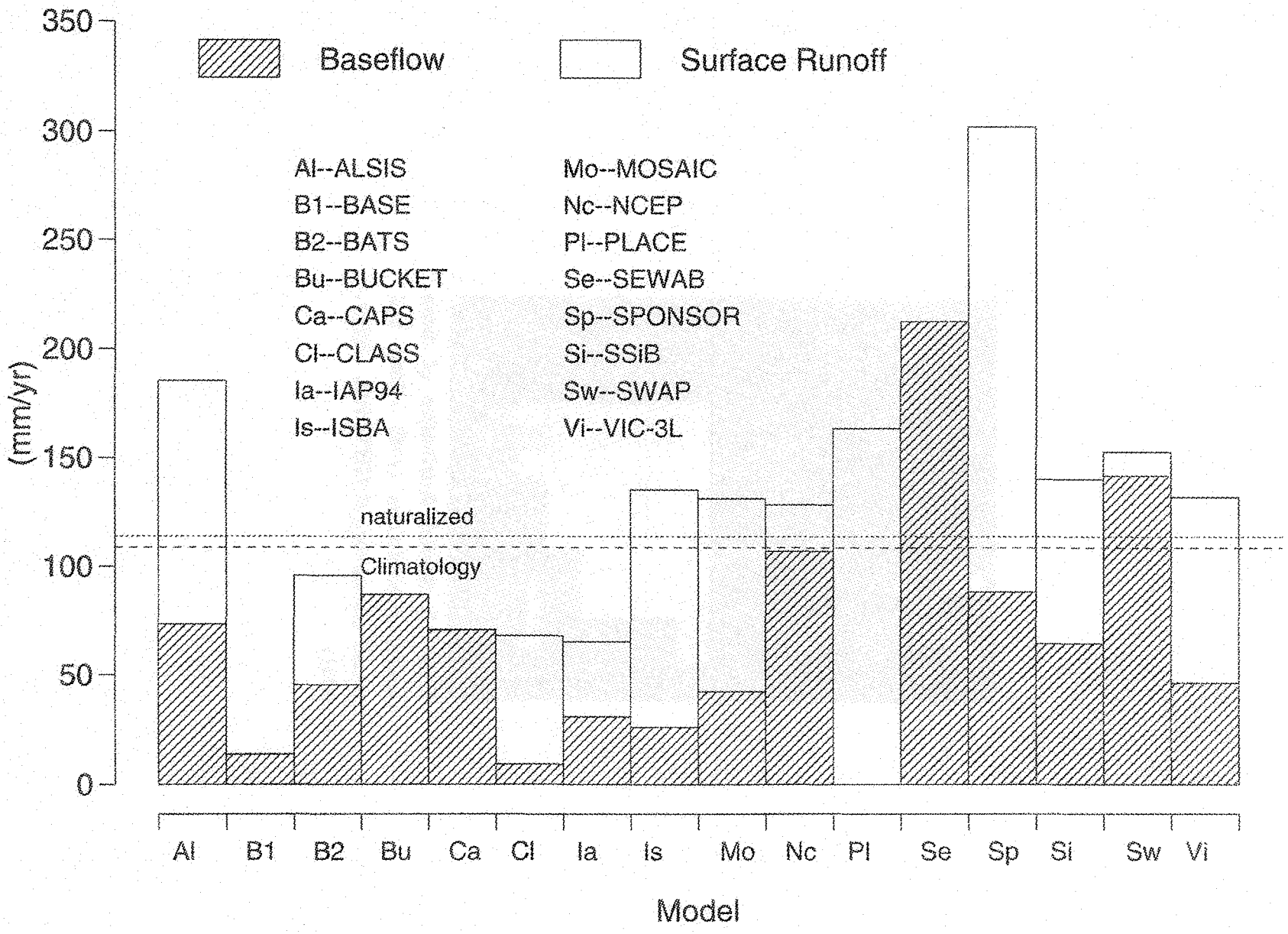

Figure 4: Model partitioning of runoff into surface and subsurface runoff.

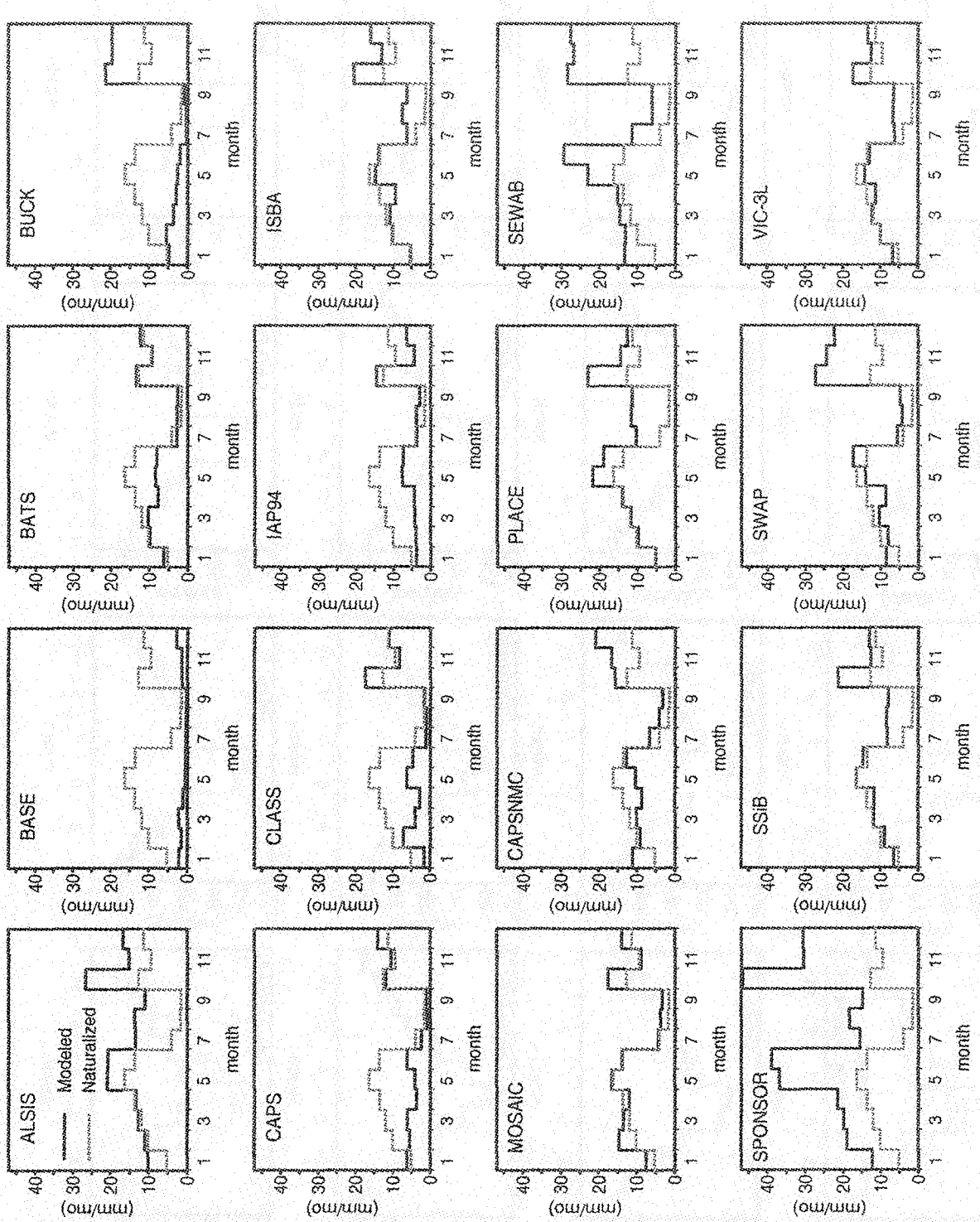

Figure 5: Meam monthly runoff (1980 - 1986) for all models compared to naturalized streamflow data.

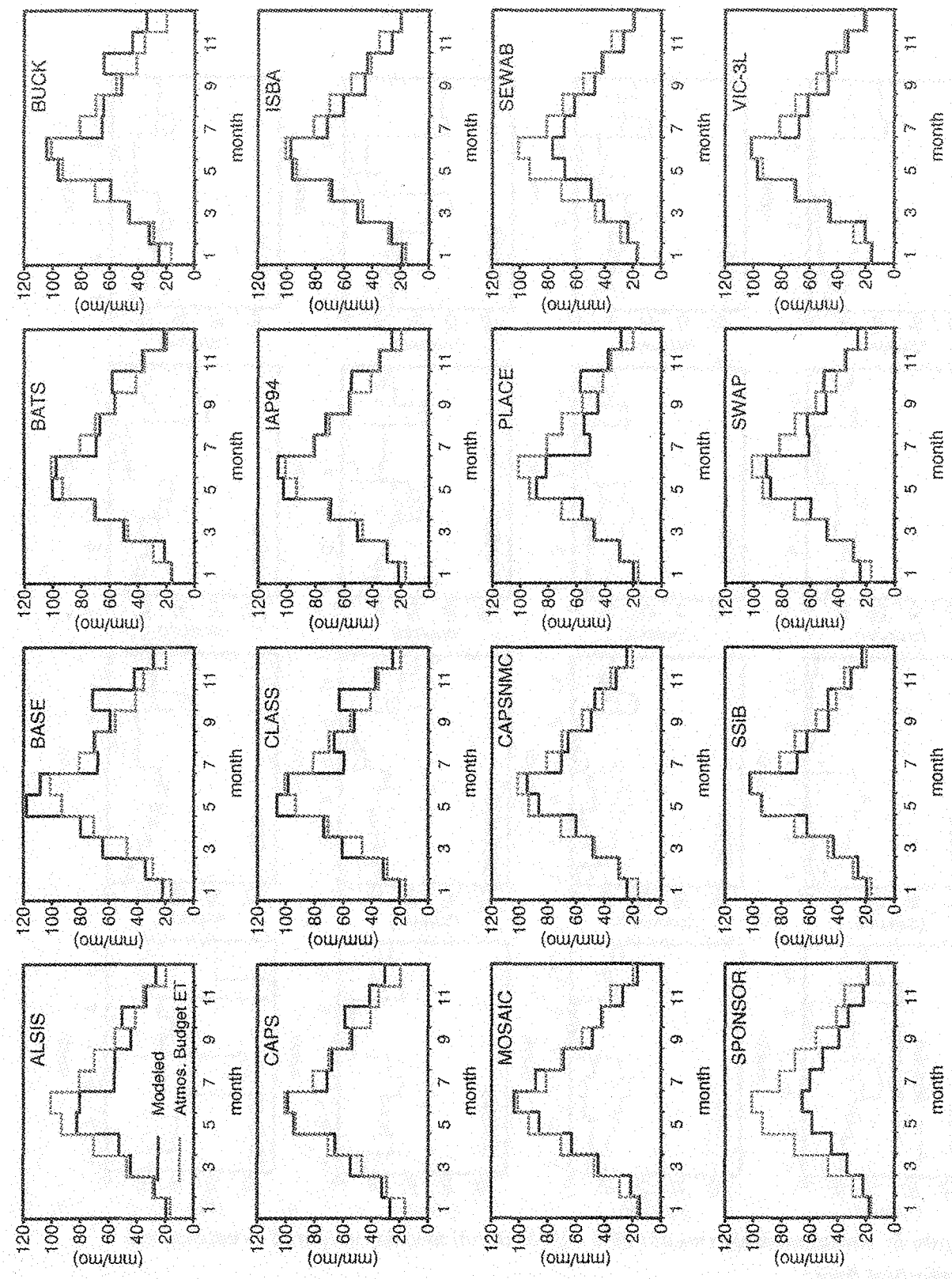

Figure 6: Mean monthly evapotranspiration (1980 - 1986) for all models compared to estimated evapotranspiration from an atmospheric budget.

REFERENCES

Henderson-Sellers, A., Z.-L. Yang, and R.E. Dickinson, 1993: The Project for Intercomparison of Land-Surface Parameterization Schemes, Bulletin of the American Meteorological Society 74, 1335-1349.

Henderson-Sellers, A., A.J. Pitman, P.K. Love, P. Irannejad, and T.H. Chen, 1995: The Project for Intercomparison of Land-Surface Parameterization Schemes (PILPS): Phases 2 and 3, Bulletin ofthe American Meteorological Society 76, 489-503.

Cogley,J.G., 1991, GGHYDRO-Global Hydrographic Data Release 2.0, Trent Climate Note 91-1, Trent University, 12.

D.P. Lettenmaier, D. Lohmann, E.F. Wood, X. Liang (Editors), 1997: PILPS-2c Draft Workshop Report, Princeton, WWW-Page: http://earth.princeton.edu

Lohmann, D., R. Nolte-Holube, E. Raschke, 1996: A large-scale horizontal routing model model to be coupled to land surface parameterization schemes, Tellus 48 A, 708-721.

SEWAB - a SVAT MODEL WITH VARIABLE INFILTRATION CAPACITY AND EXPLICIT RUNOFF FORMULATION

Heinz-Theo Mengelkamp and Kirsten Warrach
GKSS Research Center Geesthacht, Institute for Atmospheric Physics
D-21502 Geesthacht, Germany

A Soil-Vegetation-Atmosphere-Transfer (SVAT) scheme which solves the Surface Energy and Water Balance (SEWAB) equations considering partly vegetated surfaces has been developed. The scheme is based on the one-layer-concept for vegetation cover. Within the soil column the vertical diffusion equation for soil temperature and soil moisture are solved semi-implicitly at a variable number of soil layers. The model has been coupled to a one-dimensional boundary-layer model and to a three-dimensional non-hydrostatic atmospheric mesoscale model (Mengelkamp, 1991) to take into account the vertical transport of heat and moisture into the atmosphere. SEWAB participated in the World Climate Research Programme Project for Intercomparison of Land-surface Parameterization Schemes (PILPS) (Henderson-Sellers and Brown, 1992). In this paper results from experiment PILPS2c (Arkansas-Red Basin, hydrology) are presented. In this experiment runoff data modelled with SVAT schemes were compared with measured streamflow. This shows the ability of the scheme to partition the precipitation into runoff on the one hand and evapotranspiration and soil moisture storage on the other hand. The impact of the subsurface runoff parameterization (run 1, run 3) and the inclusion of a variable infiltration capacity (run 2) are investigated.

1 THE SVAT PARAMETERIZATION SCHEME

The SVAT scheme SEWAB solves the surface energy and water balance equations. The latter is given by

$$P - E - R = \Delta S \qquad (1)$$

with the precipitation P, the evapotranspiration E, the runoff R and the storage change ΔS.
Following Noilhan and Planton (1989) the evapotranspiration is calculated separately for bare soil and vegetated surfaces. The evapotranspiration from the vegetated part is calculated after Deardorff (1978). For the calculation of soil temperature T and soil moisture content η the vertical diffusion equations

$$c(\eta)\frac{\partial T}{\partial t} = \frac{\partial}{\partial z}\left(\lambda \frac{\partial T}{\partial z}\right) \qquad (2)$$

$$\frac{\partial \eta}{\partial t} = \frac{\partial}{\partial z}\left(D(\eta)\frac{\partial \eta}{\partial z} + K(\eta) \right) \qquad (3)$$

are solved semi-implicitly. $c(\eta)$ is the volumetric heat capacity and λ is the thermal conductivity. The hydraulic diffusivity $D(\eta)$ and the hydraulic conductivity $K(\eta)$ are parameterized after Clapp and Hornberger (1978). In this basic version runoff is only produced from saturated soil (run 1).

2 VALIDATION OF FLUX CALCULATIONS

A data set from 30 June - 11 July 1987 from the FIFE experiment, which was located in Kansas (USA), was used to validate SEWAB with regard to flux calculations. Figures 1 and 2 show the surface temperature and the latent heat flux, respectively, both from observations and calculations. The forcing variables measured at 2 m height were half-hourly averages of temperature, specific humidity and the radiation balance except the outgoing longwave radiation; windspeed was observed at 5.4 m. The soil type is given as silty loam and the vegetation as grass. There was hardly any precipitation.

3 VALIDATION OF RUNOFF PRODUCTION

For the experiment PILPS 2c, meteorological and hydrological data were provided for the Arkansas-Red Basin (USA) by its leading scientist Xu Liang (Princeton University). Among those is the semiarid Black Bear River catchment of 1491 km^2 (36.34°N,-96.80°E). Table 1 shows land-surface characteristics of this catchment. Meteorological forcing data from January 1979 to December 1987 were provided on a half-hourly timestep. For each catchment daily streamflow data were given for comparison with runoff data produced by the SVAT scheme.

For PILPS2c SEWAB was run in its basic version as described above with 6 soil layers (run 1). Figure 3 shows the daily sum of the runoff calculated with SEWAB (dashed) and the measured daily streamflow (solid) exemplary for 4 May - 13 June 1982 (day 1220-1260). The runoff calculated by the scheme (dashed line) increases later than measured (solid line) and decreases too slowly and not sufficiently. The water drains fully to the lowest layer where all the runoff is produced, there is no surface runoff production.

The experience from PILPS 2c resulted in a modification of SEWAB by implementing a variable infiltration capacity after the Nanjing model (run 2) described e.g. by Wood et al. (1992). The assumption is a spatial variation of the infiltration capacity due to heterogeneity in topography, soil and vegetation within the area. Dependent on precipitation and initial soil moisture a saturated fraction of the area is assumed that allows surface runoff production though the total

area is not saturated. The variable infiltration capacity has an effect on the timing of the runoff events. Figure 3 shows that there is little runoff production on days 1222 and 1228 (long-dashed line), i.e. when measured streamflow (solid line) occurs, though the amount is underestimated. The two peaks on days 1232 and 1234 and the low on 1235 are met qualitatively, but the runoff is underestimated. Afterwards the calculated runoff is dominated by subsurface runoff.

Since the results are not satisfying the calculation of the subsurface runoff was modified after the ARNO model conceptualization (Francini and Pacciani, 1991). This scheme assumes that underneath a limiting factor runoff is produced linearly dependent on the soil moisture content and above this value increases nonlinearly. This results in a higher runoff production around day 1230 due to more subsurface runoff on that day (Figure 3). Therefore, the runoff on day 1234 is less than in the previous run.

4 CONCLUSIONS

The experiments show that SEWAB is able to reproduce the runoff fairly well. At present it provides the surface fluxes as the lower boundary condition for the mesoscale atmospheric model GESIMA (Geesthacht Simulation Model of the Atmosphere).

The inclusion of a variable infiltration capacity (run 2) allows surface runoff production and causes slight improvement regarding the timing of the runoff calculation. Allowing additionally subsurface runoff already before the soil is saturated (run 3) reduced the difference between the calculated runoff and the measured streamflow not only annually but also on the daily basis.

Acknowledgment

The authors like to thank D. P. Lettenmaier, X. Liang and E. F. Wood for providing the data and organizing the PILPS(2c) workshop held from 28-30 October 1996 at Princeton University. The workshop was supported NOAA and NSF.

REFERENCES

Beven, K., 1984: Runoff production and flood frequency in catchments of the order n: an alternative approach. In V.K.Gupta et al (eds): Scale Problems in Hydrology, 107-131.

Clapp, R.B., and G.M. Hornberger, 1978: Empirical equations for some soil hydraulic properties. Water Resources Research, **14**, 601-604.

Deardorff, J.W., 1978: Efficient prediction of ground surface temperature and moisture, with inclusion of a layer of vegetation. Journal of Geophysical Research, **83**, C4, 1889-1903.

Francini, M., and M. Pacciani, 1991: Comparative analysis of several conceptual rainfall- runoff models. Journal of Hydrology, **122**, 161-219.

Mengelkamp, H.-T., 1991: Boundary layer structure over an inhomogeneous surface: simula-tion with a non-hydrostatic mesoscale model. Boundary-Layer Meteorology, **57**, 323-341.

Noilhan, J., and S. Planton, 1989: A simple parameterization of land surface processes for meteorological models. Monthly Weather Review, 117, 536-549.

Henderson-Sellers, A., and V.B. Brown, 1992: PILPS: project for intercomparison of land-surface parameterization schemes. Workshop Report and First Science Plan. IGPO Publication Series 5, Science and Technology Corporation, Hampton, VA, 51pp.

Wood, E.F., D.P. Lettenmaier, and V.G. Zartarian, 1992: A land-surface hydrology parameterization with subgrid variablity for general circulation models. Journal of Geophysical Research, **97**, D3, 2717-2728.

Table 1: Land-surface characteristics of the Black Bear River.

Parameter	Black Bear River
vegetation	mixed forest and woodland
soil depth (m)	1
root depth (90% of roots) (m)	0.3
saturated soil moisture η_s	0.48
saturated hydraulic conductivity K_s (m/ s)	2.64E-6
saturated suction head Ψ_s (m)	-0.479
sand (%)	23
clay (%)	19
Clapp and Hornberger parameter b	4.55

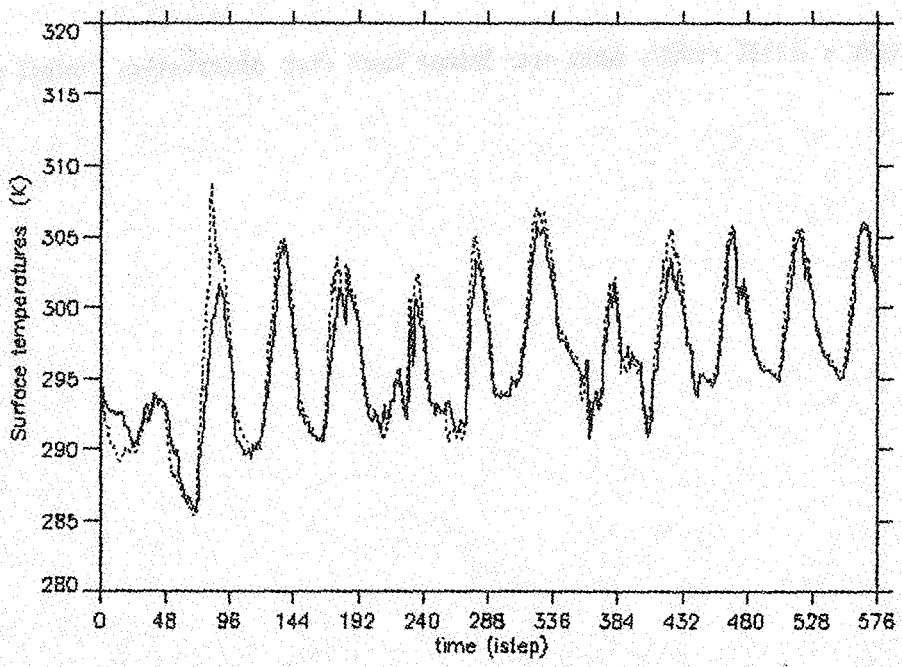

Figure 1: Comparison with a FIFE (1987) data set: surface temperature observation (solid) and calculation (dotted).

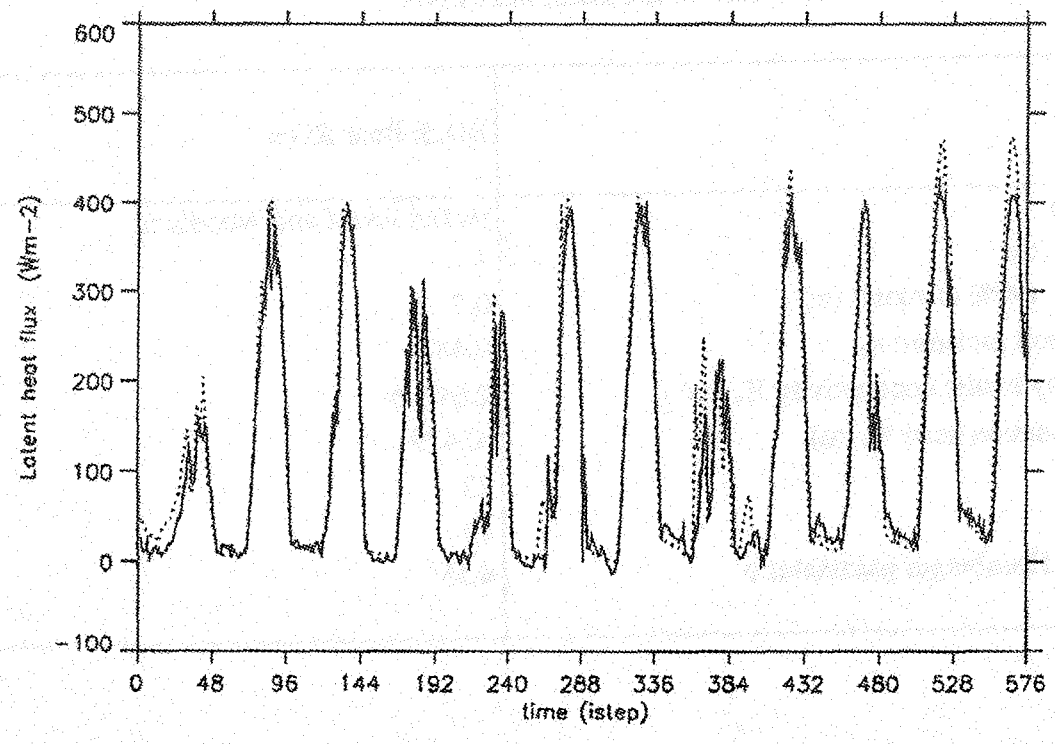

Figure 2: Comparison with a FIFE (1987) data set: latent heat flux observation (solid) and calculation (dotted).

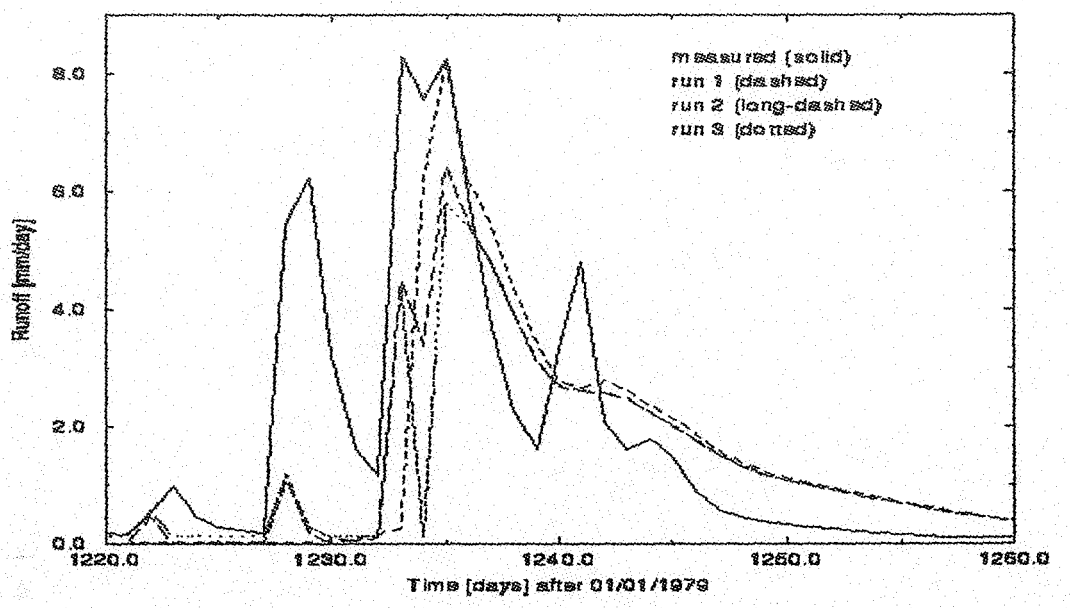

Figure 3: Daily runoff of the Black Bear River.

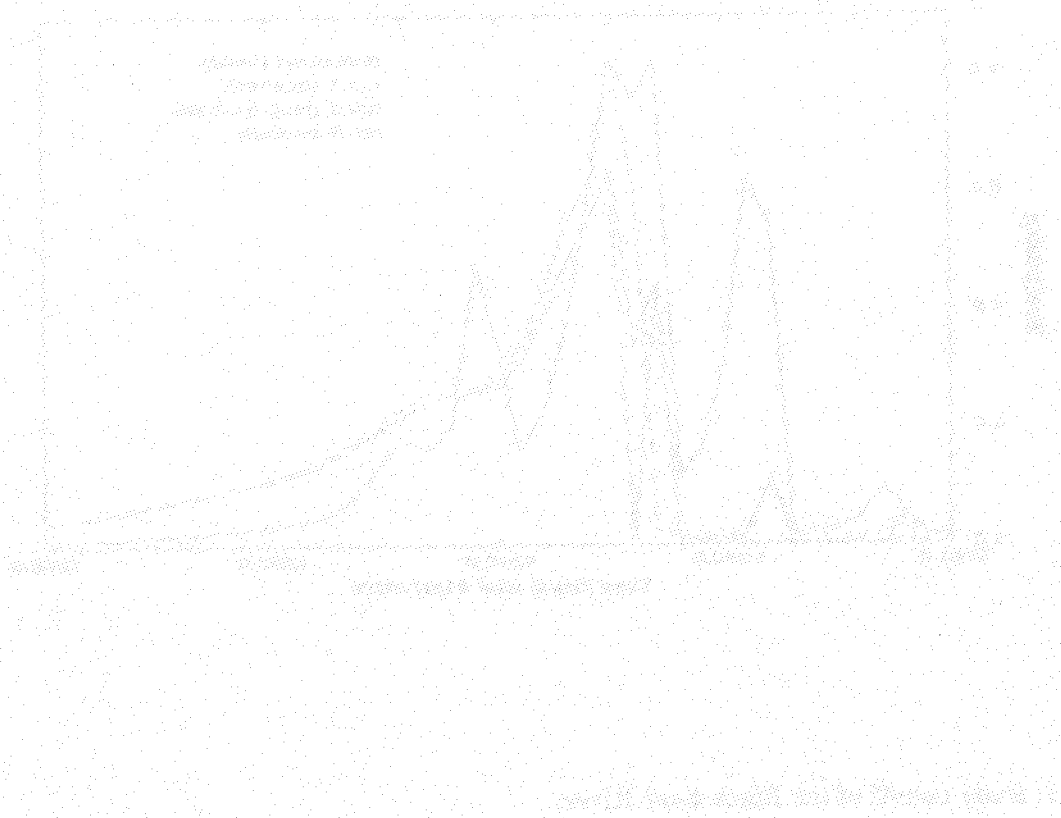

AN APPLICATION OF A LARGE-SCALE CONCEPTUAL HYDROLOGICAL MODEL OVER THE ELBE REGION

Manfred Lobmeyr
GKSS Research Center Geesthacht, Institute for Atmospheric Physics
D-21502 Geesthacht, Germany

ABSTRACT

In this paper a grid-related coupled conceptual hydrological model is presented, describing the processes of vertical and horizontal water movement separately. For the spatial scale this model is set up on a rotated grid of about 1/6 degree of the atmospheric regional scale model (REMO) used in the BALTEX project. For the time scale the physical processes of the water balance are solved on a daily base. Vertical processes are described by a SVAT scheme, as used in the VIC-2L model. Meteorological forcing is done by measured values of precipitation, temperature, pressure, wind speed, air humidity and daily sunshine duration. Output quantities are time series of fast runoff, baseflow and evapotranspiration for each grid point. Fast runoff and baseflow are routed with a horizontal routing scheme to the outlet of a catchment. Calculated and measured streamflow at prescribed gauge stations are compared. An application of this model over main parts of the German Elbe river is done.

1 INTRODUCTION

A first step towards coupling hydrological and atmospheric models is an off-line coupling of atmospheric forcing with a hydrological model. Atmospheric measurement is done by the DWD [2], at fixed climatologological stations. Data records of about 10 years are gritted on a rotated grid of about 1/6 degree of the atmospheric regional scale model REMO [3]. Vertical processes, described by a 2-layer SVAT model, are fast runoff, baseflow and evapotranpiration. Horizontal water movement is divided into transport processes inside a grid box and transport processes between neighbouring grid boxes, both are described by linear routing functions. With the help of this horizontal scheme the sum of modeled fast runoff and baseflow can be routed to the outlet of prescribed gauges and can easily be compared with measured streamflow. At first a calibration procedure for a fixed time period has to be set up, resulting in an optimal parameter set for this time period. Measured discharge at the outlet of a catchment and measured mean precipitation over this catchment is used to find a proper impulse response function, also the partitioning of total runoff in fast runoff and baseflow can be optimized. Calibration parameters for the SVAT model are the thickness parameter of upper and lower layer and the shape parameter for the variable infiltration curve of the upper layer. This model is applied over a main part of the Elbe region and comparison of discharge is done at the gauge station Magdeburg.

2 MODEL CONCEPT

2.1 SVAT-model

The VIC-2L model [4, 5] is a two layer SVAT scheme for general circulations models and numerical weather prediction models. It has participated in the PILPS [1] experiments. It includes a canopy layer and an upper and lower soil layer. A reasonable hydrologically run-off mechanism will be described, considering the variation of infiltration capacity, in the upper layer within a grid box. The effects of spatial subgrid variability of soil moisture is therefore included - it describes the saturation excess runoff in a parameterized manner. In the lower layer drainage is represented by the Arno scheme. For each vegetation type vegetation characteristics, such as leaf area index, canopy resistance, roughness length and displacement height are assigned. Percolation from the upper to the lower layer is only driven by gravity using the so-called Brooks-Corey relationship. Evapotranpiration is calculated according to the Penman-Monteith relationship. The actual evapotranspiration is dependent on the canopy layer and the transpiration from each vegetation class.

2.2. Routing model

A routing model [7] describes both the concentration time for runoff reaching the outlet of a grid box, as well as the water transport in a river network. The basis assumption is that all horizontal routing processes within a river network are linear and time invariant. The linear transfer model is characterized by its impulse response function, or Unit Hydrograph. Known time series of input are precipitation, known time series of output are measured discharge. In this system there are two unknown quantities: the amount of precipitation which becomes streamflow, the so-called effective rainfall, and the Unit hydrograph itself. Calculating the transfer function inside a grid box, as a first step, we have to separate slow flow and fast flow of the measured discharge. We can do it with a linear model approach [6], where two parameters (b and k in Figure 1) are determining the fraction of slow flow to fast flow. These two parameters are assumed to be constant over the whole time period. After this the impulse response function for the fast flow can be found by an iterative scheme with minimal least square solution. Impulse response function for the river flow can be found by the kinematic wave solution, with constant celerity and diffusivity. For the whole river network an Unit Hydrograph can be found as an appropriate superposition of the grid box and river flow impulse response function.

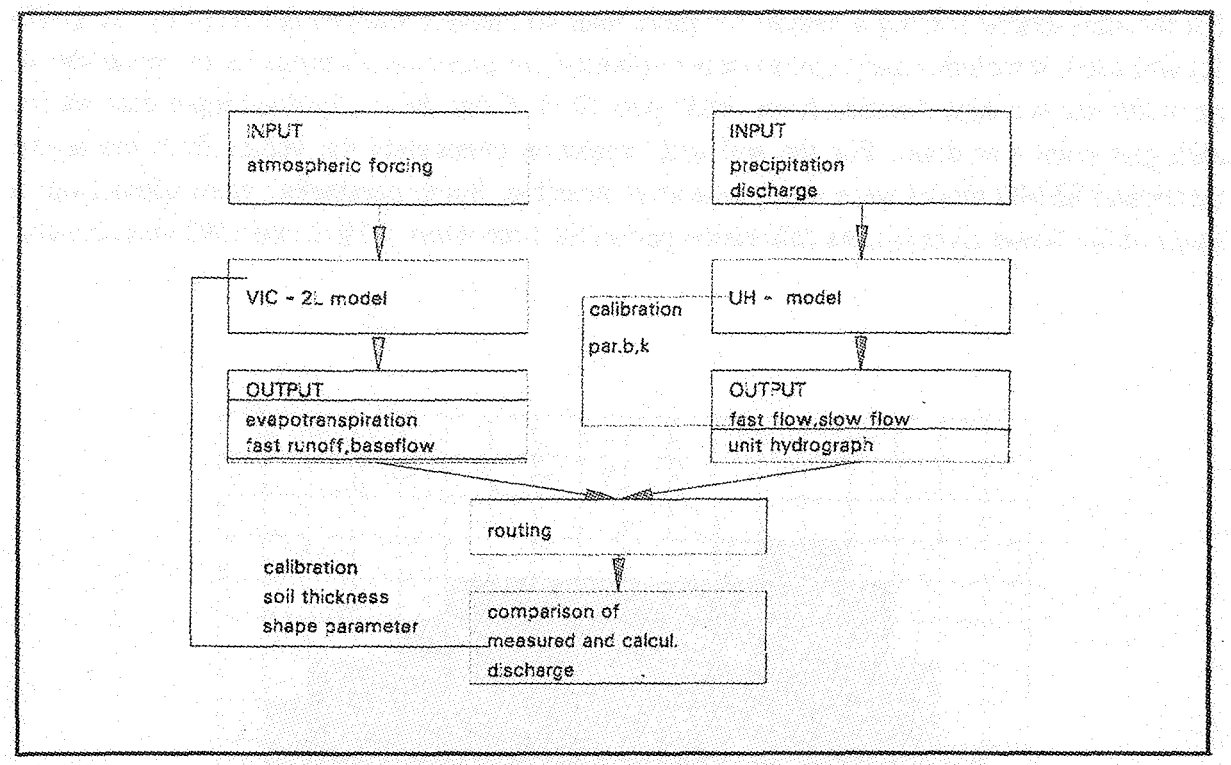

Figure 1: Calibration procedure.

3 MODEL CALIBRATION

The computational procedure for calibration of the coupled hydrological scheme can be seen in Figure 1. For the routing model input time series are measured discharge and precipitation. A first guess of parameter b and k is chosen for the separation between fast flow and baseflow. Output are fast flow, slow flow and Unit Hydrograph. Calibration is done by comparison of the routed sum of fast and slow flow with measured discharge for a time period of some months, preferably with heavy rainfall and discharge events. By changing parameter b and k, division into fast flow and baseflow can be changed.

For the SVAT model input are daily datasets of atmospheric forcing, soil and vegetation parameters. Output are evapotranspiration, fast runoff and baseflow. Fast flow and baseflow are routed with the unit hydrograph of the whole catchment as a linear product of grid box unit hydrograph and river routing impulse response function.

Balancing measured and calculated discharge the SVAT scheme can be calibrated. Calibration procedure is done by changing the soil thickness for the upper and lower layer and the shape parameter of the variable infiltration capacity curve.

4 SIMULATION OF WATER BALANCE AND RIVER FLOW

The model area includes the German part of the upper Elbe river basin, with the catchments of the Saale, Mulde and Schwarze Elster, which is a mountainous area of about 44.000 km^2. Upper and lower boundary conditions for this area are given by gauges at Schoena (B) and Magdeburg (A), respectively. The drainage area measured at Schoena is about 51.000 km^2, representing the inflow from the Czech part of the Elbe river. Therefore, the whole drainage area at Magdeburg is about 95.000 km^2.

For the atmospheric forcing a dataset for more than 40 climatic stations delivered by the DWD [2] was used. It includes daily values of precipitation, air pressure, air temperature, wind speed, humidity and sunshine duration from 1984 up to 1993. From these a gridded input data set for each grid point was done. For the soil and vegetation parameters the values from the above mentioned REMO model were used, whenever possible. Some parameters were taken from a study of the Weser river [6]. As calibration period the time interval 1992 and 1993 was chosen.

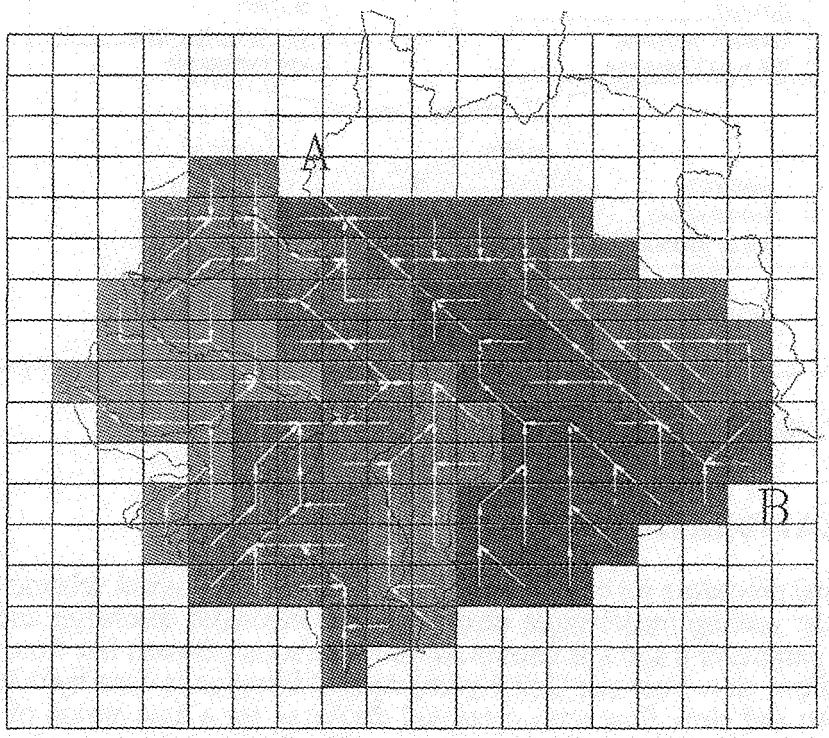

Figure 2: River network.

For the routing procedure a grid network was set up over the model area (Figure 2). The whole catchment was divided into 8 subcatchment, the outlet of each was represented by a gauge station, where time series of measured daily discharge are available. Flow direction goes in an unidirectional way from one grid box to the next, where eight directions are possible. For building up an appropriate Unit Hydrograph, the time interval from January 1993 to October 1993 was used as calibration period.

Time series of gridded fast flow, baseflow and evapotranspiration for the whole time period 1984 up to 1993 where simulated with the VIC-2L model. The sum of fast runoff and baseflow for each grid was routed with Unit Hydrograph found by the previous calibration procedure to the outlet of the subcatchment and then to the outlet of the whole area at Magdeburg. To include the inflow condition measured discharge at Schoena (B) was routed with the help of an appropriate kinematic wave solution to the outlet of Magdeburg (A).

The following figures show gridded sums for one year, namely 1991. In Figure 3 rainfall is shown. Figures 4 and 5 show the result of simulated total runoff and evapotranspiration for a one-year period. Yearly mean of rainfall over the whole region was about 550 mm. Corresponding values for runoff and evapotranspiration were about 180 mm and 370 mm, respectively.

The range of rainfall goes from 300 - 400 mm in the lower areas of Saale and Elbe but up to 900 until 1000 mm in the mountainous regions. In the same behavior are the ranges of total runoff from 100 m up to 300 mm and of evapotranpiration from 300 mm up to 500 mm.

The result of simulation for all grid points and for the time period 1985 up to 1993 is shown in Figure 6. Daily means of measured and simulated discharge is shown. Besides a good agreement in the spatial behavior there is some lack of correspondence in winter periods, when snow and ice processes are important.

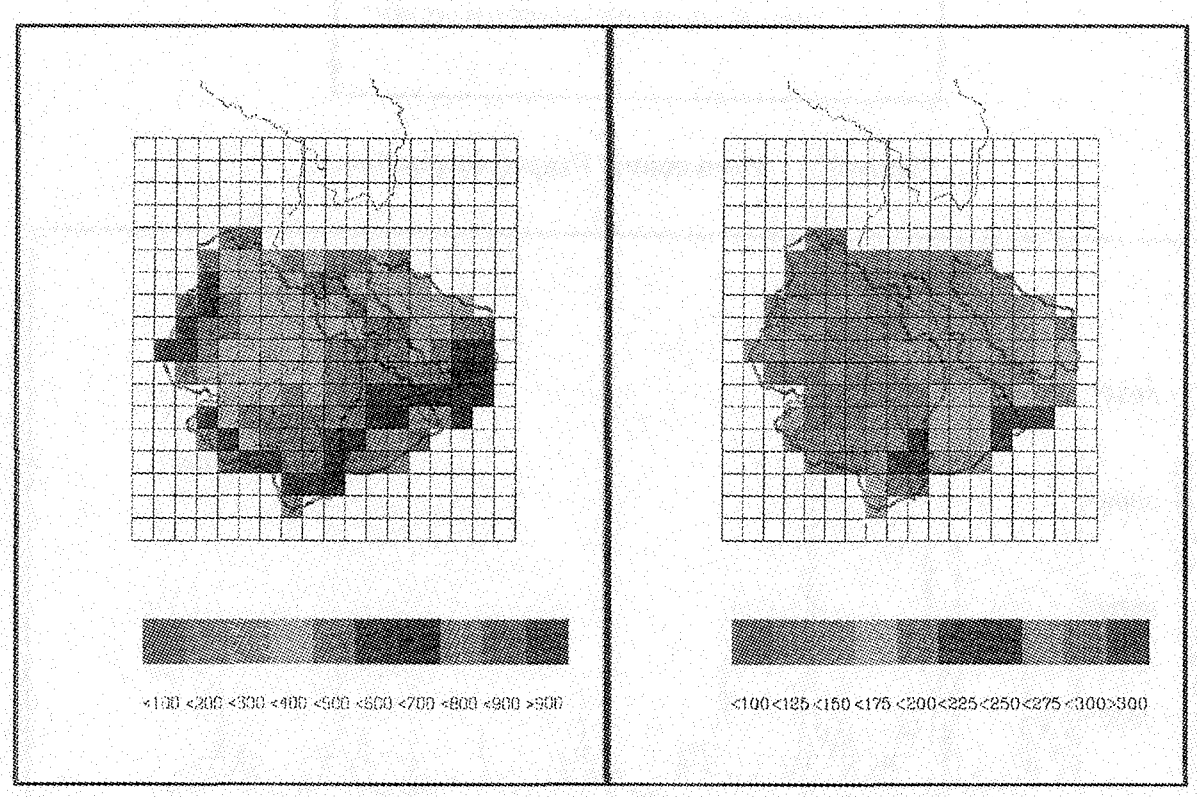

Figure 3: Mean annual rainfall.

Figure 4: Mean annual total runoff.

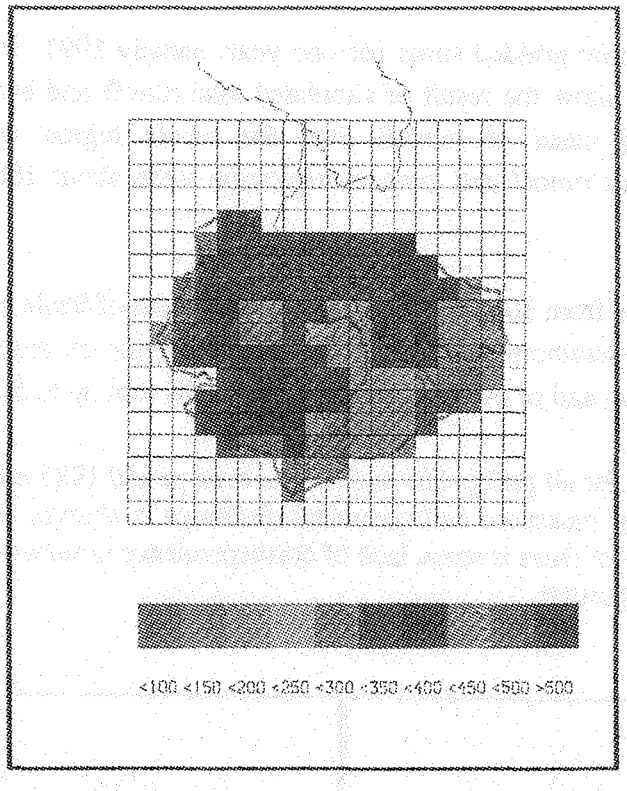

Figure 5: Mean annual Evapotranspiration.

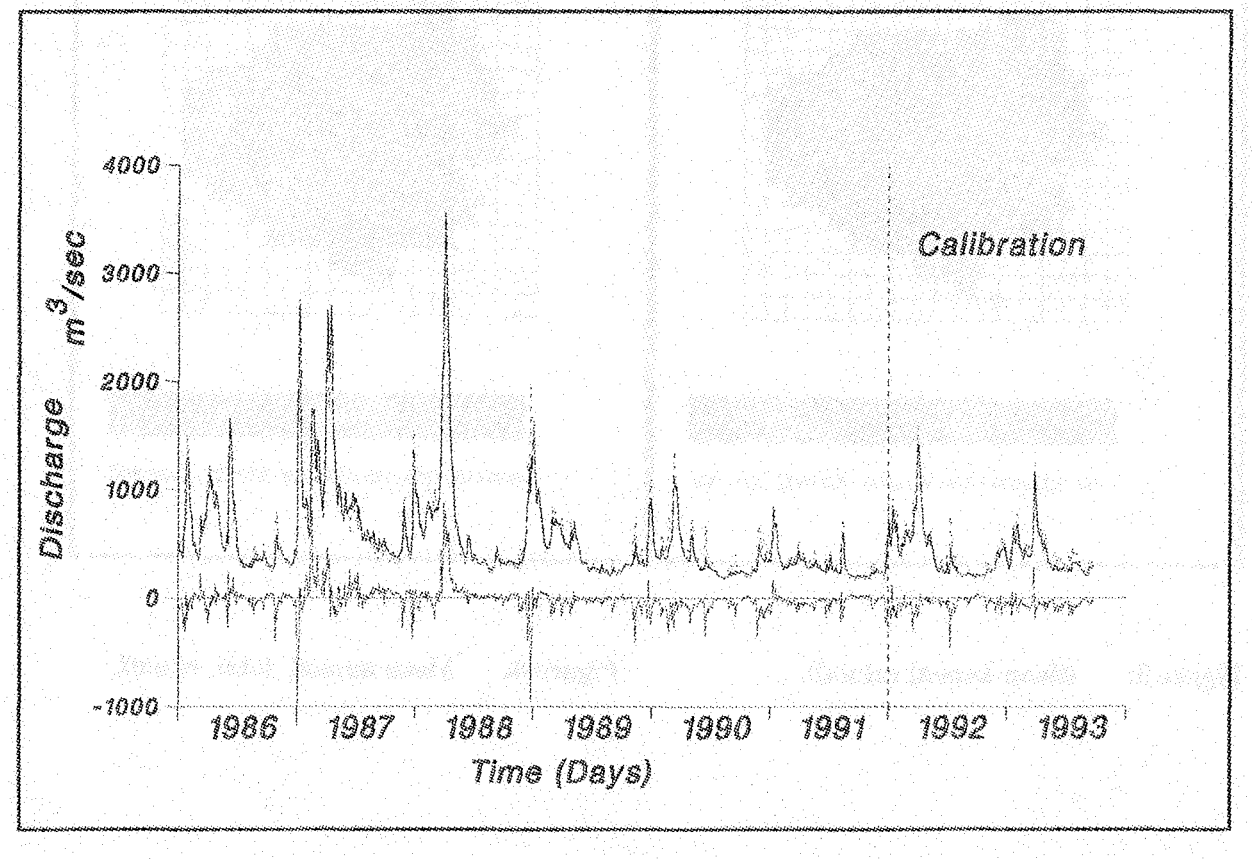

Figure 6: Discharge at gauge station Magdeburg. Red curve: simulated discharge, black curve: measured discharge, blue curve: difference between measured and simulated discharge.

6 CONCLUSIONS

As a grid network related model, describing vertical water movement processes inside each grid box a land surface parameterization scheme was used. Atmospheric forcing was done by measured daily mean values of precipitation, air temperature, humidity, pressure, wind speed and sunshine duration. Horizontal water movement was done with the help of a routing scheme. Fast runoff and baseflow were routed inside each grid box, water transport between neighbouring grid boxes were done by river routing. Calibration procedure was performed, comparing measured and simulated discharge at catchment outlet.

Measured and simulated discharge at the outlet of the whole area are in good agreement. Some discrepancies are shown for snow and ice processes. In these field more work is necessary. As a next step inclusion of the full energy and water cycle will be done. Therefore, instead of daily means the daily cycle of atmospheric forcing has to be included in the model.

7 REFERENCES

[1] Chen T.H, et al., 1996: Cabauw Experimental Results from the Project for Intercomparison of Landsurface Parameterization Schemes (PILPS), Journal of Climate, accepted for publication.

[2] DWD, 1994: Die Datenarchive der operationellen NW-Modelle des Deutschen Wetterdienstes.

[3] Karstens, U., R. Nolte-Holube, and B. Rockel, 1996: Calculation of the water budget over the Baltic Sea catchment area using the regional forecast model REMO for June 1993. TELLUS, **48A**, No. 5, pp 684 - 692.

[4] Liang, X., 1994: A two-layer variable infiltration capacity land surface representation for general circulation models, Water Resources Series Technical report No. **140**, Department of Civil Engineering, University of Washington.

[4] Liang, X., D.P. Lettenmaier, E.F. Wood, and S.J. Burges, 1994: A simple hydrologically based model of land surface water and energy fluxes for general circulation models. J.ÊGeophys. Res., **99**, D3, 14415 - 14428.

[6] Lohmann, D., 1996: Hydrologische Modellierung auf der regionalen Skala. Doctoral Thesis, Hamburg, 94 pp.

[7] Lohmann, D., R. Nolte-Holube, and E. Raschke, 1996: A large scale horizontal routing model to be coupled to land surface parameterization schemes. TELLUS, **48A**, No. 5, pp 708 - 721.

Atmospheric Fields over the Baltic Sea Derived From SSM/I Observations

R. Lindau, E. Ruprecht, and T. Jung
Institut für Meereskunde, Düsternbrooker Weg 20
D-24105 Kiel, Germany

ABSTRACT

In order to investigate the hydrological cycle - a major objective of BALTEX- results of numerical models, e.g. the Regional model REMO, are used. The results, however, have to be validated. With our study we will provide validation data, based on Special Sensor Microwave/Imager (SSM/I) observations over the Baltic Sea. Two problems appear: (1) the development of retrieval algorithms which are capable to derive atmospheric fields with high accuracy and (2) the application of microwave data in small-scale regions such as the Baltic Sea. The latter requires the development of new methods to remove land and sea ice influences. The applied retrieval algorithms are based on neural networks, which give the highest accuracies. It will be shown, that the new techniques to remove the influence of land and sea ice work well.

1 INTRODUCTION

The investigation of the hydrological cycle over the Baltic Sea and its catchment area is the main objective of BALTEX (1995). Regional models will be one of the tools to perform such an investigation. A careful validation of the model results is a prerequisite for this undertaking. Over land there exists a large, though not satisfactory, number of observations for the validation. Over sea, however, the data base is smaller.

In this study we describe the processing method of satellite observations, which should be applied to validate the results of the regional model REMO over the Baltic Sea. The data come from the Special Sensor Microwave/Imager (SSM/I) onboard the satellites of the Defense Meteorological Satellite Program (DMSP). Data are available at 4 frequencies in 7 channels; vertically and horizontally polarized at 19.35, 37.0, and 85.5 GHz and vertically polarized only at 22.235 GHz (Hollinger et al. 1987). Using these measurements, it is possible to derive fields of total water vapour content (TWV), cloud liquid water path (LWP), near surface wind speed (V) and specific humidity (q).
The SSM/I scans an arc of 1600 km at the earth's surface, containing 64 (128 at 85.5 GHz) individual pixels. The pixel size ranges from 15 (85.5 Ghz) to 69 km (19.35 GHz). The satellite crosses the Baltic Sea twice a day; southward at about 9 am and northward at about 7 pm UTC. Thus, the SSM/I data combine high temporal with relatively low spatial resolution. For the Baltic Sea this is indeed crucial, because all available retrieval algorithms were developed for applications over oceanic surfaces only and therefore are not valid over land surfaces. Since oceanic surfaces in contrast to land and sea ice surfaces represent relatively cold and

homogeneous radiometric backgrounds (in the microwave domain) land as well as sea ice can bias the retrieved fields.

A large number of algorithms are published in the literature, which can be used to determine hydrological parameters from SSM/I observations. Algorithms based on neural networks become more and more interesting, because they are easy to implement, computer cost is relatively low, and their accuracies are in general higher than those of regression algorithms (e.g. Stogryn et al. 1994; Jung et al. 1997).

2 RETRIEVAL ALGORITHMS

Most of the retrieval algorithms which are published in the literature are based upon regression techniques (e.g. Simmer 1994; Karstens et al. 1994). However, since the last five years neural network based algorithms became more and more popular (e.g. Stogryn et al. 1994). Neural networks have several properties that make them attractive to develop retrieval algorithms: First, they are able to detect and approximate multiple, nonlinear correlations without a priori information on the problem under consideration; second, they are able to approximate relationships using only the data presented, i.e. they do not depend on model equations like regression techniques; and finally, once training has been finished they are easy to implement and computer cost is relatively low. Due to the first two facts, neural network based algorithms are more accurate than standard regression algorithms (Jung 1996). We adopted in this study the algorithm of Jung (1996) in order to retrieve the total water vapour content. A case study during the PIDCAP period has shown, that the new liquid water path algorithm from Jung et al. (1997) is able to correctly estimate the overall structure as well as small-scale features like the Norwegian Föhn.

3 LAND AND SEA ICE INFLUENCE

For the removal of the land effects the full orbit geometry of the satellite and the viewing geometry of the radiometer has to be known. The satellite is looking downward in flight direction under 45°, so that the pixels form an ellipse on the earth's surface, which is elongated in view direction. The fast movement of the SSM/I scanner in the scan direction weakens but does not totally cancel this deformation. The 19 GHz pixels, for example, extend 69 km in view and 43 km in scan direction, when the pixel boundary is defined by the half power beam width, which is located where the antenna function has decreased to -3 dB. In order to determine the portion of land within a pixel, the orientation of the ellipse has to be known, which depends on the actual flight direction and scan angle. The former is solely a function of the orbit parameters. Using spherical geometry, the flight direction is given by

$$\frac{dy}{dx} = \frac{\cos \alpha}{\tan (\phi_0 - 90°)} \qquad (1)$$

where α denotes the phase angle and ϕ_0 the inclination angle of the satellite orbit. Taking additionally into account that the pixels precede the foot point of the satellite by 8°, and eliminating the effect that the earth is rotating while the satellite is passing, the flight direction can be calculated for each date. Assuming further that the scan rotation axis of the sensor is directed towards the earth's center, the scan angle may simply be added to the flight direction to obtain the current pixel orientation.

After the exact position and orientation of the footprint ellipses are known a 1/10-degree land-sea mask was applied to determine the portion of land within each individual pixel. In order to quantify the radiative effect of the land-sea distribution within a pixel, the contribution of each area has to be weighted according to the antenna function. All pixels with land influence are rejected from the further process.

The retrieved fields of total water vapour content (TWV) for individual overpasses seemed to be reasonable after the land influence had been removed with the method described above; but monthly averages show that the land influence was not totally removed. The un-removed "warmer" land surfaces produce an increase of the brightness temperatures, which leads to an overestimation of TWV near the coast, resulting in TWV gradients perpendicular to the coastlines (Figure 1). Obviously land surfaces outside the nominal pixel boundary (defined by the half power line), which were not taken into account by this land identification scheme, significantly influence the results.

In order to estimate these effects we assume, that the antenna sensitivity is circularly symmetric and can be approximated by a quadratic function in a semi-logarithmic figure, i.e.,

$$s = s_0 \cdot \exp\left(- a \frac{r^2}{R^2}\right) \qquad (2)$$

where r is the distance to the center of the ellipse, R is the distance of the nominal pixel boundary to the center, and s_0 is the center sensitivity. Since the sensitivity at the pixel boundary is -3 dB, the constant a is equal to ln 2. In order to get the total sensitivity S within the ellipse, Eq.(2) has to be integrated, which gives

$$S = \frac{\pi s_0}{\alpha}\left(1 - \exp\left(- a \frac{r^2}{R^2}\right)\right) \qquad (3)$$

The results show that the sum of all sensitivities inside and outside R are equal. Since brightness temperatures over land are approximately 100 K higher than those over water, land influ ence has to be restricted to about 1 per mille in order to retain an accuracy of 0.1 K. However, the total contribution does not reach 99.9 % for $r < 3R$. Thus, if we accept an error smaller than 0.1 K, all grid points within an ellipse of 200 by 130 km for the 19 GHz channel have to be without any land influence. In the Baltic Sea this condition is nearly nowhere fulfilled; the entire area is more or less influenced by land. A land identification scheme, which rejects all land influenced pixels, is therefore not appropriate. Thus, a different method was developed.

The SSM/I observations for June 1993 were used. It was assumed that the pixel size is 130 by 200 km. The land portion in each of these large pixels was calculated. The relationship between the land portion within a pixel and its corresponding brightness temperature (T) was fitted by a cubic function. This allows to calculate T_0, the brightness temperature of a total water pixel, from the actual brightness temperature, if the relation T/T_0 is assumed to be universal. So the brightness temperatures can be corrected for each land influence and channel. However, this procedure was only used, if land influence was less than 20 %.

The land influence in the retrieved fields is obviously removed using this kind of correction, since the TWV gradients perpendicular to the coast are disappeared (Figure 2).

Similar to land, sea ice, which occurs primarily over the northern part of the Baltic Sea during the winter season, can introduce large systematic errors in the retrieved fields, since sea ice emissivities are significantly higher than those of water. The algorithm from Cavalieri (1992) was adopted in order to identify sea ice. It relies on the observations of the 19 and 37 GHz channels and estimates the sea ice concentration. Cases studies for the first part of May 1993 indicate that the patterns of sea ice in the Baltic Sea were correctly estimated.

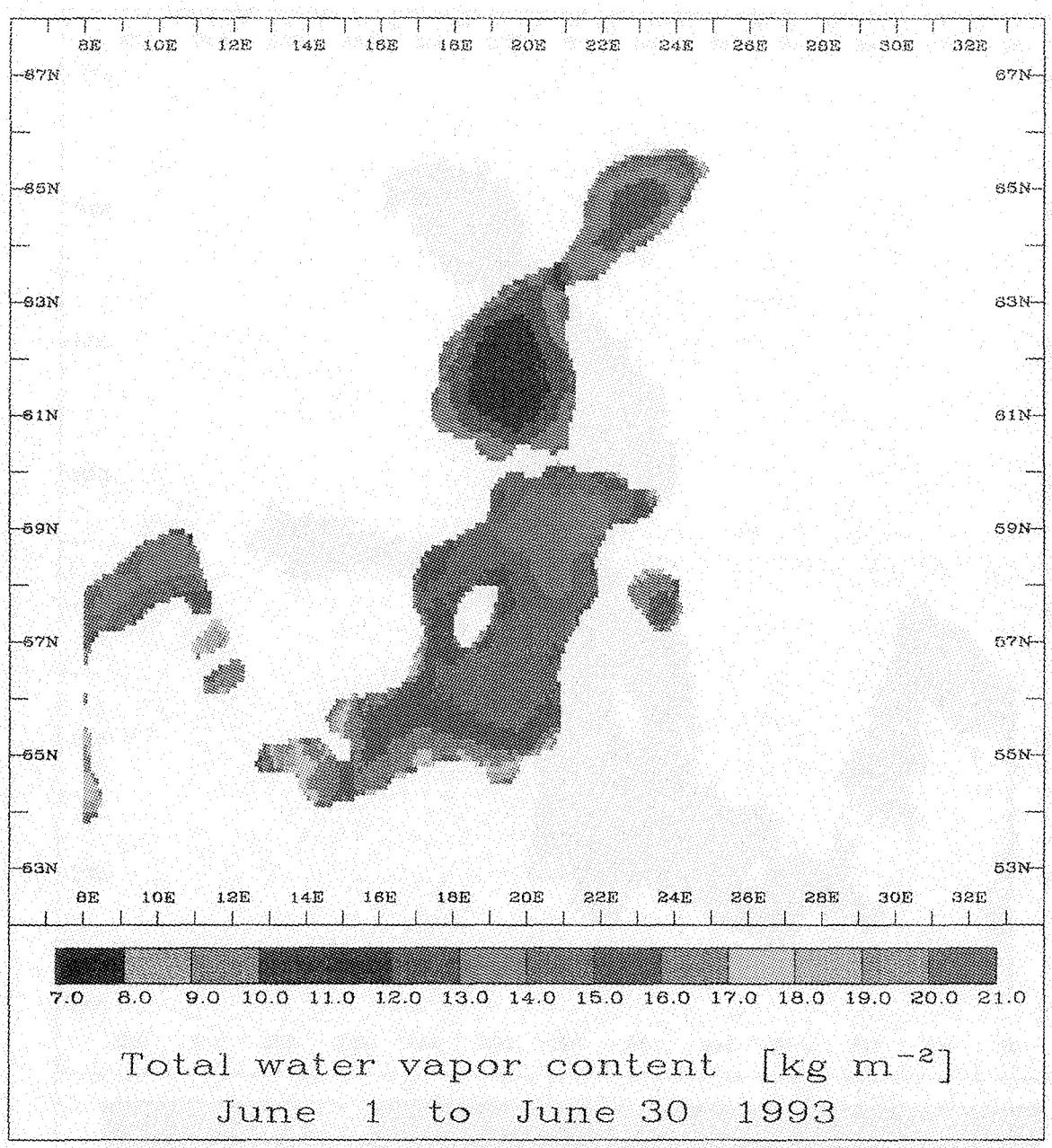

TJ;

Figure 1: Monthly mean total water vapour content for June 1993, estimated with the neural network based algorithm from Jung (1996). Land influences inside the half power beam width are removed.

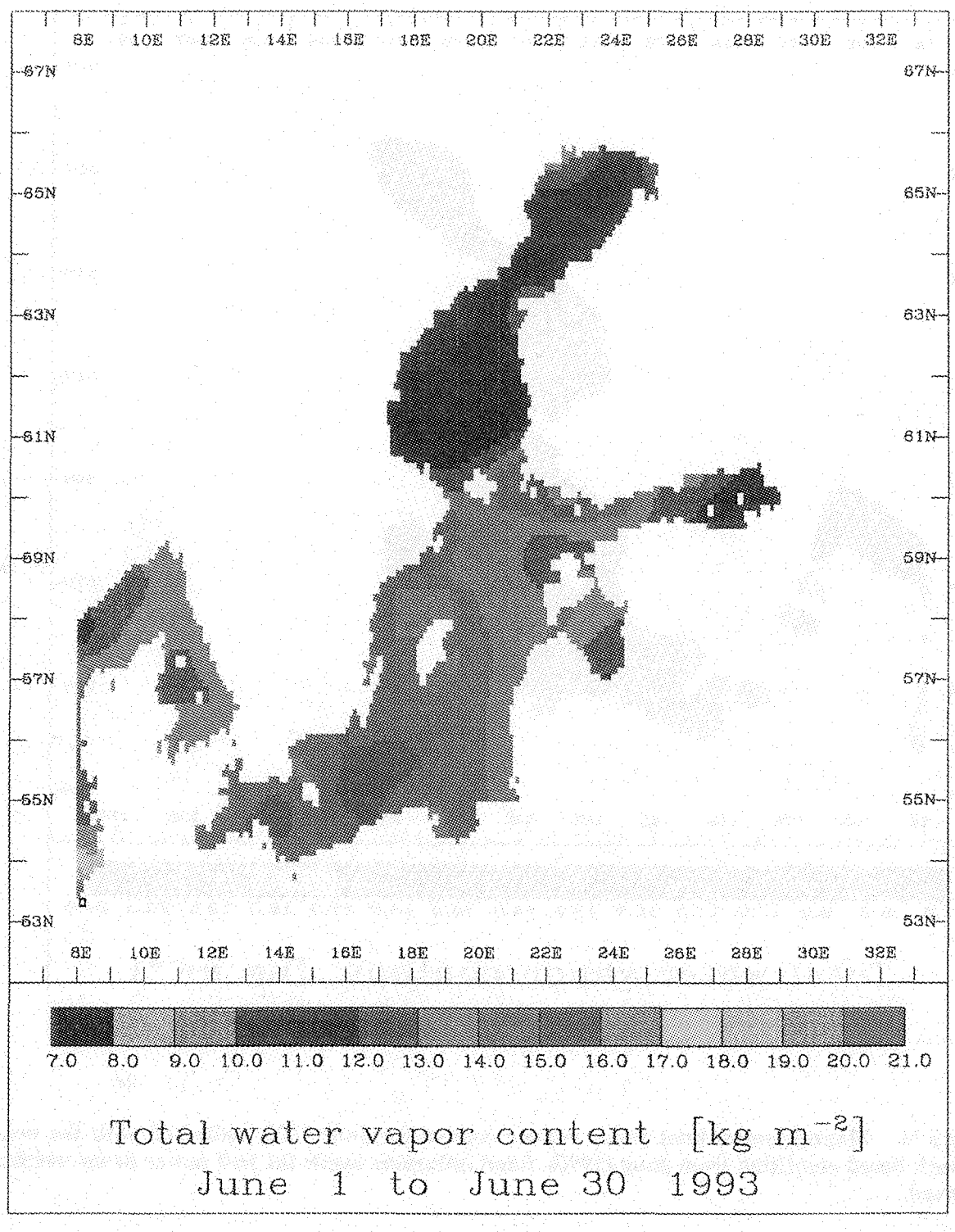

Figure 2: As in Figure 1, but all land influences are removed.

3 CONCLUSION

Neural network based algorithms were (1) used to retrieve hydrological fields over the Baltic Sea, and (2) validated with radiosonde observations during the PIDCAP period. Land and sea ice influences were removed from these fields with satisfying accuracy. However, it was necessary to correct the brightness temperatures even in the middle of the Baltic Sea, because nearly all SSM/I pixels are effected by land influence, at least for the lower frequencies.

RERERENCES

BALTEX, 1995: Baltic Sea Experiment BALTEX Initial Implementation Plan. International BALTEX Secretariat. Pub No.2

Cavalieri, D.J., 1992: NASA Sea Ice Validation Program for the Defense Meteorological Satellite Program Special Sensor Microwave/Imager: Final Report. Technicial Report NASA Technicial Memorandum 104559, Goddard Space Flight Center, Greenbelt, MD.

Hollinger, J.P., R. Lo, G. Poe, R. Savage, and J. Peirce, 1987: Special Sensor Microwave/Imager user's guide. Tech. Rep., Naval Research Laboratory, Washington, D.C., 120 pp.

Jung, T., 1996: Bestimmung des Wasserdampf- und Fluessigwassergehaltes aus simulierten SSM/I-Daten mit Hilfe von neuronalen Netzen. Dipl. degr., Institut für Meereskunde, Kiel.

Jung, T., E. Ruprecht, and F. Wagner, 1997: Determination of Cloud Liquid Water Path Over the Oceans From SSM/I Data Using Neural Networks. submitted to Journal of Applied Meteorology.

Karstens, U., C. Simmer, and E. Ruprecht, 1994: Remote Sensing of Cloud Liquid Water. Meteorology and Atmospheric Physics, **54**: 157-171.

Simmer, C., 1994: Satellitenfernerkundung hydrologischer Parameter der Atmosphäre mit Mikrowellen. Verlag Dr. Kovac, Hamburg.

Stogryn, A.P., C.T. Butler, and T.J. Bartloc, 1994: Ocean surface wind retrievals from special sensor microwave/imager data with neural networks. Journal of Geophysical Research, **99**: 981-984.

Spatial Variability of Surface Radiation Budget Components inferred from Satellite Data

Franz H. Berger[1], Susanne Mecklenburg[1] and Sven Jagdhuhn[2]
[1]Technische Universität Dresden,
[2]Freie Universität Berlin

1 INTRODUCTION

To predict changes in the global climate or to understand all relevant processes governing the hydrological cycle and the energy cycle in the climate system, an improved knowledge about water vapour in the atmosphere is needed [Chahine, 1992]. To observe and characterize the full hydrological cycle, an international programme known as the Global Energy and Water Cylce Experiment (GEWEX) is implemented [WMO, 1990]. This programme itself consists of several components, projects or experiments. One of these regional continental-scale projects is the European contribution, the Baltic Sea Experiment (BALTEX) [Raschke, 1995]. The key objectives are to explore and to model the various mechanisms determining the energy and water budgets of the BALTEX region including the surroundings, to relate these mechanisms to the large-scale circulation systems, and to develop transportable methodologies in order to contribute to basic needs of climate, climate impact, and environmental research.

Thus, one important element is the observation of relevant components describing the energy and water cycle. This is the motivation for the current study, based on satellite data analysis for the BALTEX region. To infer the main important component of the energy budget at surface, the net radiation, NOAA-AVHRR data as well as Meteosat data were analysed. This gives either high spatial resolved or high temporal resolved net radiation fields at surface. Here the general scheme will be presented with results from the NOAA-AVHRR analysis, applied to data in May and June 1993.

2 METHOD AND DATA ANALYSIS

The scheme to infer all surface radiation budget components and the net radiation, separately for NOAA-AVHRR and Meteosat, can be divided into a few main parts: cloud classification, determination of cloud optical properties, and determination of surface fluxes.

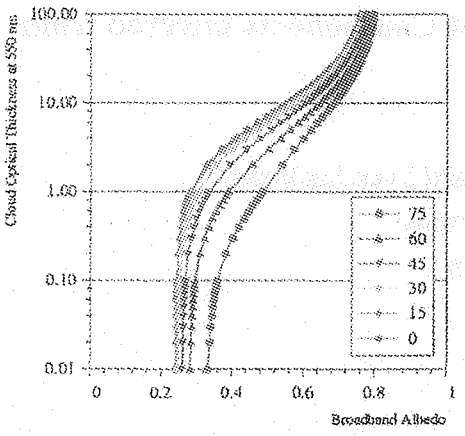

Figure 1: Broadband planetary Albedo related to Cloud Optical Thickness at 550 nm for a high cloud over land (for different solar zenit angles).

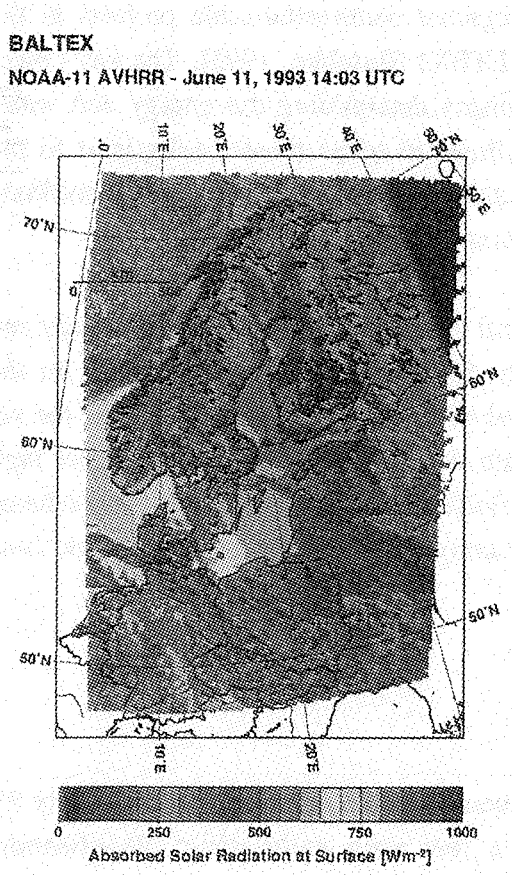

Figure 2: Absorbed Solar Radiation at Surface at June 11, 1993; inferred from NOAA-AVHRR data.

After calibration and transformation into a stereographic map, a detailed cloud classification could be carried out. This cloud classification, comparable for NOAA-AVHRR and Meteosat data, is based on the maximum likelihood method and classifies more than twenty cloud classes. The needed trainings data to define individual cloud classes were determined automatically using reflectances in the solar and emitted fluxes in the terrestrial spectrum [Berger, 1995]. These basic informations are related to different geographical and atmospheric conditions, like a variable tropopause temperature [Oort, 1983]. In a further step, the classified clouds were used to define their microphysical properties and their cloud base heights [Stephens et al., 1984]. The cloud base heights could be defined using synoptical observations. To complete this part of the analysis, a threshold technique could be used to distinguish snow and sunglint from clouds and a second for a land use classification. Both techniques could only be applied to NOAA-AVHRR data, where the results could be used for both. Deriving cloud optical properties and surface radiation budget components from remotely sensed data, additional information about atmospheric conditions are needed. Therefore, synoptical observations were analysed with respect to relative humidity, horizontal visibility near the surface and cloud base height.

In the next two steps, cloud optical thickness and surface radiation budget components were inferred based on an inverse remote sensing technique. It takes into account comprehensive radiative transfer calculations considering mostly all atmospheric and cloudy conditions. For the solution of the radiative transfer a delta-two-stream approximation is used with a 40 layers atmosphere for different

geometrical conditions. Considering the different cloud and surface types, relations between cloud optical thickness and broadband shortwave reflectance at top of atmosphere or shortwave reflectance at top of atmosphere for an individual satellite band could be determined. These results (Figure 1) show that increasing solar zenith angles and/or increasing cloud depths lead to a non-linear increase of shortwave reflectances [Berger et al., 1996].

Using the results from the radiative transfer calculations, further relations (look-up tables) for surface radiation budget components could be established. These look-up tables consider as an additional parameter, the cloud optical depth. For June 11, 1993 the absorbed solar radiation at surface is displayed in Figure 2. Figure 2 shows the result on a reduced spatial resolution (18x18 km^2), which is similiar to the current model resolution of REMO [Karstens et al., 1996]. The net solar radiation includes also the results from the simple landuse classification (typical reflectance characteristics) and shows a reduction of absorbed shortwave radiation below the convective clouds over Poland up to 100 Wm^{-2}, i.e. difference between diffuse and reflected diffuse radiation. It can further be seen that in the clear-sky regions the net solar radiation is about 750 Wm^{-2} (ocean) and about 600 Wm^{-2} for land surfaces. Comparisons of satellite inferred results with ground based observations show reasonable agreement, where in general a slight underestimation of the satellite results can be noticed [Berger et al., 1996; Mecklenburg et al., 1997]. This can be explained due to an underestimation of cloud optical thickness. New estimates using only reflectances in the individual spectral band show that cloud optical thickness (larger than 10) could be more accurately determined. Concerning the longwave components, simple empirical relations could be found for cloudy conditions to modify the clear-sky estimates. The first, very preliminary assumption has assumed that the outgoing longwave radiation at surface below the clouds is the same as for the nearest clear-sky pixel.

The new empirical relationships are based on the decrease of outgoing longwave radiation due to cloud occurrence, cloud optical thickness, and spatial resolution [Mecklenburg et al., 1997, Sedlak, 1996]:

$$M^{\uparrow}_{LW,Cloud} = M^{\uparrow}_{LW,Clear} + f(a + b\delta_{Cloud})\ [Wm^{-2}]$$

where $M^{\uparrow}_{LW,Cloud}$, $M^{\uparrow}_{LW,Clear}$ are the outgoing longwave fluxes for cloudy and clear-sky conditions. f is a geometrical parameter, which considers the surroundings of center pixel depending on cloud type. For low clouds a 5x5 pixel area, for mid-level clouds a 9x9 pixel area and for high clouds a 21x21 pixel area were taken into account. a and b are empirical coefficients to determine the reduction of outgoing fluxes at surface, which depend further on cloud optical thickness δ_{Cloud} at 550 nm. The empirical coefficients are summarized in Table 1.

Table 1: Empirical coefficients to determine the reduction of the outgoing longwave radiation due to clouds.

	a	*b*
Low clouds	-50	-0.12
Mid clouds	-30	-0.40
High clouds	-15	-0.10
Convective Clouds	-15	-1.30

These relations could be applied to compute cloud base temperatures more accurately, depending on their climatological heights.

Thus, the net radiation at surface, the main relevant component of the energy balance, could be computed as the sum of all four components (Figure 3). It can be seen, that there are high energy fluxes over sea surfaces (up to 600 Wm^{-2}) and lower fluxes over land surfaces (up to 450 Wm^{-2}). These differences can be explained by the differences in surface reflectances, which can also be seen in Figure 2. Below clouds the energy flux is reduced up to 50 Wm^{-2}, which corresponds mainly to the net shortwave radiation.

In a further additional step the net radiation at top of atmosphere as well as in different atmospheric levels could be determined. This allows a more detailled description of the energy cycle in this limited area.

3 OUTLOOK

This investigations shows that meteorological satellite data can be used to infer surface radiation budget components, where the accuracies of the inferred results are in the same order of magnitude as ground based observations. Despite the large scatter of cloud properties, and therefore of net radiation, a more detailed information about the spatial variability of the radiation field can be given. In ongoing studies, the surface topography will be included in the computation of surface radiation components. Finally, the temporal variability on an hourly basis and the spatial variability on 18x18 km^2 resolution will be studied in more detail. This will also allow the validation of the model inferred surface net radiation fields.

Acknowledgment: This work was supported by the German Ministry of Education and Research (BMBF) under contract 07 VWK 01-06.

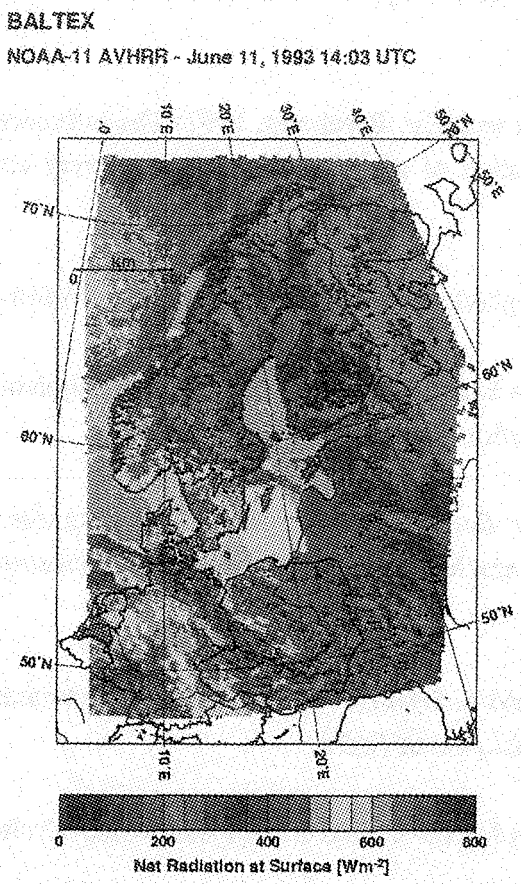

Figure 3: Net Radiation at Surface at June 11, 1993; inferred from NOAA-AVHRR data.

REFERENCES

Berger, F.H., 1995: Inference of climatic efficiency of clouds from satellite measurements. *Int. J. Remote Sensing*, **16**, 2903-2926.

Berger, F.H., S. Jagdhuhn, B. Rockel and R. Stuhlmann, 1996: Radiation Budget Components inferred from NOAA-AVHRR and Meteosat data for the Baltic Sea. in: *IRS'96: Current problems in atmospheric radiation.*

Chahine, M., 1992: The hydrological cycle and its influence on climate. *Nature*, **359**, 373-380.

Karstens, U., R. Nolte-Holube and B. Rockel, 1996: Calculation of the water budget over the Baltic Sea catchment area using the regional forecast model REMO for June 1993. *Tellus*, **48A**, 708-721.

Mecklenburg, S., F.H. Berger and Chr. Bernhofer, 1997: The influence of cloud optical thickness on terrestrial longwave radiation of a spruce forest for different cloud types. *submitted to Z. Meteor.*

Oort, A., 1985: Global atmospheric circulation statistic. *Techn. NOAA-Report*, No. 14.

Raschke, E., 1995: Baltic Sea Experiment (BALTEX) - Initial Implementation Plan, International BALTEX Secretariat, Publication No. 2.

Sedlak, I., 1996: *Studie zur Berücksichtigung von Bewölkungsdaten aus Satellitenbildern in einem eindimensionalen Grenzschichtmodell.* Diplomarbeit, Meteorologisches Institut der Freien Universität Berlin.

Stephens, G., S. Ackerman and E. Smith, 1984: A shortwave parameterization revised to improve cloud absorption. *J. Atmos. Sci.*, **41**, 687-690.

WMO, 1990: Scientific Plan for the Global Energy and Water Cycle Experiment, WMO report No. 376.

Detection and determination of rainfall with the SSM/I over Germany

G. Müller and C. Simmer
Meteorological Institute, Bonn University
D- 53121 Bonn, Germany

ABSTRACT

Precipitation is investigated with Special Sensor Microwave Imager (SSM/I) data over land. These data are correlated with in situ measurements. The algorithm of *Grody* (1991) adapted to the conditions over Germany and an artificial neural network were used for rain detection. We found that for optimized thresholds the scattering indices calculated according to Grody and those obtained with the neural network give similar results. Applying the neural network in a direct manner improves the number of correctly identified rainfall and no rainfall cases considerably. A further improvement was achieved by applying the vegetation index NDVI and its standard deviation as an additional input into the neural network. The in situ measured rain rates can be reproduced from SSM/I data with an uncertainty factor of 2.5 (confidence level of 68 %).

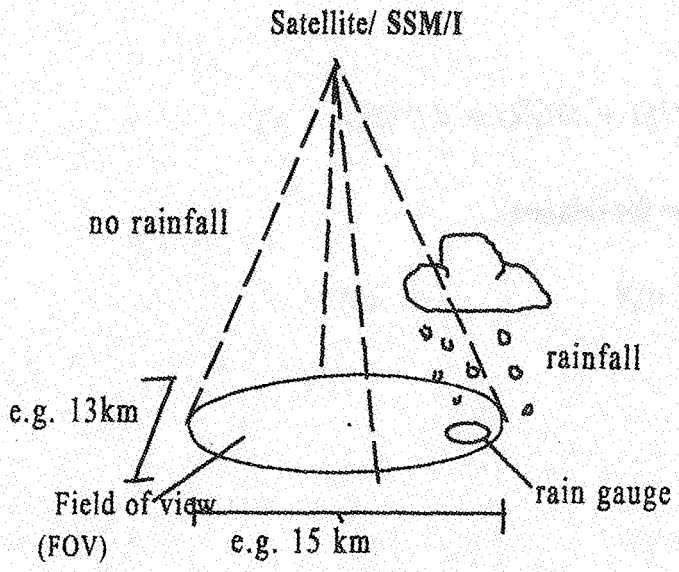

Figure 1: Scheme of the SSM/I measurement.

1 INTRODUCTION

Within BALTEX (Baltic Sea Experiment) soil moisture and rainfall are investigated by the Special Sensor Microwave Imager SSM/I installed on the polarorbit DMSP satellites (Defense Meteorological Satellite Program). Their orbit period is approx. 100 minutes so that together with a swath width of 1400 km most areas in Germany are viewed about twice a day. The emitted radiation intensities are measured at frequencies of 19, 22, 37, and 85 GHz and converted into brightness

temperatures (*Hollinger*, 1987). Over land surfaces the 85 GHz (λ = 3.5 mm) temperature is reduced to a measurable extent by extinction and scattering due to raindrops while the lower frequencies remain largely uneffected. This is the basis of rain detection according to *Grody* (1991). The scheme of the measurements is illustrated in Figure 1. The 3 dB field of view (FOV) for the 85 GHz channel has an almost elliptical area of 15 x 13 km^2.

The SSM/I measurements are correlated with in situ measurements in order to classify the SSM/I measurements into rain and no rain cases. Those cases were selected in which the SSM/I measurements and the in situ measurements were performed simultaneously. Only rain gauges with a high temporal resolution (few minutes) are suitable to ensure simultaneous measurements. The SSM/I and the rain gauge data are from Mai and June 1993. The rain gauge data have been provided by the Deutscher Wetterdienst DWD (75 stations), the Emscher-Lippe-Verband (70 stations) and the University of Bonn (10 stations) (Figure 2). To account for the area average due to the satellite FOV the rain gauge data have been time-averaged over 20 minutes.

2 RAIN DETECTION ACCORDING TO GRODY

A general algorithm for the detection of rain and land surface type based on SSM/I data has been developed by *Grody* (1991). His concept is based on the so-called scattering index *SI*:

$$SI(85) = F - T(85) \qquad (1)$$

with

$$F = T_{cal.}(85) = a + bT(19) + cT(22) + dT^2(22)\,. \qquad (2)$$

The condition for precipitation is fullfilled by the relation:

$$SI \geq TH \text{ with } TH \sim 10K\,. \qquad (3)$$

	orginal coefficients (Grody)	recalculated coefficients (University of Bonn)
a	451.9	603.97
b	-0.44	-0.9274
c	-1.775	-2.4223
d	0.00574	0.007835

Table 1: Coefficients of equation (2).

In Eq. 1 the 85 GHz temperature T(85) represents the value measured in the actual rain or no rain case. The F value represents a 85 GHz temperature assumed in case the measurement is not disturbed by rain. F is calculated by the measured temperatures at 19 and 22 GHz according to Eq. 2. The coefficients are determined by linear regression with no rain cases only. Grody assumes rain under the condition that the scattering index is greater than a certain threshold, e.g. 10 K (Eq. 3). This simple scheme works in cases without desert and snowcover. While Grody used a global data set we determined the coefficients with linear regression for Germany since they are assumed to be dependent on the underlying surface. The results are shown in Table 1. The differences between the two coefficient sets are partially due to the difference in surface types and partially due to an uncertainty of the mathematical formalism which is not significant for the application on a regional scale.

In addition we used the artificial neural network NETS (*Baffes*, 1991) to derive the F value. Neural networks supply an alternative which models the relation between a set of input data and the desired output data without an a priori model function. The comparison between the calculated and the measured T(85) for 677 no rain cases is presented in Figure 3.

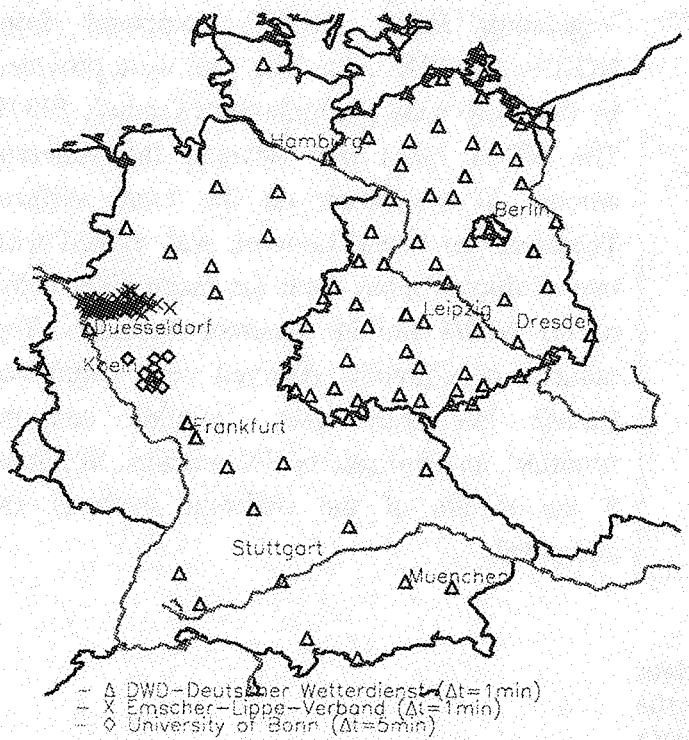

Figure 2: Location of the rain gauges.

To test the Grody algorithm a test data set of 63 'rainfall' and 1354 'no rainfall' data was used. The results are shown in Figure 4 (left). The horizontal axis represents the threshold and the vertical axis the percentage of correctly detected cases for both 'rainfall' and 'no rainfall'. Reducing the threshold increases the number of correctly detected rain cases. Simultaneously, the number of correctly detected 'no rain' cases decreases. With optimal thresholds all three algorithms give results of similar quality. By corresponding choice of the thresholds e.g. 76% of the rainfall cases and 76% of the no rainfall cases can be correctly detected. Obviously, the use of neural networks in the

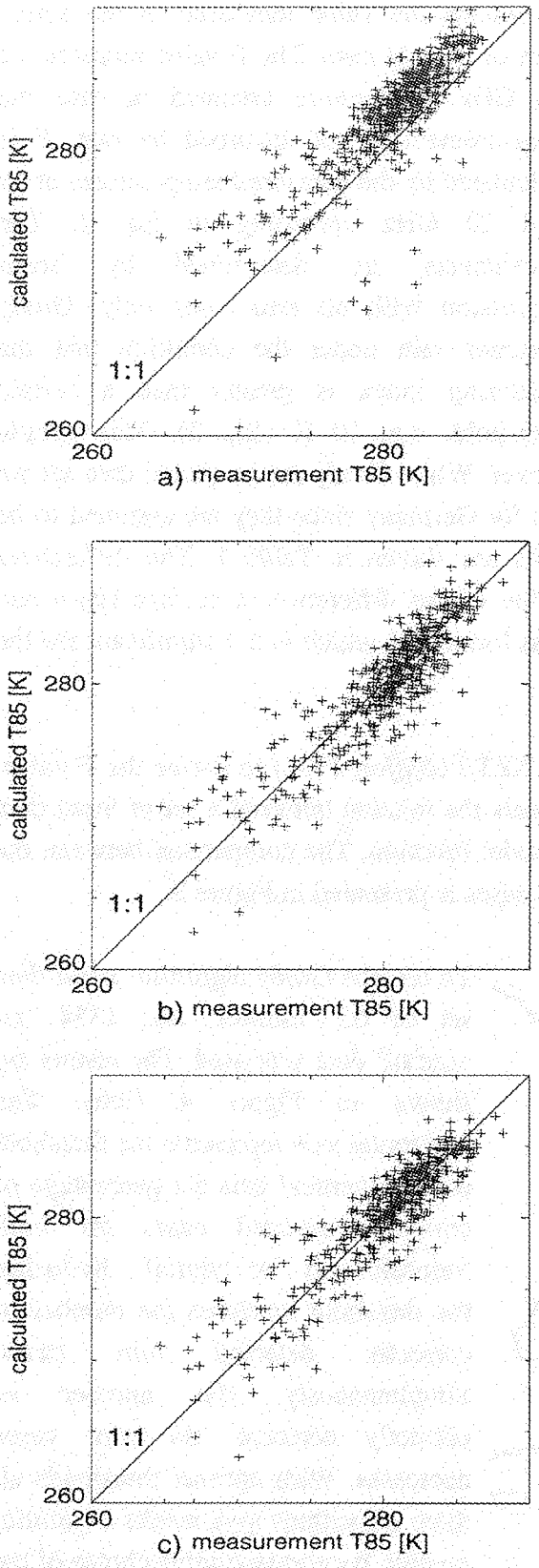

Figure 3: Scatter diagram for the test data set of the calculated F = $T_{cal}(85)$ versus the measured T(85) by means of no rain data with (a) the orginal coefficients, (b) the coefficients recalculated by linear regression and (c) by the neural network for no rain cases.

Grody formalism does not result in an improvement.

3 DIRECT APPLICATION OF NEURAL NETWORKS FOR RAIN DETECTION

We trained the neural network directly in order to predict 'rain' or 'no rain' without relying on the Grody formalism. Input data were the brightness temperatures at 19, 22 and 85 GHz. The demanded output was zero for 'no rainfall' and unity for 'rainfall'. The result for the test data shows that for both rainfall and no rainfall cases approximately 90% were correctly detected.

Apparently, neural networks make a better use of the available information. Since the surface type has substantial influence on microwave radiation temperatures we tested the effect of an independent surface information, the Normalized Vegetation Index (NDVI) computed from NOAA- AVHRR- data. The data were provided by the DLR- Oberpfaffenhofen (*Kramer*, 1997). The NDVI takes into account the different amount of vegetation on the earth surface. Therefore the neural network was trained with two additional input data: the mean pixel value of the NDVI and its standard deviation. The number of correctly detected cases improves further. For both cases, 'rainfall' and no 'rainfall', an error rate of 8% remains. In Figure 5 the results of the different methods are compared.

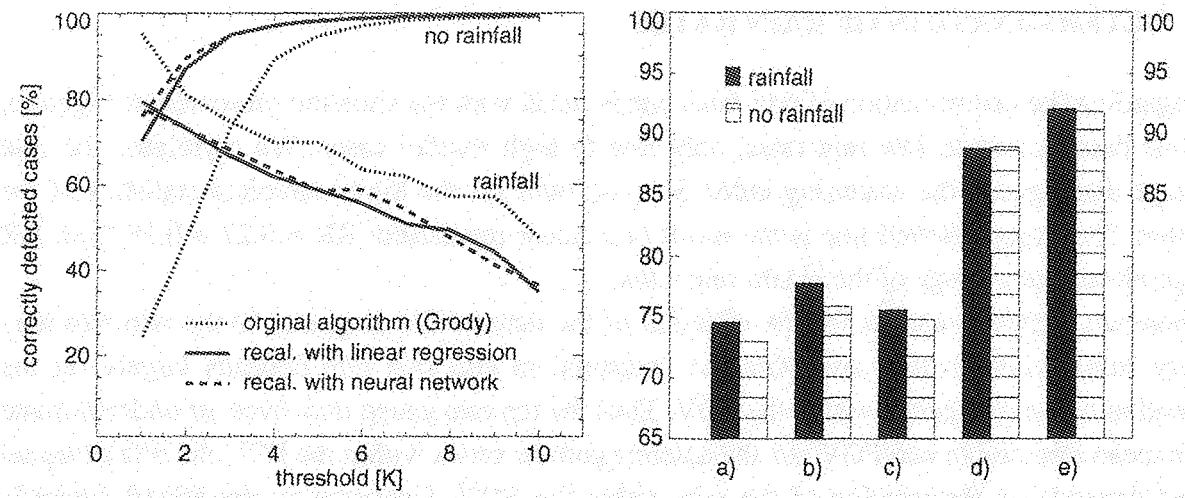

Figure 4: Left: Results for testing the Grody formalism with both a 'rainfall' and a 'no rainfall' data set using the orginal coefficients, the coefficients recalculated by linear regression and by the neural network over Germany.

Figure 5: Comparison of the different methods for rain detection. The first six columns are the result of the Grody algorithm calculated with (a) the orginal coefficients (TH = 3 K), (b) the coefficients recalculated by linear regression (TH = 1 K) and (c) by the neural network (TH = 1.5 K). The last four columns are the result of applying the neural network in a direct manner with (d) the brightness temperatures as input data and (e) additionally with the mean pixel value of the NDVI and its standard deviation.

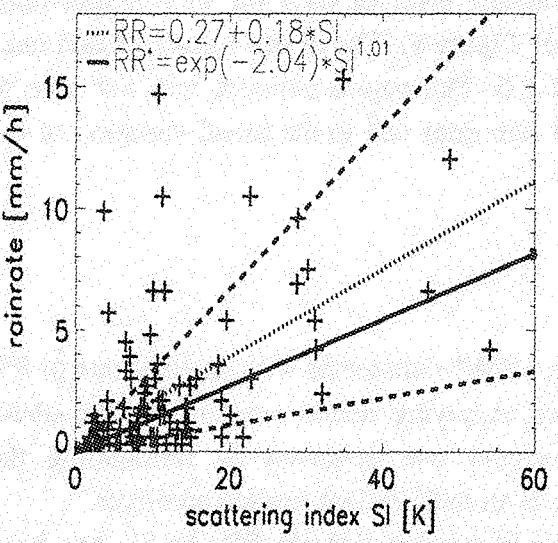

Figure 6: Scatter diagram of the in situ rain rates RR versus the scattering index SI.

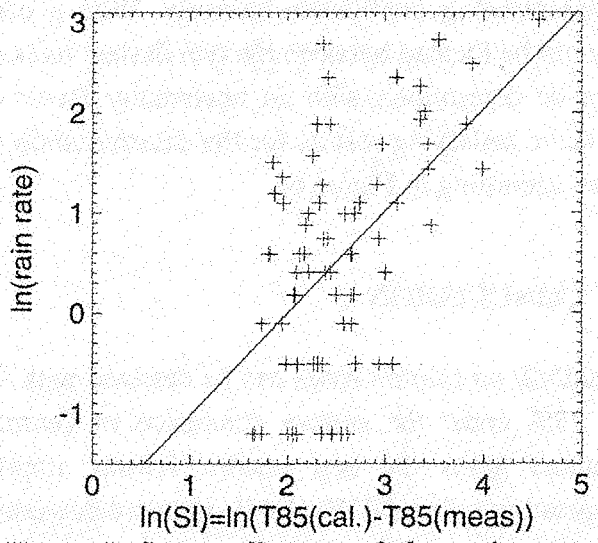

Figure 7: Scatter diagram of the rain rates logarithms of the (ln RR) versus the logarithms of the scattering index (ln SI). The line is the sult of a linear regression on the level of logarithms (ln RR* = -2.04 + 1.01* ln SI).

4 DETERMINATION OF RAIN RATES

Regarding the determination of rain rates one is faced with the situation presented in Figure 6. Most data pertain to low rain rates, only few to high rainfall cases. We correlated the rain gauge data against the scattering index SI to account for the lower sampling statistics of the latter. The straight dotted line is the result of a linear regression: RR = 0.27 + 0.18 * SI. RR reproduces the average of the in situ rain rates.

There are different reasons for the variation of the data in this diagram. As the rain rate may vary substantially within one FOV the measured in situ rain rate depends largely on the location of the rain gauge within the FOV. Thus the the rain gauge may over- or underestimate the mean rain rate in one FOV. As the antenna pattern varies within the FOV the SSM/I signal also depends on the location of the rain within the FOV. Furthermore, the SSM/I signal is influenced by varying diameters of rain drops and by ice particles in the clouds. Finally the geographical position of the FOV is uncertain by 5 to 15 km.

The linear regression in Figure 6 misses the condition that the differences between the data and the regression line should be independent along the line. This should be true especially when comparing data above and below the line. The solution could be a weighted regression. As an alternative we considered the situation on the level of logarithms: the logarithm of the scattering index and the logarithm of the rain rate. For the scattering index SI $\geq$ 5 K (ln SI $\geq$ 1.6 K resp.) the situation is represented in Figure 7. The line gives the result of the linear regression with the logarithmically transformed data (ln RR* = -2.04 + 1.01* ln SI). Around the regression line the differences are quite reasonably Gaussian distributed (Figure 8). On the basis of this Gaussian distribution it is possible to determine the uncertainty factors with corresponding confidence intervals. With a confidence level of 68% the in situ rain rates should be located between the two dashed lines (see Figure 6). The in situ measured rain rates can be determined with an uncertainty factor of 2.5. The neural network was not able to achieve satisfying results for the determination of rain rates due to the broad variation of the data according to Figure 6.

5 CONCLUSION

Rainfall/ no rainfall cases can be detected with the SSM/I radiometer with an error rate of 8% to 23% under the surface conditions of Germany. Applying neural networks in the direct manner gives the best results. Further improvement was achieved by introducing the vegetation index NDVI and its standard deviation as an independent surface qualifyer.

The variation of the in situ rain rates around the regression line (ln RR, ln SI) has been quantified by an uncertainty factor of 2.5 (confidence level of 68%) within a Gaussian distribution on the level of logarithms.

The results should be further valdidated on the basis of a greater amount of data e.g. other seasons and years.

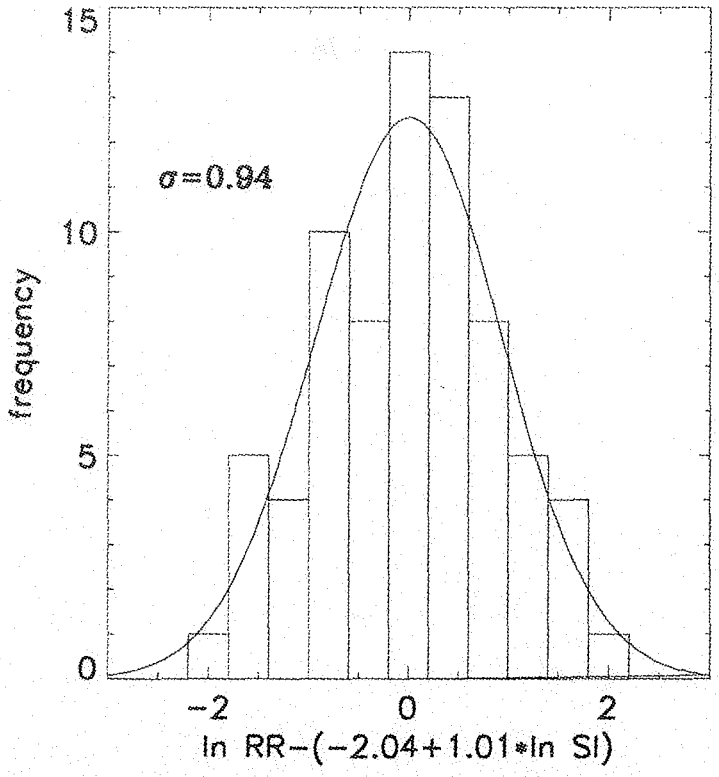

Figure 8: Histogram of the differences between the measured rain rates and the recalculated rain rates on the level of logarithms.

Acknowledgement

We wish to thank the Deutscher Wetterdienst and the Emscher- Lippe- Verband for providing the rain gauge data and the DLR for providing the vegetation index data.

References

Baffes, P.T., R.O. Shelton, R.O & T.A. Phillips, (1991): NETS User's Guide, NASA Johnson Space Flight Center, 103pp. [Available from COSMIC, University of Georgia, 382 East Broad ST., Athens, GA30602.]

Grody, N.C. (1991): Classification of snowcover and precipitation using the special sensor microwave imager, J. Geophys. Res. vol. 96, D4, pp.7423- 7435

Hollinger, J., R. Lo, G. Poe, R. Savage, & J. Pierce, (1987): Special Sensor Microwave/Imager User's Guide, Naval Res. Lab., Washington, DC

Kramer, J.H. (1997): DFD Product Guide, German Remote Sensing DATA Center (DFD), DLR D- 82234 Oberpfaffenhofen

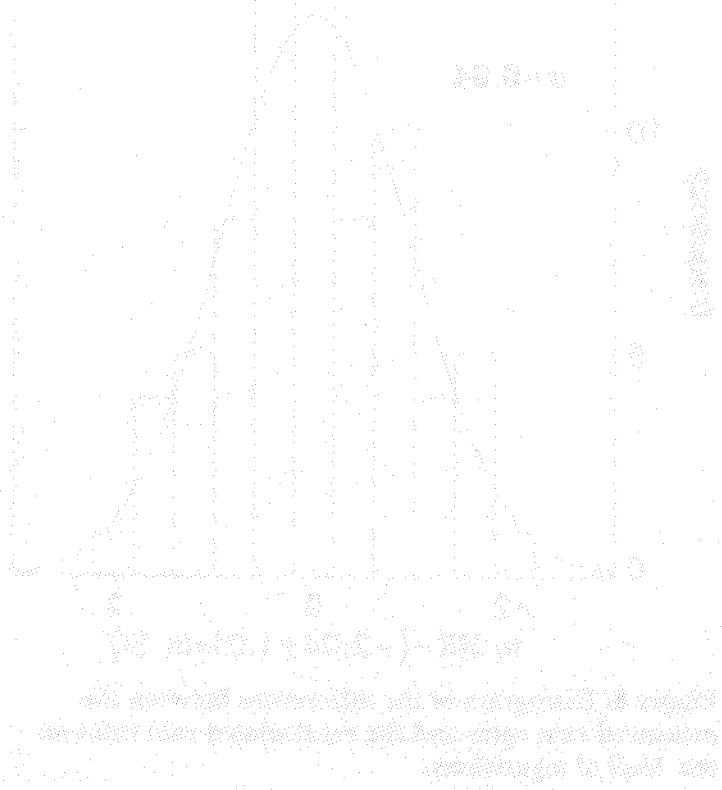

Soil moisture retrieval with SSM/I overvegetated areas in Central Europe

M. Drusch and C. Simmer
Meteorological Institute, Bonn University
D- 53121 Bonn, Germany

ABSTRACT

The antecedent precipitation index (API) is calculated for the German area, using REMO (REgional MOdel) predictions and measured precipitation. This soil moisture index is scaled up to SSM/I (Special Sensor Microwave/ Imager) footprint size taking the nonlinear antenna pattern into account. Comparisons with measured SSM/I 19 GHz polarisation ratios were performed for 10 climatological stations. Time series at nine stations show the expected positive correlations, in five cases the correlation coefficients are in the range of .59 to .75. Dense vegetation cover attenuates the soil moisture signal and inhomogeneities in surface parameters have a strong influence on the polarisation ratios due to the non-linear relationship between brightness temperatures and geophysical parameters. These effects might be responsible for the large deviations in some cases.

1 INTRODUCTION

Several studies have shown that surface soil moisture is one of the most important parameters in many hydrological and meteorological applications. On the one hand it effects the hydrological cycle in the soil and is the limiting factor for plant growth in large areas of the world. On the other hand latent and sensible heat flux between the land surface and the atmosphere strongly depend on this parameter. Therefore the knowledge about the spatial distribution of surface soil moisture on large scales is of high interest [8], [10], [2]. Since in situ measurements are always point measurements available for small areas only, remote sensing methods have been developed to infer soil moisture from satellite-borne radiometers to obtain large area coverage. Generally low frequency microwaves are most suited, since they are related directly to surface soil moisture and less to atmospheric parameters [11]. Aircraft measurements with passive microwaves at L-band show a strong linear relationship between polarisation ratio and soil moisture even for rough and vegetated soils [6]. The low spatial resolution and technical problems prevented the operational use on satellite plattforms so far. With increasing frequency the influence of the vegetation cover and its water content increases too. However, SSM/I measurements with almost global, daily coverage provide a unique potential data set for the last ten years.

2 API CALCULATION

For most hydrological applications mesurements or ground truth data are not available, especially if larger scales and/or long time periods are concerned. Saxton and Lenz [9] determined a daily soil moisture index, the API, using the rainfall from the previous day (j - 1) and a recession factor K:

$$API_j = (API_{j-1} + RR_{j-1}) * K_{j-1} \qquad (1)$$

K depends on the potential evaporation E_{pot} soil depth Z, and plant available field capacity $(\theta_{fc} - \theta_{wp})$ and describes the decrease of soil moisture with time:

$$K_j = \exp\left(-\frac{E_{pot_j}}{Z(\theta_{fc} - \theta_{wp})}\right)$$

It must be noted that complex physical processes like infiltration, runoff, or interception are negleted when we use this index. However, it is not possible to quantify these parameters for large scales.

The potential evapotranspiration was calculated using the Penman equation described in [1]. The atmospheric parameters were obtained from REMO predictions at a spatial resolution of 17 km. Soil properties were taken from the climatological data set defined in the soil module of REMO at the same resolution.

Averaging daily sums of rainfall, measured at 8000 rain gages from the German Weather Service, the API was calculated for May and June 1993 for the area of Germany at the REMO grid resolution.

The API values calculated for the first half of May are not reliable since we do not know the initial API for April 30th.

3 SCALING UP TO SSM/I FOOTPRINT SIZE

The effective field of view, or 3dB resolution, of SSM/I depends on the wavelength. For the 19 GHZ channel, which is most sensitive to surface soil moisture, the EFOV (Effective Field Of View)-footprint has an elliptical shape with 69 and 43 km semi-axis. The actual ground resolution is about three times larger, since the area inside the -3dB footprint includes only 50 %

of the area monitored by the SSM/I measurement. Since the vegetation and soil properties show a high degree of variability in the study area, the measured 19 GHz signal is a composite of radiation emitted from several homogeneous patches. Since the relation between the surface parameters and the brightness temperature is generally non-linear, scaling up to area weighted averages will lead to errors [7]. The second non-linear process in the up-scaling procedure is the antenna gain function of the SSM/I radiometer. To take into account the antenna pattern we used a Gaussian function for the up-scaling of API to SSM/I pixel size. Calculating the exact location and shape of each footprint we obtained weights for each 17 km element within the ground resolution area.

4 RESULTS

Calculations with radiative transfer models have shown that optical thick clouds and rain can have a strong influence on microwave measurements at frequencies exceeding 10 GHz [3]. To separate rain events we adjusted a screening algorithm developed by Groody to the BALTEX area [5]. Moreover, measurements from up to four DMSP F10 and F11 overpasses were averaged to minimize atmospheric effects and to obtain daily means.
For comparisons between the up-scaled API and SSM/I measurements the normalized PR (polarization ratio) at 19 GHz was calculated. This parameter is less sensitive to the surface temperature than the actual brightness temperature.

However, the measurements are still influenced by various soil and vegetation parameters, e.g. roughness, plant water content or vegetation cover. To keep the distribution of these variables within the footprints constant, we examined time series of Mai and June 1993 at 10 fixed locations. Only footprints with distance less than 10 km between the climatological station and the footprint center were used for the comparisons.

For the period from 16th of May to the end of June we obtain correlation coefficients between .59 and .75 at five stations (Fig.1). At four stations the timeseries show the expected shape with a decrease in PR when the soil dries up. The low correlations at Bocholt and Würzburg are related to the second half of June. An increase in surface soil moisture can not be found in the PR time series. Whether this is due to an increase in vegetation water content, which attenuates the soil moisture signal, must be examined in the future. For the period prior to these events correlation coefficients of .66 (Bocholt) and .63 are obtained.

Examining the PRs, we find a negative trend in the time series from May to June, which can be related to an increase in vegetation water content and cover. NOAA NDVI (Normalized Difference Vegetation Index) scenes for this period confirm this interpretation.

In order to investigate the uncertainties related to the non-linear effects of the surface properties in the radiative transfer the NDVI was scaled up as described in section 3. The mean values and the standard deviations were calculated for both, the NDVI and the API. Separating SSM/I measurements connected to low standard deviations in NDVI and API, e.g. homogeneous distributed surface parameters, correlations of .6 for PR and the API were found, independent of their geographical locations. On the other hand the whole ensemble is described by a correlation coefficient of .2.

This study outlines that a correlation of .6 to .7 seems to be a maximum value for surface soil moisture retrievals with SSM/I measurements in vegetated areas. Inhomogeneities in surface parameters and vegetation layers with NDVI values exceeding 0.4 attenuate the surface soil moisture signal to correlations of .2 or less. However, it should be noted, that the API describes the soil moisture in a 20 cm deep layer, whereas the penetration depth of 19 Ghz microwaves is in the order of 1cm. A more detailed surface soil moisture scheme [4] will probably enhance the correlation under certain conditions.

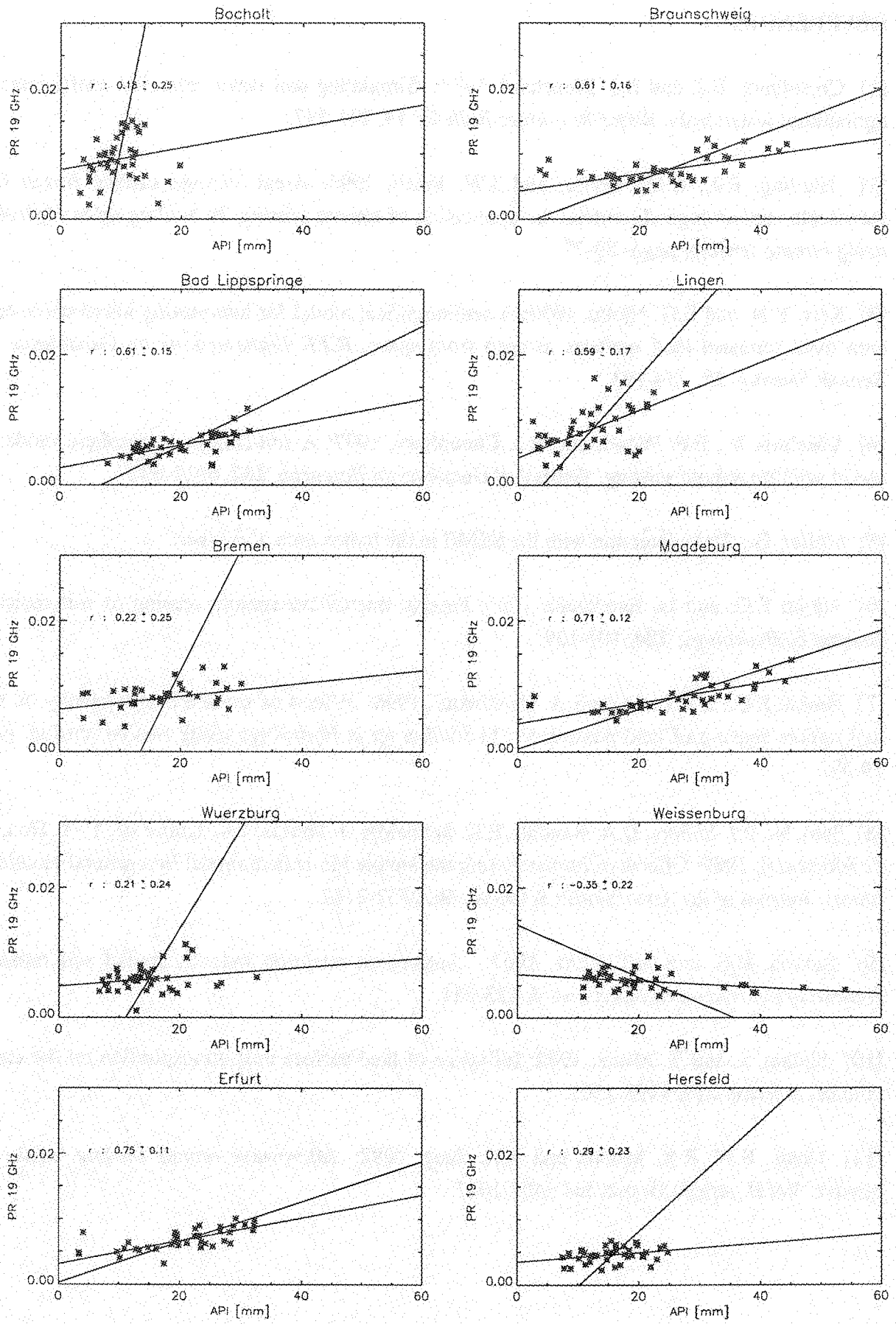

Figure 1: API vs. PR for the period from 16.5.93 to 30.6.93

REFERENCES

[1] Choudhury, B.J. and B.J. Blanchard, 1983: Simulating soil water recession coefficients for agricultural watersheds. *Water Resources Bulletin,* **19**, 241-247.

[2] Harding, R.J., C.M. Taylor, and J.W. Finch, 1996: Areal average surface fluxes from mesoscale meteorological models: the application of remote sensing. In *Scaling up in Hydrology using remote sensing,* pages 59-77.

[3] Kerr, Y.H. and E.G. Njoku, 1990: A semiempirical model for interpreting micro-wave emission from semiarid land surfaces as seen from space. *IEEE Trans-actions on Geoscience and Remote Sensing,* **28**, 384-393.

[4] Lakshmi, V., E.F. Wood, and B.J. Choudhury, 1997: A soil-canopy-atmosphere model for use in satellite remote sensing. *Journal of Geophysical Research,* **102**, 6911-6927.

[5] Müller, G.: Rain detection with the SSM/I in the baltex area. *this issue.*

[6] Njoku E.G. and D. Entekhabi, 1996: Passive microwave remote sensing of soil moisture. *Journal of Hydrology,* **184**, 101-129.

[7] Njoku, E.G., S.J. Hook, and A. Chehbouni, 1996: Effects of surface hetero-geneity on thermal remote sensing of land parameters. In *Scaling up in Hydrology using remote sensing,* pages 19-39.

[8] Sato, N., P.J. Sellers, D.A. Randall, E.K. Schneider, J. Shukla, J.K. Kinter III, Y.-T. Hou, and E. Albertazzi, 1989: Effects of implementing the simple bio-sphere model in a general circulation model. *Journal of the Atmospheric Sciences,* **46**, 2757-2782.

[9] Saxton, K.E. and A.T. Lenz, 1967: Antecedent retention indexes predict soil moisture. *Journal of the Hydraulics Division,* **4**, 223-241.

[10] Shukla, J. and Y. Mintz, 1982: Influence of land-surface evapotranspiration on the earth's climate. *Science,* **215**, 1498-1501.

[11] Ulaby, F.W. R.K. Moore, and A.K. Fung, 1982: *Microwave remote sensing: active and passive. Vol II.* Artech House, Inc., 457-1047.

DEVELOPMENT AND VALIDATION OF NEW SSM/I-ALGORITHMS FOR THE RETRIEVAL OF VERTICALLY INTEGRADED CLOUD LIQUID WATER OVER THE BALTIC SEA

Holger Gäng
Institut für Meereskunde der Universität Kiel
Duesternbrooker Weg 20, D-24105 Kiel, Germany

ABSTRACT

New algorithms for the estimation of the vertically integrated cloud liquid water (liquid water path, LWP) from data of the SSM/I-radiometer were developed. This new approach was derived from a database method, applied on the principal components of a wide set of brightness temperatures, calculated from measured atmospheric profiles using different combinations of radiative transfer models with ocean surface reflectivity estimations. The resulting algorithms are compared with some older commonly used LWP algorithms and with a new neural network estimation method.

Compared with the older retrieval schemes a much higher potential of accuracy regarding the RMS error of the retrieved LWP is stated, whereas the comparison with the neural network gives errors of the same order. Validation with ship borne radiometric data during the PIDCAP period of the BALTEX project in 1995 and a measuring campaign during summer 1996 shows the improvement of accuracy by a factor of 3 when thin clouds are present. High values of LWP are difficult to validate, because deviations in estimating the ground truth data are hiding the systematic errors of the SSM/I algorithms. During rainy conditions all algorithms do underestimate more or less the amount of cloud liquid water.

1 MOTIVATION

The presence of clouds as part of the hydrologic cycle plays a important role for the global atmospheric and oceanic energy budget. Correct modelling of the cloud characteristics like the liquid water path (LWP) should improve the accuracy of climate sensitivity studies and also the quality of numerical weather prediction models, like REMO for the Baltic Sea region, that is supported by the GKSS. A strong disadvantage of handling cloud properties is the unaccuracy of the validation on a larger scale, that means, that the retrieval methods of the LWP, that should provide the average cloud liquid on an area with typical dimensions in order of the model grids are very unaccurate at present. Today the best methods of measuring the liquid water amount are microwave remote sensing methods [14], applied over sea regions. This was done mainly by the

SSMR sensor (1978 - 1987) and since 1987 by the SSM/I sensors on board of the DMSP (Defense meteorological program) satellites.

Typical errors for lower LWPs in terms of bias and random deviation are 50 - 100 g/m^2, that is much compared with the mean global LWP of about 100 g/m^2.

The algorithms, that use statistical information about real atmospheric conditions like [7], [2], [1] often provide better results, than the physically based retrieval schemes, that perform a simplification of the radiative transfer model [4], [10], [12], or use a strong limitation of the variability concerning the atmospheric profiles. The latter is done by most of the iteration schemes with a least square approximation like [3], [16].

The ground truth validation of existing algorithms is very difficult, caused by the great problems to estimate the true data concerning the cloud liquid water.

This was done only in certain regions with stratiform and homogenous clouds, accepting ground based radiometric data as true values [17] and thus there is a great necessity to validate LWP algorithms in other than subtropical subsidence regions.

The aim of this study is therefore defined to develop new algorithms, using a database method and to validate existing retrieval schemes together with the new algorithms with data, sampled over the Baltic Sea.

2 ALGORITHM DEVELOPMENT METHOD

Combining the advantages of the statistical methods and the physical approaches led to the decision to use a semi-statistical background for the development of LWP algorithms like in [7]. The main input dataset consists of an ensemble of 11000 radiosonde ascents with vertical profile data, sampled over globally distributed ocean regions. From every profile the 7 brightness temperatures TB_i, that should be seen by a SSM/I sensor are calculated by the use of the radiative transfer model "MWMOD" [14], briefly described below in section 4. It is assumed, that the atmosphere doesn't contain raindrops, restricting the resulting algorithms to non rainy conditions. Note, that the LWP value of a certain profile not necessarily represents the unknown actual amount of liquid water, but rather gives a physically meaningful solution of liquid water content (LWC) distribution with a resulting LWP. It is only important, that this solution is not too far away from the real but unknown state, ensuring a correct statistic behavior of the data set.

The resulting dataset consists now of LWP values on the one side and values of the TB_i on the other side.

The aim to minimize the regression errors suggested to choose a data base method, that relates every possible set of TB_i to a certain value of LWP. With respect to the strong correlation of the TB_i, an analysis of the empirical orthogonal functions (EOF) concerning the TBs was performed.

After performing the EOF analysis, the principal components ETB_i instead of the TB_i are used building up the data base. The maximum and minimum values $MAX(ETB_i)$, $MIN(ETB_i)$ for every dimension i of the whole dataset define 7 ranges and are building a cube of 7 dimensions within the space of the ETB_i, if the maximum order number is used. Now a regular grid must be defined within this cube, and all LWP values can be interpolated on this array after adding a gaussian distributed random error to all ETB_i independently.

When applying this database array to estimate the LWP for a given set of TB_i, the ETB_i must be calculated, and after this the desired LWP is found by multilinear interpolation between the LWP values of the next grid neighbours. The number of neighbours is 2^d, with d meaning the number of used dimensions (order of EOFs) within the array of ETB_i.

3 RADIATIVE TRANSFER MODEL "MWMOD"

This RTM calculates the emitted microwave radiation at the top of the atmosphere as seen by the SSM/I with an incident angle of 53.0° [14].

The atmospheric absorption due to the oxygen line complex at 50 GHz, the strong water vapour line at 22.35 GHz and the water vapour continuum absorption is calculated by use of Liebes model "MPM89" or "MPM93" [8][9], dividing the atmosphere into 45 layers with homogenous properties. The layers are assumed to be horizontally infinite, classifying this RTM as a 1-dimensional model. The treatment of scattering at the cloud droplets is done by the method of succesive order of scattering.

Due to the assumption of not rainy conditions and no ice crystals beeing present, the scattered radiation is computed by the use of the rayleigh approximation. The cloud droplets are introduced into the atmosphere following the modified adiabatic method. The main feature of this is, that clouds are assumed to be present at relative humidities RH > 93 %, having a liquid water content LWC that increases with height assuming adiabatic behaviour [7]. Additionally entrainment takes place, that tends to decrease again the LWC at higher levels obove the cloud base. The microwave emission and reflection at the ocean surface is a big disadvantage for SSM/I methods, because the behavior of the sea surface is not exactly known, but has a great effect on the SSM/I TBs. The microwave properties are modelled, using one of two parameterisation schemes. The first model is that of Hollinger [5] with the estimation of foam coverage from Stogryn [6], the

second one is a 3-scale model with limited fetch, according to the not fully developed waves in the Baltic Sea [13], dividing the rough surface into facettes and treating the short and long waves separately (1st and 2nd scale). The parameterisation of foam coverage and whitecaps, defining the 3rd scale, is done according to Monahan and O'Muircheartaigh [11].

4 SSM/I ALGORITHMS FOR COMPARISON

The following comparison study is performed using always the same set of published algorithms together with the new lookup table models. The choosen algorithms are listed below. (Abbreviation used: e.g. '22v' means 22 Ghz, vertically polarized; 'h' means horizontally polarized.)

- Semistatistical algorithm following Karstens, 22v,37v, denoted as "KAR" [7]
- Physical algorithm following Petty, 19v,19h,22v,37v,37h, denoted as "PET" [12]
- Statistical algorithm following Alishouse, 19v,19h,22v,37v,37h, 85h, denoted as "ALI" [1]
- Semistatistical algorithm following Bauer, 19v,19h,22v,37v,37h, 85v,85h, denoted as "BAU" [2]
- Semistatistical algorithm using neural network technique following Jung, 19v,19h,22v,37v,37h,85h, denoted as "JUN" [18]
- Lookup table algorithm, 19v,19h,22v,37v,37h, 85v,85h, atmospheric model "MPM89" from Liebe, ocean surface model from Hollinger and from Stogryn, denoted as "IFM 1"
- Lookup table algorithm, 19v,19h,22v,37v,37h, 85v,85h, atmospheric model "MPM93" from Liebe, ocean surface model from Hollinger with foam parameterisation from Stogryn, denoted as "IFM 2"
- Lookup table algorithm, 19v,19h,22v,37v,37h, 85v,85h, atmospheric model "MPM89" from Liebe, ocean surface model from Schrader with foam parameterisation from Monahan and O'Muircheartaigh, denoted as "IFM 3"6 SSM/I dataset of validated situations over the Baltic Sea.

During the summer of 1995 and 1996 two ship cruises with the German research vessel "ALKOR" took place. The goal was to validate SSM/I LWP algorithms with a upward looking

microwave radiometer on board of the ship. The radiometer was able to receive on 3 separate channels with the frequencies 21.3, 23.8, 31.7 GHz. Using tip curve calibration procedures the LWP could be measured very stable with different two-channel algorithms or also with the use of the here described lookup table method. Tests of the different algorithms for the ground based radiometer showed, that all algorithms do not differ very much at higher LWP values, but that the lookup table method gives the best results for low values or LWP=0. Based on comparisons of the calculated TBs from additively released radiosondes using the RTM "MWMOD" with measured Tbs the model from Liebe "MPM89" was found to be the best for this frequencies. Therefore, all ground truth LWPs are that of the lookup table method with Liebe's model "MPM89".

The main problem is the statistical error when estimating the mean LWP of an area, comparable with the SSM/I footprint, because the radiometer was held at a fixed position of 37° elevation angle and therefore is only able to scan a small stripe within this area.

The ground truth was calculated by averaging the ship radiometer LWP values from 30 minutes before to 30 minutes after SSM/I overpassing time. The corresponding SSM/I TBs must be modified due to the land influence, because most of the sea area has a minimum coastal distance in the order of the half width of the footprint. The antenna pattern function was digitized and the fraction of land A_l seen by the SSM/I was calculated according to the pixel center position and frequency of the channel. Now the unknown brightness temperature, assumed 100 % sea coverage TBs, can be calculated from the equation

$$TB = (1-A_l)*TBs + A_l*TB_l. \qquad (1)$$

The brightness temperature over land was set to TB_l = 270 K. The TBs of an SSM/I overpass were taken within the dataset only if the distance between pixel center and ship position during the overpassing time was not greater than 20 km, according roughly to the size of footprint.

5 RESULTS FROM BALTIC SEA DATASET

The choosen set of algorithms was used to derive the LWP, as seen from the SSM/I, according to the dataset, sampled over the Baltic Sea during 1995 and 1996 (section 5). The results are shown in Figures 1 to 8. The solid line marks the function of an ideal algorithm with a slope of 1. Both dashed lines are the regression functions for regression y(x) and x(y). The line with the lower slope, denoted as r1, means the regression y(x), treating the x data as true, the more steep line (slope r2) corresponds to the regression x(y), treating y data as true. Both lines are crossing each other in the statistical center of the scatterplot. The correlation coefficient c is also given within the pictures.

For all algorithms the RMS error is within the range 240 to 300 g/m^2 and they show a linear best fit y(x) within the range 0.28 for the "IFM 3" algorithm (Figure 8) to 0.46 for the "PET" formulation (Figure 2).

The regression x(y), treating the y data as free of error, leads to regression coefficients between 0.75^{-1} for "ALI" in Figure 3 and 1.17^{-1} for "BAU" in Figure 4.

This means, that the slope of the true linear function LWP_ssmi(LWP_ship) is less than unity for all algorithms, namely the geometric average of r1 and r2, if the error estimate of the ship radiometer data and the SSM/I data are assumed approximately as equal. The underestimation during strong cloud coverage of all algorithms is found to be dependent from rainrate. As an example Figure 9 displays the differrence of Karstens algorithm "KAR" to the LWP value derived by the ship radiometer over the rainrate, measured by ship rain gauge.

It is seen, that for moderate rainrates of 1 to 1.5 mm/h the algorithm "KAR" underestimates the LWP by about 1000 g/m^2. The other algorithms, including the new database types, show also this behaviour. It is assumed that the reason is, that all algorithms used here are developed without consideration of the special effects produced by the presence of raindrops. The main effect is, that due to the larger size of the raindrops a greater portion of the emitted or reflected radiation from the ocean surface will be scattered, leading to a lower brightness temperature seen from the SSM/I.

The best representation of the higher amounts of LWP is achieved by the physically based algorithm from Petty (Figure 2).

A comparison of the algorithm results for the situations with LWPs less than 100 g/m^2, that corresponds with non precipitating conditions gives the following results. The algoritms "BAU" and "PET" overestimate these very small LWP values, whereas the algorithm from Alishouse gives mostly negative estimates for true values near zero. The algorithm from Karstens shows no bias for this cases. The uncertainty, expressed as standard deviation in this LWP region reaches from 20 g/m^2 for "BAU" to 50 g/m^2 for the Petty algorithm. All the different database type algorithms (Figures 6 to 8) and the neural network algorithm in Figure 5 show negligible bias for the cloudfree situations. It seems, that the "IFM 2" approach often underestimates LWP in cases of ship radiometer values between 0 and 100 g/m^2. The best representation is found by the "IFM 3" algorithm. The uncertainty for LWP = 0 is only about 8 g/m^2. The result of the neural network is similar to the output of the "IFM 3" algorithm.

6 CONCLUSIONS

The new algorithms based on a lookup table method regarding the EOF transformed SSM/I brightness temperatures reduce the RMS error for cloudy scenes with only low vertically integrated liquid water path by a factor of 3, compared with most of the published algorithms. Only the neural network algorithm give the same very small error for cloudfree and thin cloud situations.

For higher LWP values, all algorithm show a strong underestimation of LWP, according to the rainrate. The algorithm from Petty gives the best results for situations when rain is present, while the other algorithms do not differ very much regarding their retrievals.

The validation for the higher LWPs is very problematic in midlatitude regions, caused by the statistical error of the ground truth values from ship born radiometer, so that a definite decision of the algorithm quality in the high LWP region was not possible. The main advantages for this method should come from assimilation of rain data into the sets of atmospheric profiles, used for building up the lookup tables.

REFERENCES

[1] Alishouse, J.C., S. Snyder, J. Vongsathorn, and R.R. Ferraro, 1990: "Water vapour and cloud water validation," in DMSP Special Sensor Microwave/Imager, Calibration/Validation Report, vol.2. J.P.Hollinger, Ed. Washington D.C.: Naval Research Laboratory, pp. 7.1-7.24.

[2] Bauer, P., 1992: "Wasserdampf, Gesamtwasser und Niederschlagsrate aus Daten passiver Mikrowellenradiometer ueber dem Ozean",Forschungsbericht Nr. DLR-FB92-37 der Deutschen Forschungsanstalt fuer Luft- und Raumfahrt, Koeln: DLR 1992.

[3] Francis, C.R., D.P. Thomas, and P.L. Windsor, 1983: "The evaluation of SMMR retrieval algorithms," in Satellite Remote Sensing, T.D. Allan, Ed. Chichester: Ellis Horwood Limited, pp. 481-498.

[4] Greenwald, T.J., G.L. Stephens, T.H. Von der Haar, and D.L. Jackson, 1993: "A Physical Retrieval of Cloud Liquid Water Over the Global Oceans Using Special Sensor Microwave/Imager (SSM/I) Observations," J. Geophys. Res., vol. 98, pp. 18,471-18,488.

[5] Hollinger, J.P., 1971: "Passive microwave measurements of sea surface roughness," IEEE Trans. Geos. Electron., vol. GE-9, pp. 165 ff.

[6] Stogryn, A., 1972: "The emissivity of sea foam at microwave frequencies," J. Geophys. Res., vol. 77, pp. 1658-1666.

[7] Karstens, A., C. Simmer, and E. Ruprecht, 1994: "Remote Sensing of Cloud Liquid Water," Meteorol. Atmos. Phys., vol. 54, pp. 157-171.

[8] Liebe, H.J., and D.H. Layton, 1987: "Millimeter-wave properties of the atmosphere: Laboratory studies and propagation modelling," NTIA Report, vol. 87-224. U.S. Dept. of Commerce, Natl. Telecomm. and Inf. Adm., Inst. for Comm. Sciences, 325 Broadway, Boulder, CO 80303-3328, 80 p.

[9] Liebe, H.J., G.A. Hufford, and M.G. Cotton, 1993: "Propagation Modeling of Moist Air and Suspended Water/Ice Particles at Frequencies below 1000 GHz," AGARD 52nd Specialists Meeting of the Electromagnetic Wave Propagation Panel, Proceedings, Paper 3, Palma de Mallorca 1993.

[10] Liu, G. and J.A. Curry, 1993: "Determination of Characteristic Features of Cloud Liquid Water From Satellite Microwave Measurements," J. Geophys. Res., vol. 98, pp. 5069-5092.

[11] Monahan E.C. and I.G. O'Muircheartaigh, 1986: "Whitecaps and the passive Remote Sensing of the Ocean Surface," International J. of Remote Sensing, vol. 7, pp. 627-642.

[12] Petty, G.W. and K.B. Katsaros, 1990: "New geophysical algorithms for the Special Sensor Microwave/Imager," Fifth Conference on Satellite Meteorology and Oceanography," London: American Meteorological Society, pp. 247-251.

[13] Schrader, M., 1995: "Ein Dreiskalenmodell zur Berechnung der Reflektivität der Ozeanoberfläche im Mikrowellenfrequenzbereich," Berichte aus dem Institut fuer Meereskunde, Nr. 274.

[14] .Simmer, C., 1994: "Satellitenfernerkundung hydrologischer Parameter der Atmosphaere mit Mikrowellen," Habilitationsschrift am Institut fuer Meereskunde der Christian-Albrechts-Universitaet Kiel, Kiel: IFM, 1994.

[15] Weng, F. and N.C. Grody, 1994: "Retrieval of cloud liquid water using the special sensor microwave imager (SSM/I)," J. Geophys. Res., vol. 99, pp. 25,535-25,551.

[16] Wentz, F.J., 1983: "A model for ocean microwave brightness temperatures," J. Geophys. Res., vol. 88, pp. 1892-1908.

[17] Westwater, ED.R., Jack B. Snider and Michael J. Falls, 1990: "Ground-Based Radiometric Observations of Atmospheric Emission and Attenuation at 20.6, 31.65, and 90.0 GHz: A Comparison of Measurements and Theory," IEEE Transactions on Antennas and Propagation, vol. 38 (10), pp. 1569-1579.

[18] Jung, T., E. Ruprecht and F. Wagner "Determination of Cloud Liquid Water Path Over the Oceans From SSM/I Data Using Neural Networks", J. App. Met., submitted paper.

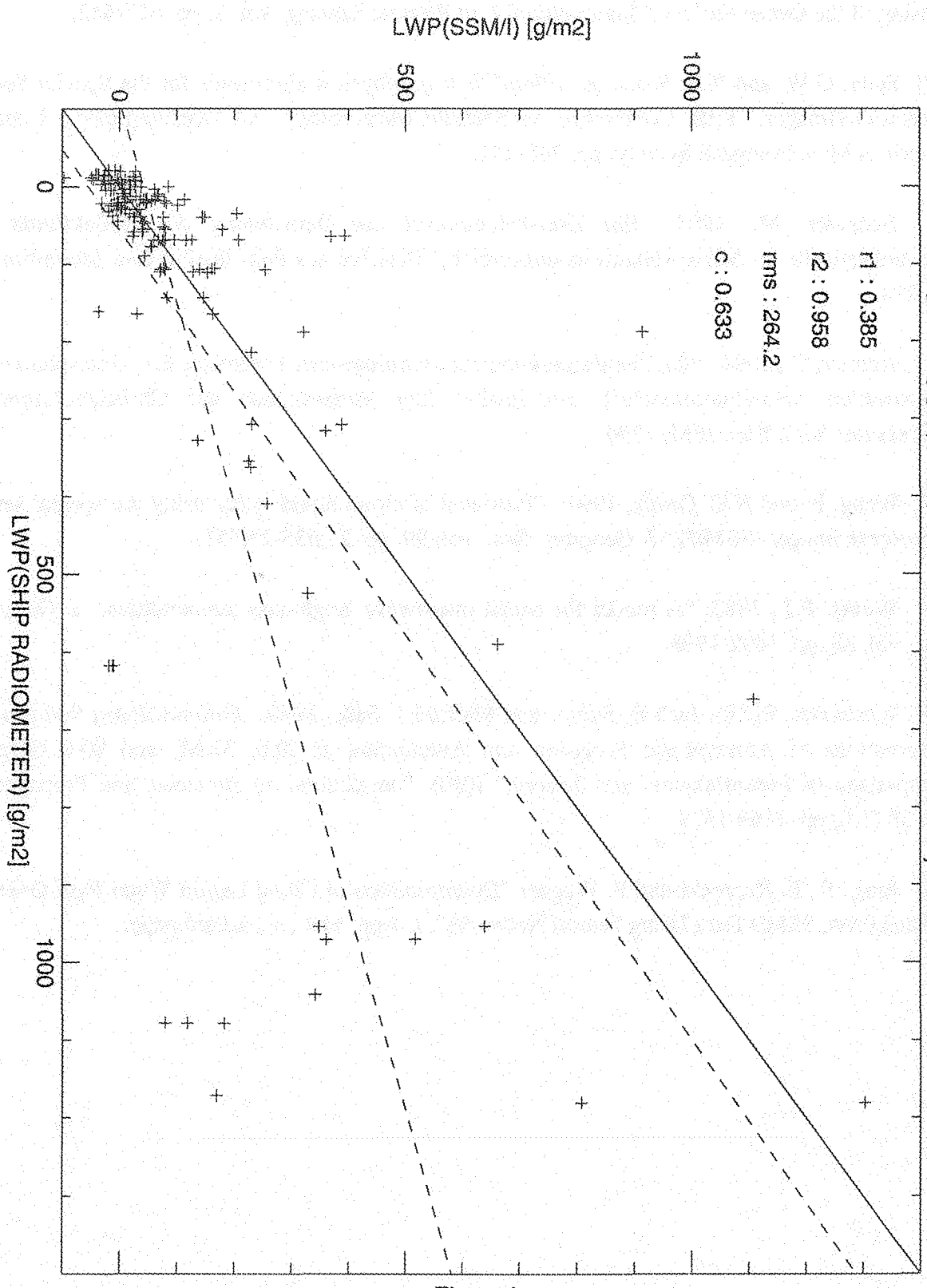
FIG. 1 SSM/I TBS OVER THE BALTIC SEA , ALGORITHM: KAR
r1 : 0.385
r2 : 0.958
rms : 264.2
c : 0.633
LWP(SSM/I) [g/m2]
LWP(SHIP RADIOMETER) [g/m2]
0
500
1000

Figure 1

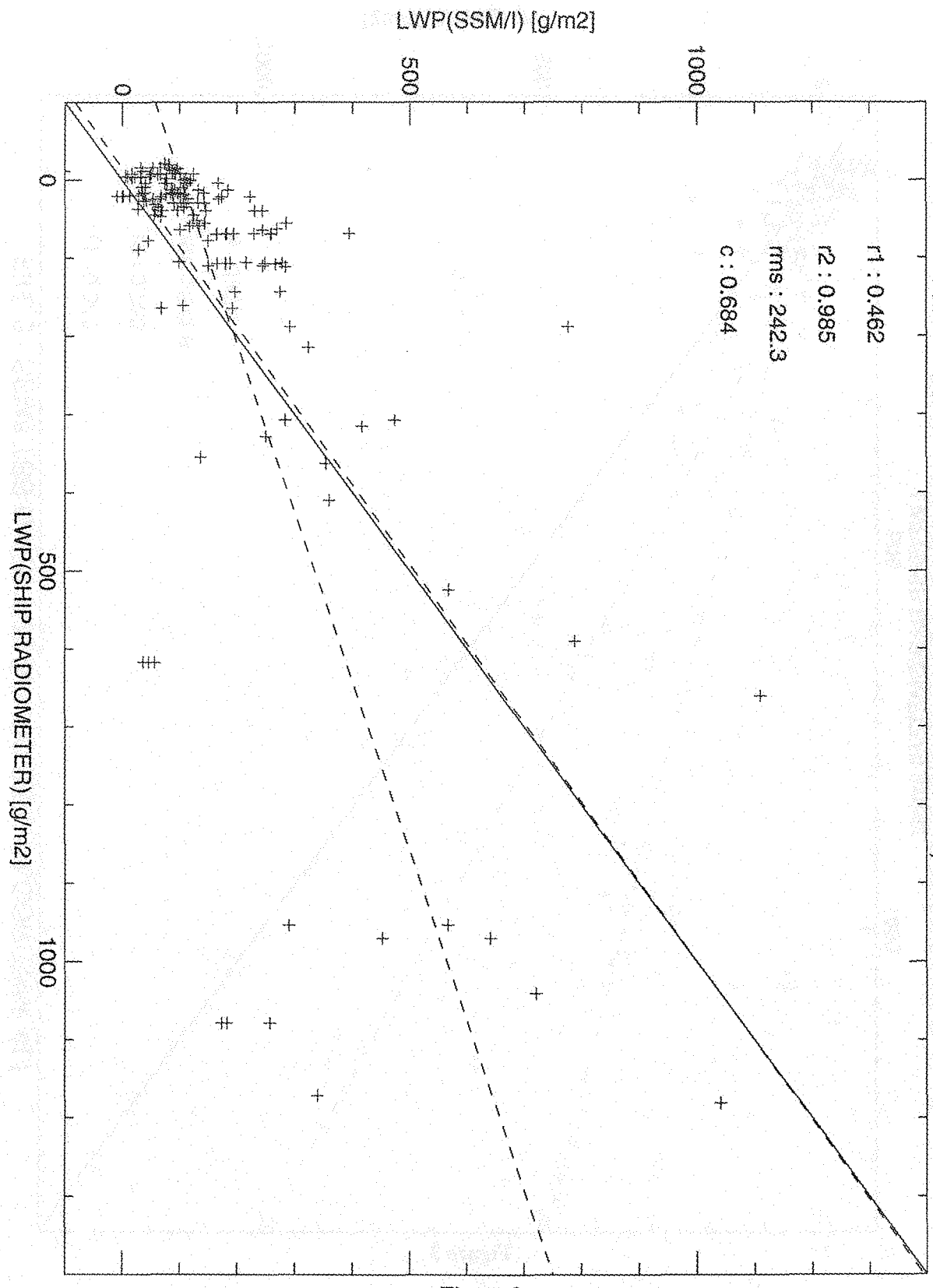
FIG. 2 SSM/I TBS OVER THE BALTIC SEA , ALGORITHM: PET
r1 : 0.462
r2 : 0.985
rms : 242.3
c : 0.684
LWP(SSM/I) [g/m2]
LWP(SHIP RADIOMETER) [g/m2]
0
500
1000

Figure 2

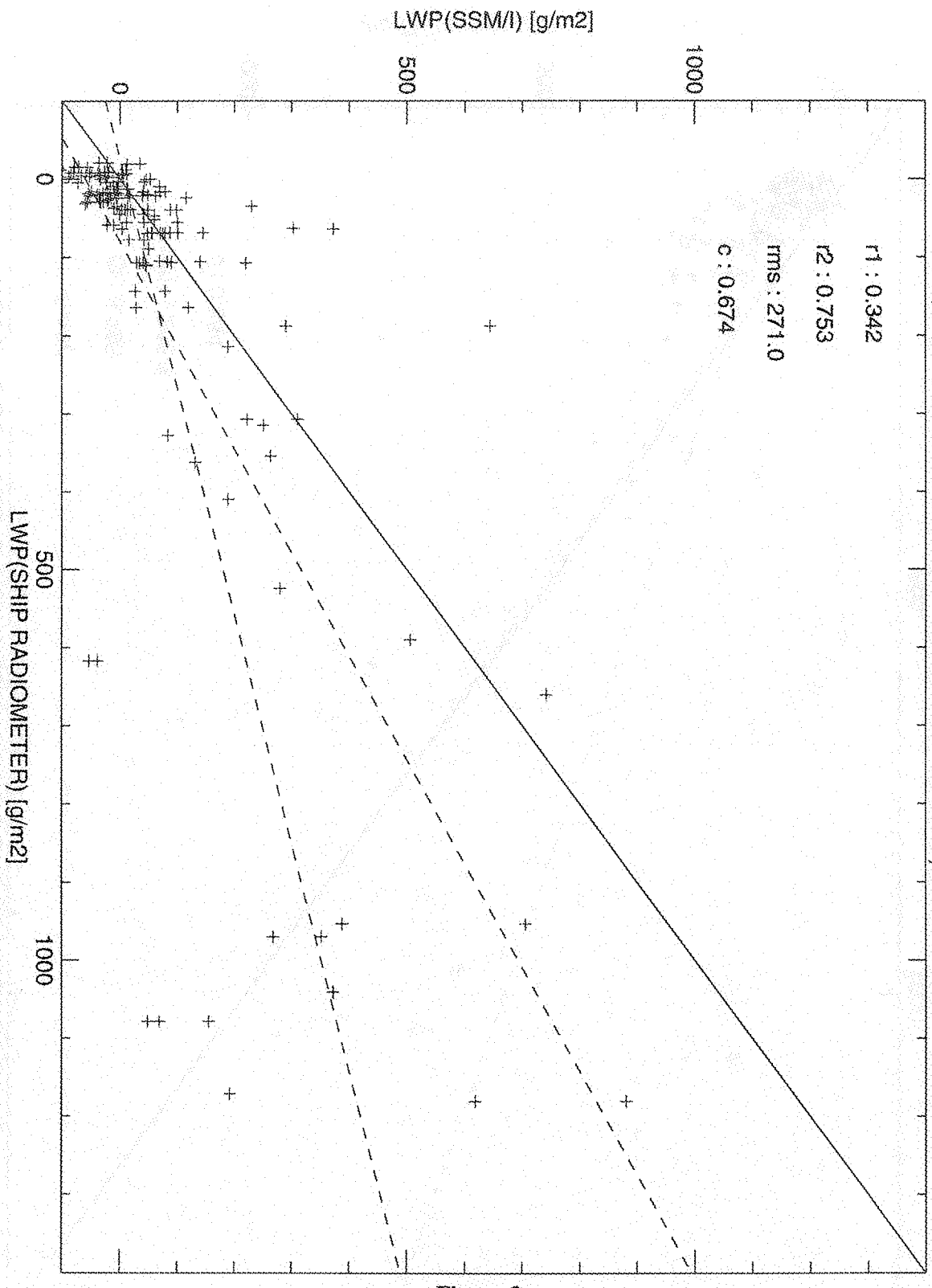
FIG. 3 SSM/I TBS OVER THE BALTIC SEA , ALGORITHM: ALI
r1 : 0.342
r2 : 0.753
rms : 271.0
c : 0.674
LWP(SSM/I) [g/m2]
LWP(SHIP RADIOMETER) [g/m2]
0
500
1000

Figure 3

FIG. 4 SSM/I TBS OVER THE BALTIC SEA , ALGORITHM: BAU

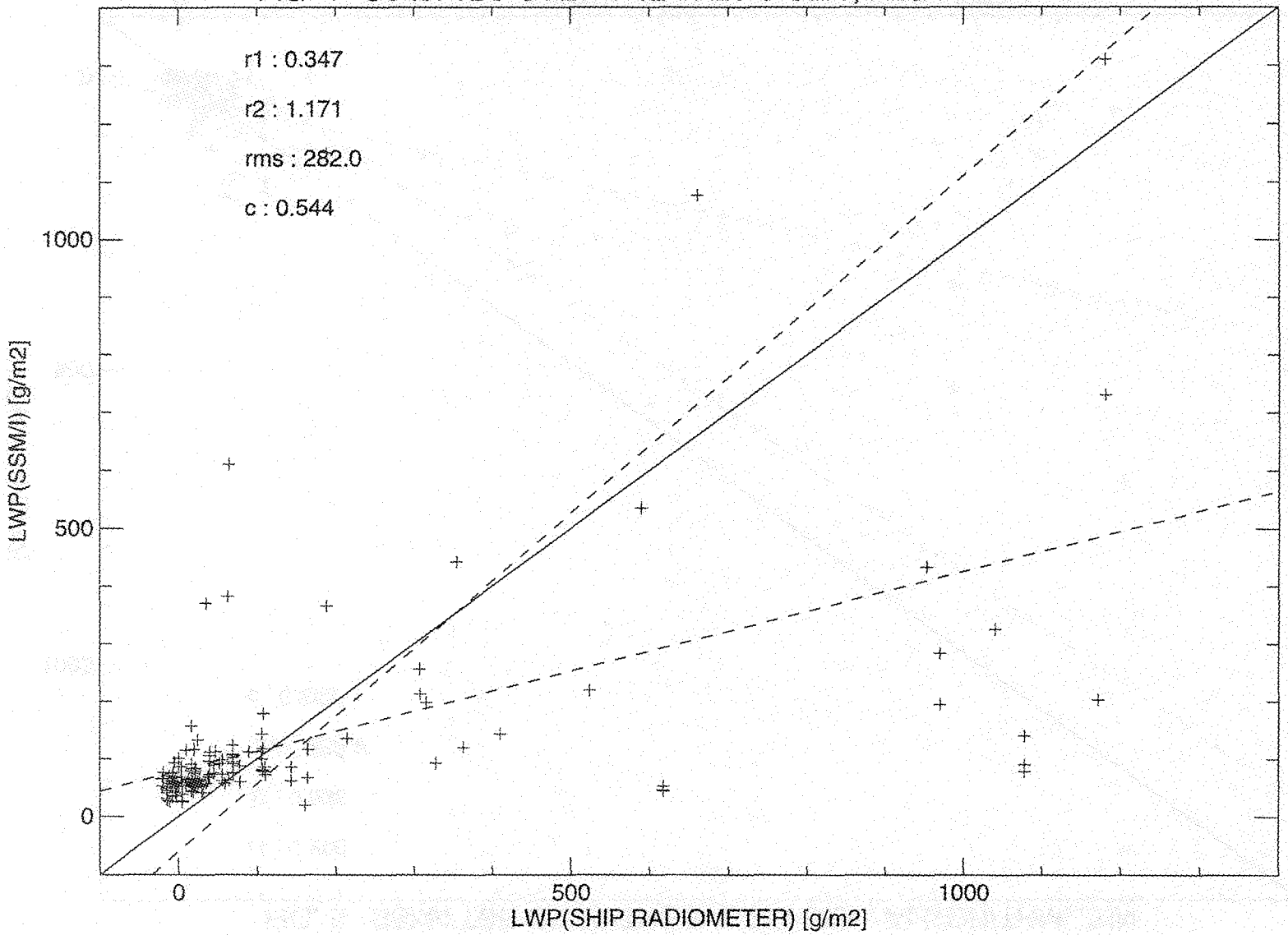

Figure 4

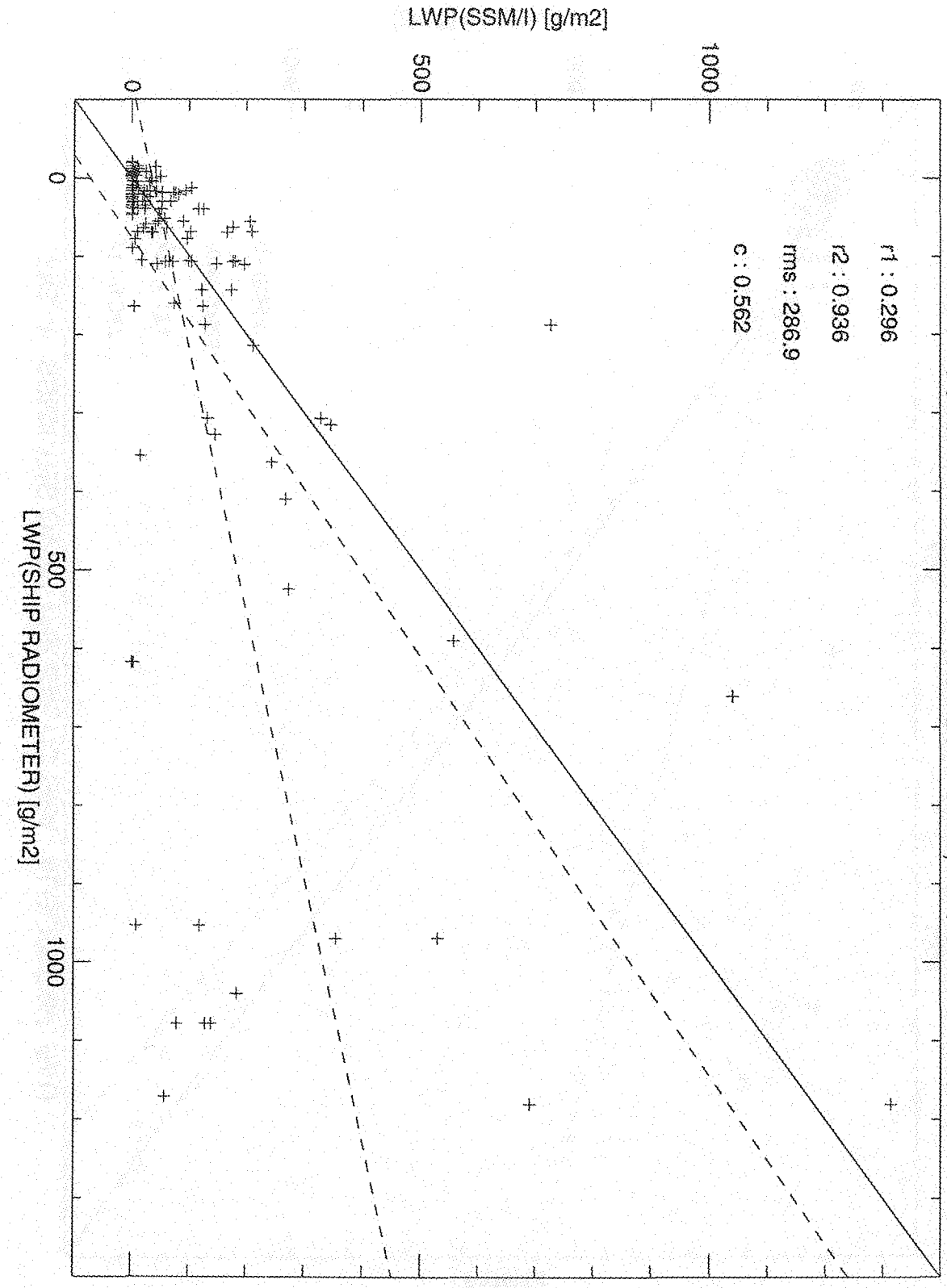
FIG. 5 SSM/I TBS OVER THE BALTIC SEA , ALGORITHM: JUN
LWP(SSM/I) [g/m2]
LWP(SHIP RADIOMETER) [g/m2]
r1 : 0.296
r2 : 0.936
rms : 286.9
c : 0.562
0
500
1000

Figure 5

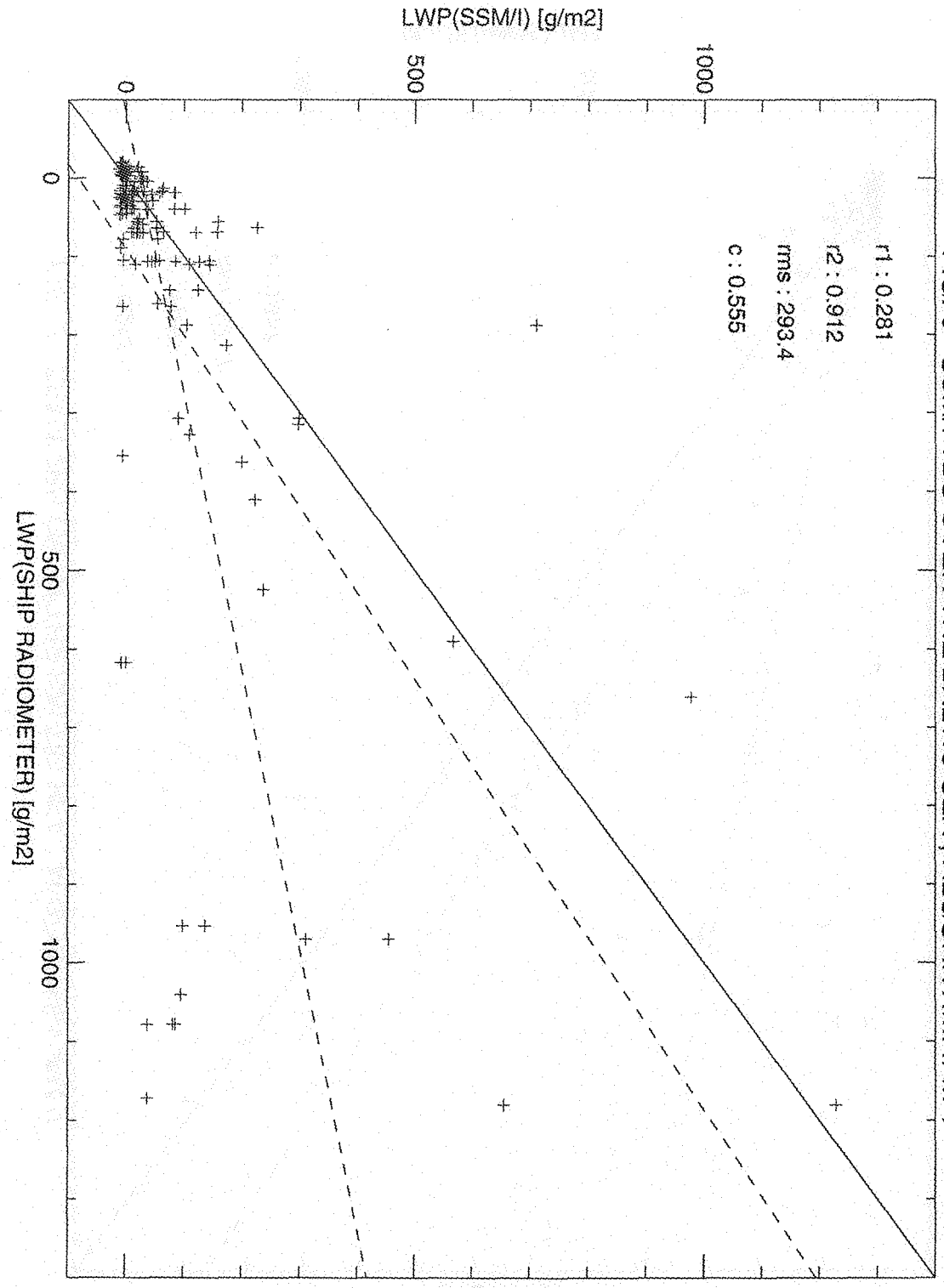
LWP(SSM/I) [g/m2]
0
500
1000
r1 : 0.281
r2 : 0.912
rms : 293.4
c : 0.555
FIG. 6 SSM/I TBS OVER THE BALTIC SEA , ALGORITHM: IFM 1
LWP(SHIP RADIOMETER) [g/m2]
0
500
1000

Figure 6

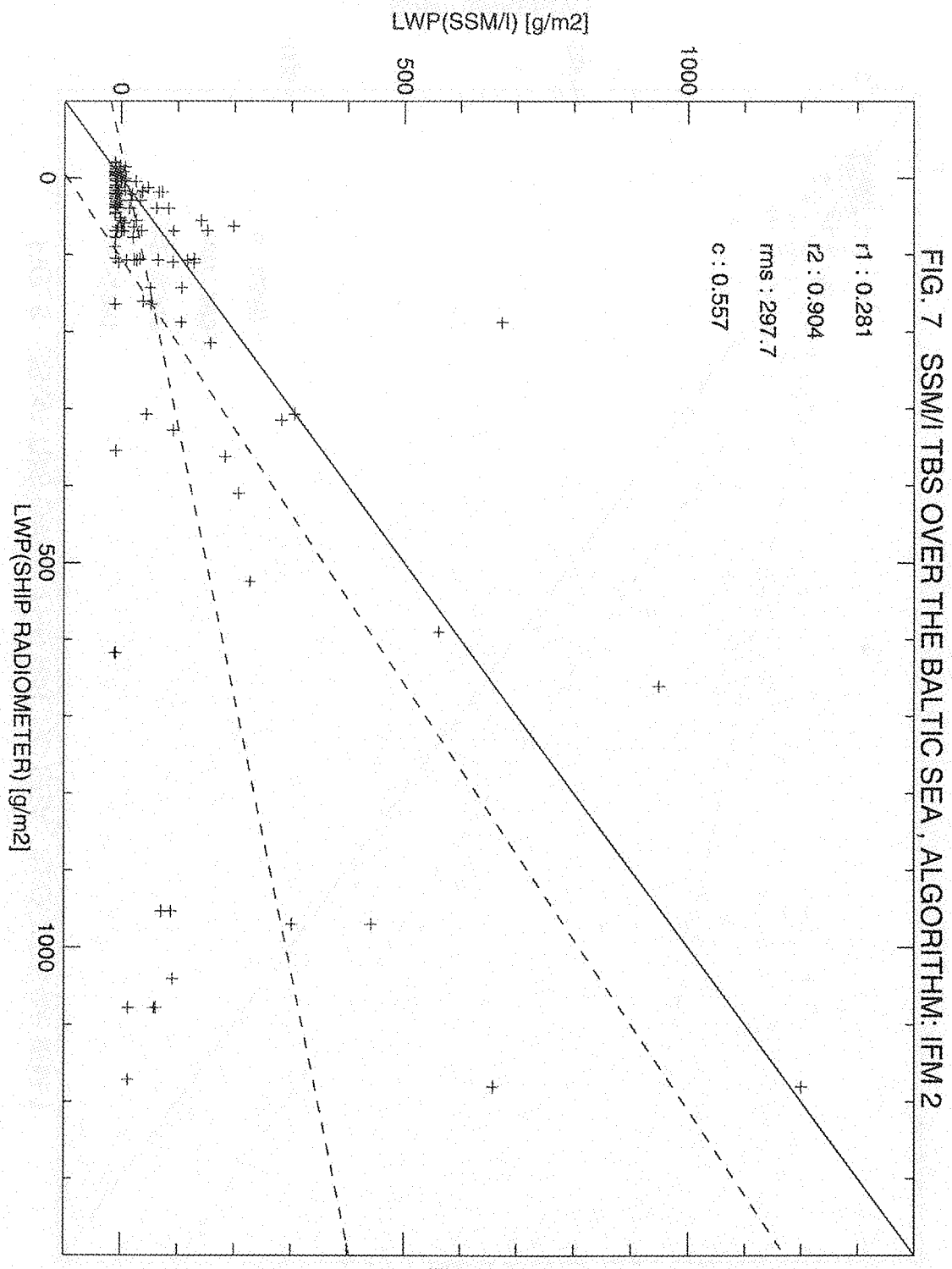
FIG. 7 SSM/I TBS OVER THE BALTIC SEA , ALGORITHM: IFM 2
r1 : 0.281
r2 : 0.904
rms : 297.7
c : 0.557
LWP(SSM/I) [g/m2]
LWP(SHIP RADIOMETER) [g/m2]
0
500
1000

Figure 7

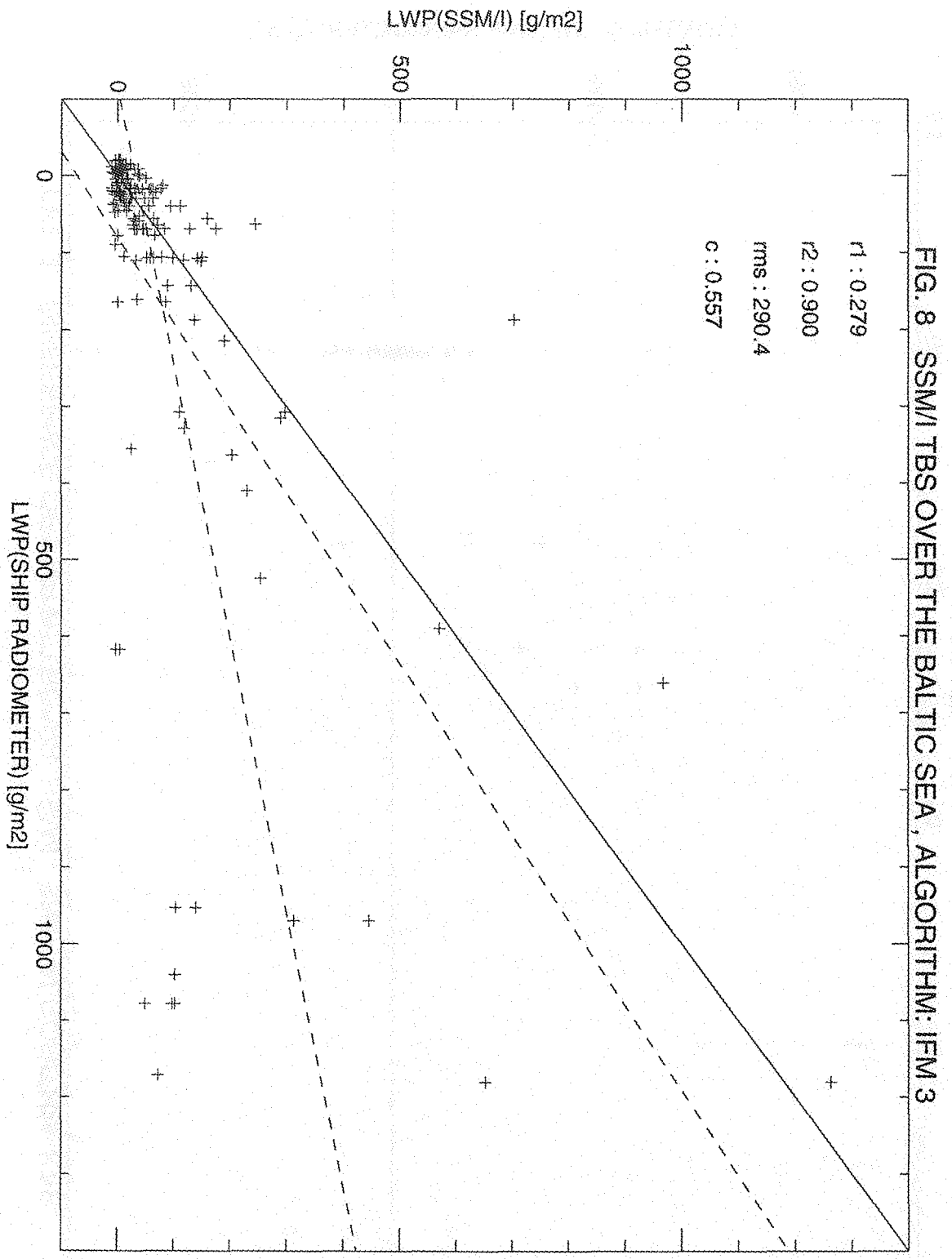
FIG. 8 SSM/I TBS OVER THE BALTIC SEA , ALGORITHM: IFM 3
r1 : 0.279
r2 : 0.900
rms : 290.4
c : 0.557
LWP(SSM/I) [g/m2]
LWP(SHIP RADIOMETER) [g/m2]
0
500
1000

Figure 8

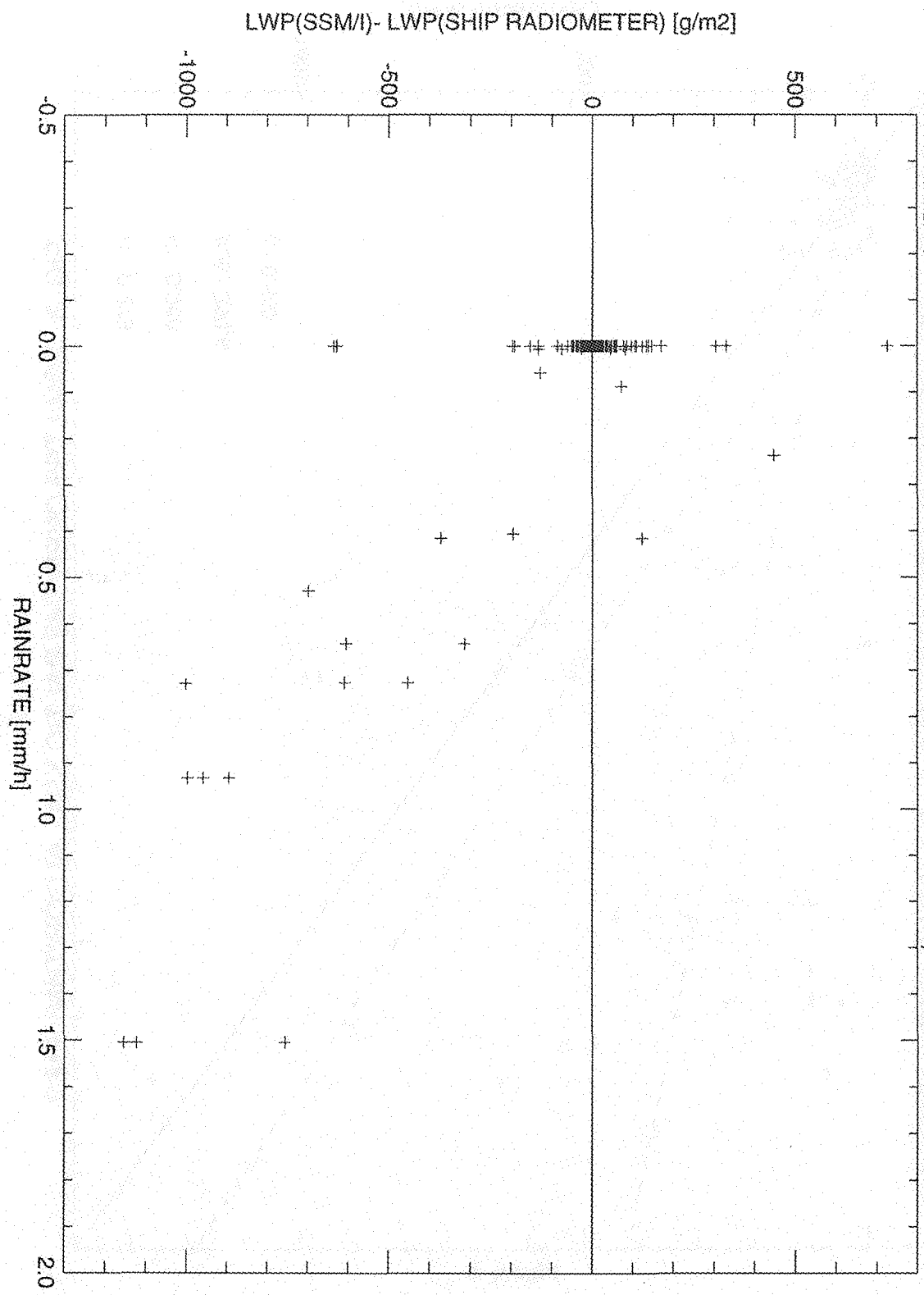
LWP(SSM/I)- LWP(SHIP RADIOMETER) [g/m2]
-1000
-500
0
500
-0.5
0.0
0.5
1.0
1.5
2.0
RAINRATE [mm/h]
FIG. 9 DIFFERENCE OF LWP RETRIEVAL SSM/I - SHIP, ALGORITHM: KAR

Figure 9

Sub-gridscale properties of atmospheric budgets for BALTEX

F. Hamelbeck, M. Hantel
Institute of Meteorology and Geophysics, University of Vienna
Hohe Warte 38, A-1190 Vienna., Austria

ABSTRACT

A central goal of BALTEX is to quantify the processes determining the time and space variability of the water and energy cycle. We consider this from two aspects: the integral of the atmospheric column covering the Baltic drainage basin and the details of vertical profiles. 1) The integral budget for BALTEX is controlled by the gridscale transports and the molecular transports across the surface. 2) Resolving the vertical structure of the atmospheric column the sub-gridscale fluxes come into play. The specific profiles describe the mechanism by which the budget is executed in detail. The vertical sub-gridscale fluxes, gained by indirect diagnostic techniques, are shown. For pronounced convective situations the upward convective fluxes are stronger than 300 W/m^2 across the 700 hPa surface. Also results for a statistical evaluation of averaged profiles is presented.

1 INTRODUCTION

The budgeting efforts of BALTEX require a well defined scale for each evaluation. Here we look at two different scales: The complete atmosphere on top of the Baltic drainage basin (the BALTEX box) and the 3D budget on a 55 km and $\Delta p \approx 30$ hPa grid. The first allows to calculate the exchange of the study area with its surrounding, while the second offers insight, how the budget is executed in detail.

2 BALTEX BUDGET

Looking at the atmosphere over the catchment as one box, the energy balance can be concluded from the gridscale dynamics, radiation fluxes and turbulent fluxes at the surface. Throughout this study we use data from ECMWF (atmospheric fields are taken from initialized analysis and fluxes from forecasts) and from optimal interpolation of rain gauge measurements (Rubel 1996). The energy content of the BALTEX box was calculated for different cases. The internal and potential energy vary quite slowly. The latent and kinetic energy show strong relative fluctuations. For a five day period starting at Aug. 27 1995 6 UTC until Aug. 31 6 UTC we present the

result for dry enthalpy (all quantities in W/m^2; fluxes positive, when entering the BALTEX box): Inflow from the Earth's surface 92 (sensible heat 22, latent heat release by precipitation 126, terrestrial 56, solar radiation -112), radiation at the top of the atmosphere -30 (terrestrial -237, solar 207), advection of enthalpy 116 and energy conversion -135 balance a tendency of 45 with an imbalance of -2. In the moisture budget the latent heat flux across the surface 66, precipitation -126 and advection 49 balance the tendency of 7 with an imbalance of -18.

3 CONVECTIVE BUDGET

Enhancement of resolution shows the vertical and horizontal structure of the budget and allows to study the different processes, which establish the energy balance. We look at the Gibb's equation for moist enthalpy, represented by the equivalent temperature $\vartheta = c_p T + L_q$. Transports on all scales occur. The contribution of the gridscale dynamics defines the gridscale part of the budget

$$\text{bud} \equiv c_p \left[\frac{\partial \bar{\vartheta}}{\partial t} + \nabla \cdot \left(\bar{\vartheta} \bar{V} \right) - \frac{\kappa}{p} \bar{T}\, \bar{\omega} \right] - \overline{Q_{rad}} \qquad (1)$$

The averaging operator is written as an overbar, the deviation as a prime. We include the radiation into the gridscale budget, as we take it to be known. The most important sub-gridscale fluxes are believed to be the vertical transports by eddies. We calculate the eddy correlation flux $c(p) = g^{-1} c_p \overline{\vartheta' \omega'}$ necessary to balance the gridscale budget:

$$\text{bud}(p) + g \frac{\partial c(p)}{\partial p} - g \frac{k}{p} \frac{c(p)}{1 + 1/\beta(p)} = 0, \qquad (2)$$

where $\beta(p)$ is the generalized Bowen ratio and all other quantities have standard meaning. The convective flux is fixed at the surface by the sum of molecular fluxes of latent and sensible heat across the surface. This overspecifies this differential equation, which allows to estimate the imbalance present in the dataset. We refer to eq. (2) as convection equation. A corresponding equation for the water content is the moisture equation.

This method is implemented in the diagnostic model DIAMOD, established at the University of Vienna (Haimberger 1995). Figure 1 shows three selected columns over the BALTEX domain, valid for 31 October 1995. Convection penetrates the entire atmospheric column in a warm sector at the Kattegat, where is sizeable rain. At the Polish coast in the cold sector there is very little convection, but stratiform rain. Further north at Aland the convective transport is limited to the boundary layer over a warm sea.

A systematic study was applied to the year 1991: For each month's first day the convective situation was examined for a square grid of Å 1000 columns over Europe. It is possible to sort most of the resulting vertical profiles into the three destinct categories of Figure 1 in a objective way. Figure 2 shows averaged results for classified types at night, Figure 3 during the day. For the

night period 18 UTC-6UTC (6 UTC - 18 UTC, day period), 39 % (27 %) show deep convection, 11 % (40 %) boundary layer convection and 6 % (4 %) precipitation, without sizeable convection. Deep convection is more prominent during the night, boundary layer convection during the day. Stratiform precipitation is characterized by insignificantly small convection and occurs rarely.

4 CONCLUSIONS

The budget of the BALTEX box can be calculated from the fluxes across the top of atmosphere and the surface and the gridscale transports. Resolving the three-dimensional structure sub-grid-scale fluxes cannnot be neglected, else the budget would not be closed. This condition was used to calculate the convective flux for the Baltic Sea. The application of the convective flux to examine the mesoscale situation is described elsewhere (Dorninger 1997, Hantel and Hamelbeck 1997). We plan to extend the case studies of the PIDCAP-period to cover the whole period, accessing the average convective types in BALTEX, as was done for Europe.

Acknowledgments

This work was in part supported by the EC Environment and Climate Research Progamme (contract: NEWBALTIC, No ENV4-CT95-0072, Climatology and Natural Hazards) and in part by the Austrian Ministry of Science, Transport and Art. We are indebted to our international partners, especially to the ECMWF and the DWD. Furthermore to the Central Institute for Meteorology and Geophysics, Vienna, which provided the synoptic data. The support and advice of M. Dorninger, M. Ehrendorfer, O. Frauenfeld, L. Haimberger, and M. Ungersböck is gratefully acknowledged.

REFERENCES

Dorninger M, 1997: Der konvektive Wärmefluß bei verschiedenen synoptischen Lagen. PhD Thesis, University of Vienna, in German, 162 pp.

Haimberger, L., M. Hantel and M. Dorninger, 1995: A thermodynamic diagnostic model for the atmosphere. Part III: DIAMOD with orography and improved error model. Meteorol. Zeitschr., N.F., 4, 162-182.

Rubel, F., 1996: PIDCAP - Quick Look Precipitation Atlas. Österreichische Beiträge zu Meteorologie und Geophysik, Heft 15, 97 pp.

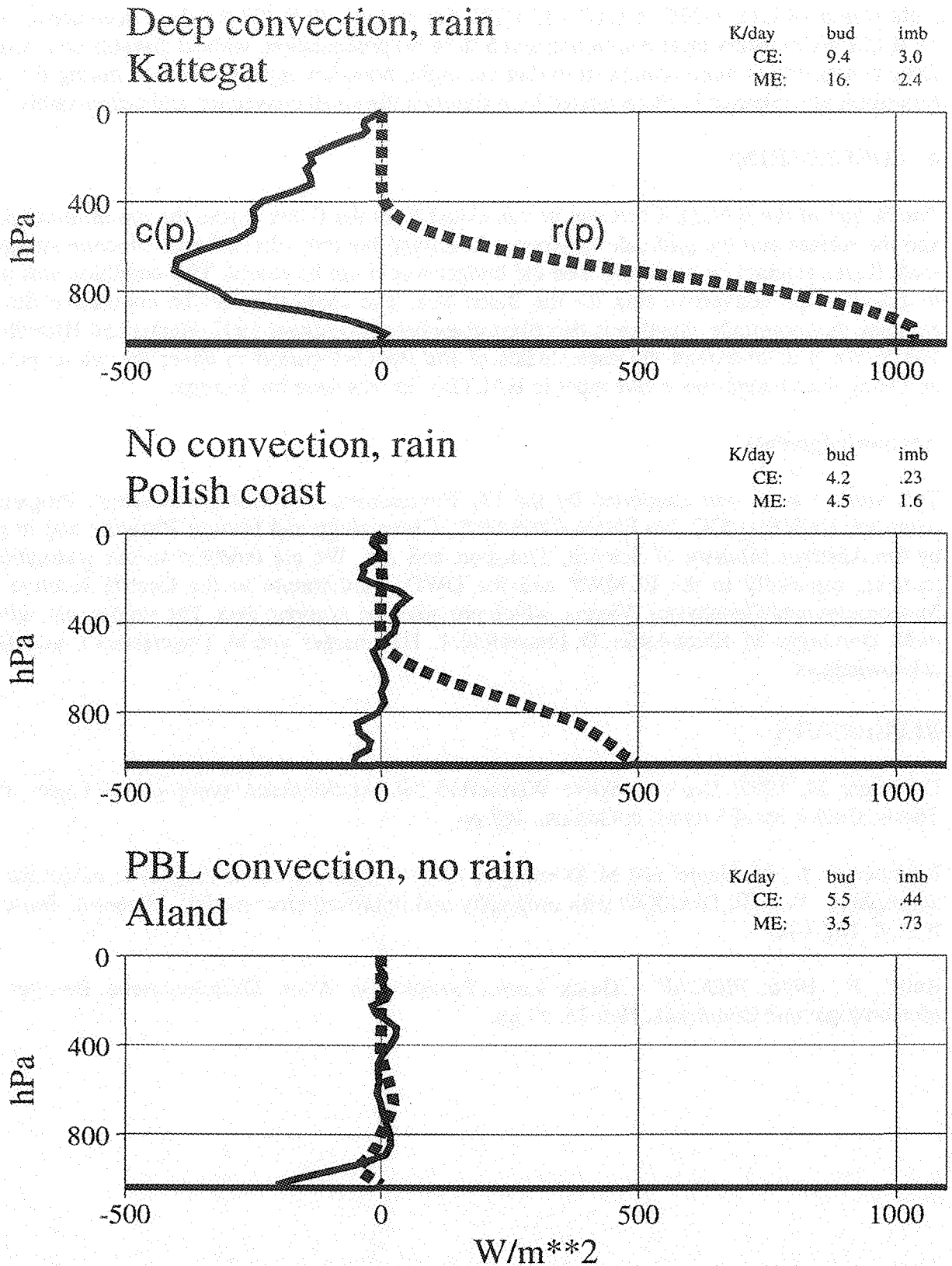

Figure 1: Vertical profiles of convective heat flux c(p) and rain flux r(p) in W/m^2, downward fluxes positive; for each column rms-values for budget and imbalance of convection equation (CE) and moisture equation (ME) presented. Date: 31 October, 1995, 6 - 18 UTC (Note: 1.7 mm/12 h ≈ 100 Wm^{-2}).

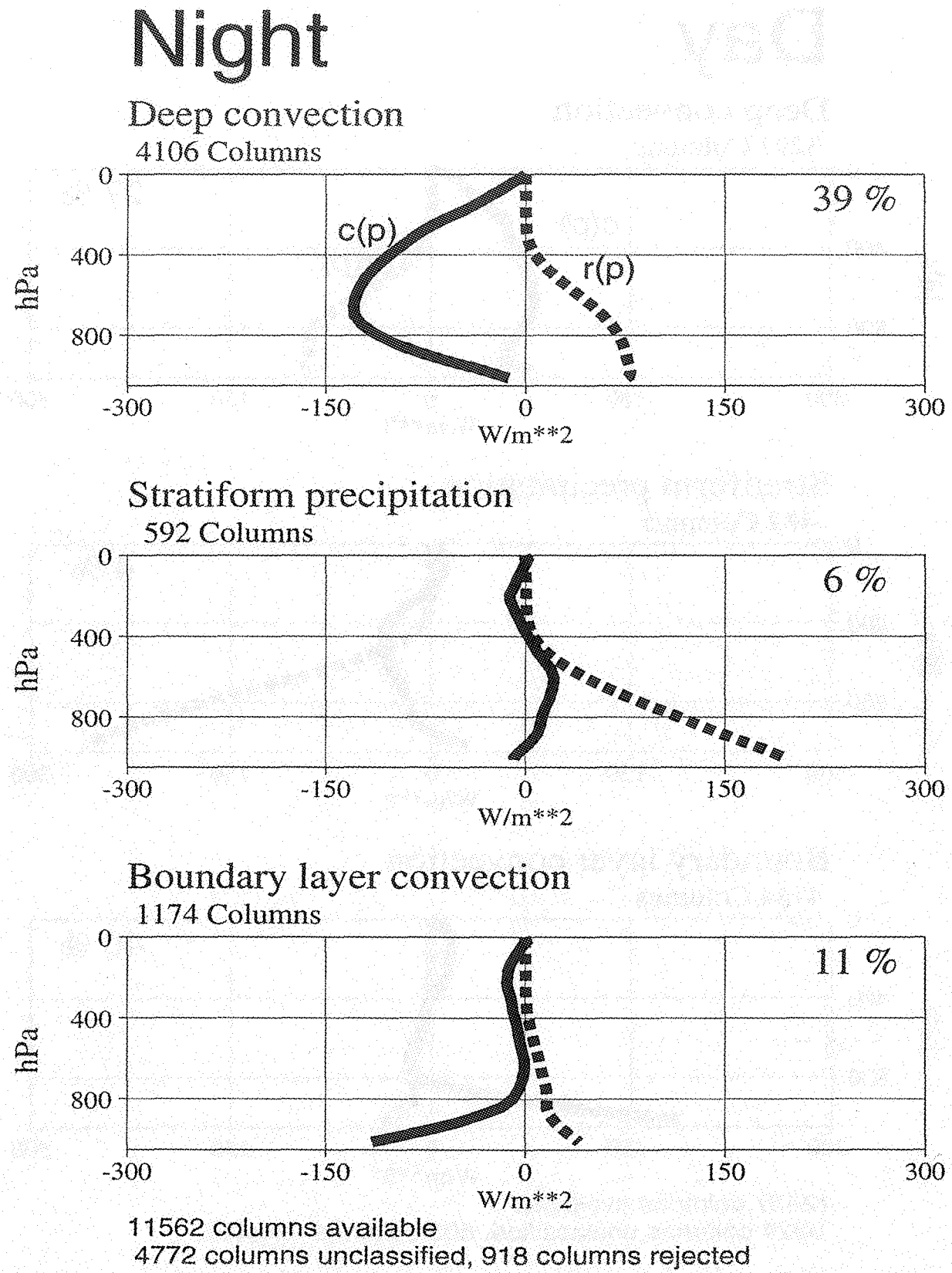

Figure 2: Averaged profiles for objectively sorted columns for three different types; both convective heat and rain fluxes shown. Relative frequency given in upper right corner. Valid from 18 UTC - 6 UTC. Dataset 32 x 32 columns over Europe for first day of each month for 1991, using ERA data.

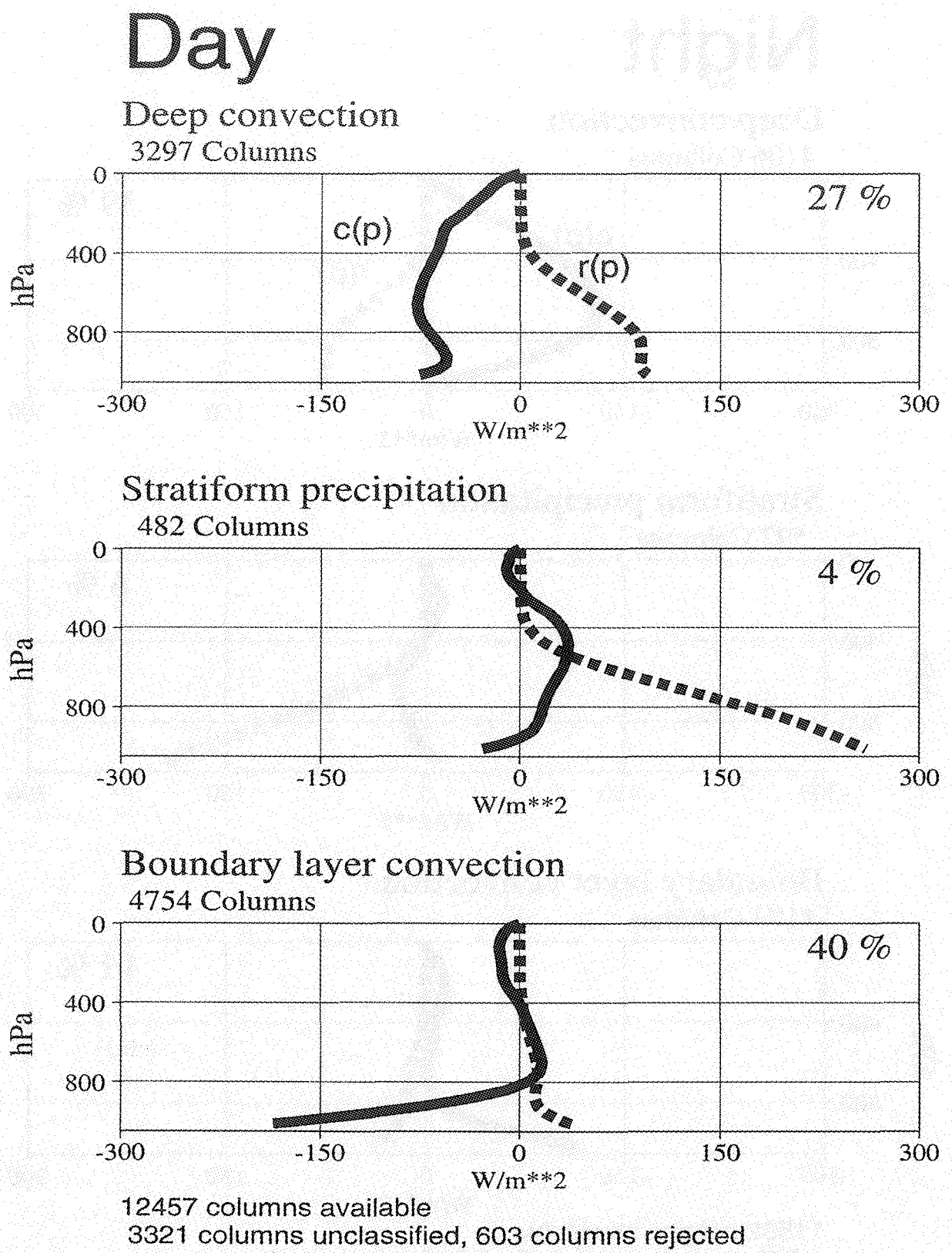

Figure 3: Averaged profiles for objectively sorted columns for three different types, as in Figure 2 but valid for 6 UTC - 18 UTC.

INVESTIGATIONS OF THE WATER AND ENERGY CYCLE OF THE BALTIC SEA USING GLOBAL AND REGIONAL CLIMATE MODELS

Daniela Jacob, Martin Windelband
Max-Planck Institute for Meteorology, Hamburg
Ralf Podzun
Deutsches Klimarechenzentrum, Hamburg
Phil Graham
Swedish Meteorological and Hydrological Institute, Norrköping

ABSTRACT

The interaction between the atmosphere and hydrosphere takes place on several scales and determines the water and energy cycle. To simulate processes correctly improved regional and global models are necessary which are carefully validated. First steps towards a validation on different time and space scales have been presented at the EGS meeting 1997 in Vienna. Three talks demonstrated some important aspects of the validation and they are summarized in the following. This contribution contains the talks titled:

- Are perfect boundaries really perfect ?
- Hydrological and energetic cycle for the baltic catchment simulated with regional and global models
- A hydrological and a climatological view of the Baltic water balance.

1 INTRODUCTION

The water and energy cycles over the Baltic Sea are influenced by meteorological phenomena on a variety of scales. Therefore an intense study of weather events on a wide range of spatial and temporal scales linked to hydrological macro-scale models is one of the important issues. The conceptual HBV hydrological model has been applied to the entire Baltic basin and will be used for intercomparison and validation of output from the ECHAM4 global climate model. The global climate model delivers information on long time scales and provides lateral boundary condition for the regional climate model.

Recently it has been shown that the lateral boundary conditions are strongly influencing the simulation of a regional climate model. This is not only true for long time series, but also for short episodes. Furthermore analyses or re-analyses data can be used as lateral boundary conditions for regional models. These data are assumed to be 'perfect' or 'as close to reality as possible'. A careful validation will include sensitivity studies comparing the influence of different analyses (provided by different weather prediction centers for the same time period).

For regional studies of the hydrological and energy cycles over the Baltic Sea and its drainage basin the hydrostatic model REMO based on the operational forecast model of the DWD was used. In close cooperation with the DKRZ an additional physical parameterization scheme, identical to the one of the global MPI climate model (ECHAM4) for the atmosphere was

successfully implemented. The REMO model can now be used with two complete physical parameterization .

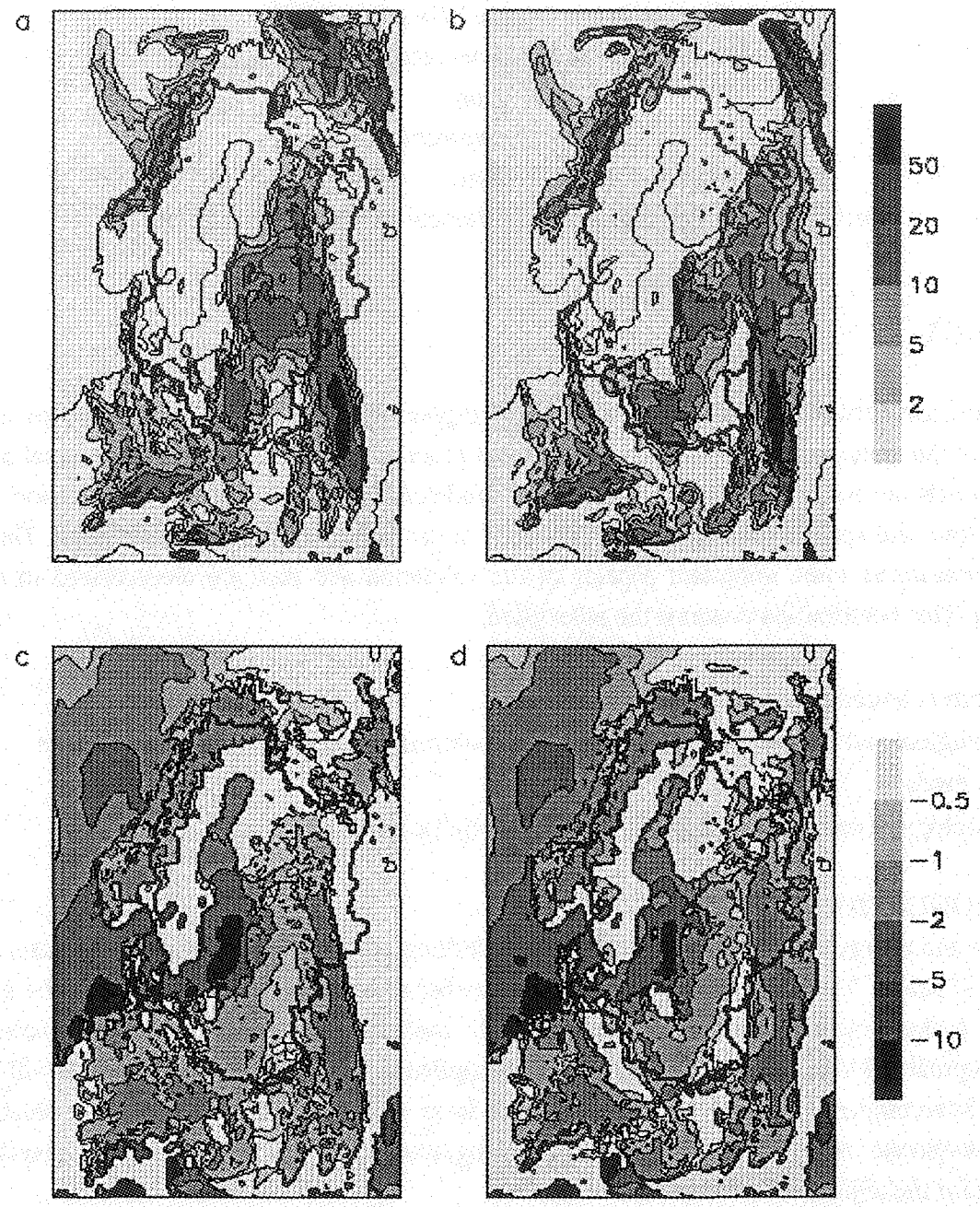

Figure 1: Total precipitation [mm/day] and evaporation [mm/day] simulated with REMO-EC4 and DMI-Analyses for August 29th 1995. a: 30h (tot. prec); b: 78h (tot. prec); c: 30h (evap); d: 78h (evap).

Figure 1: Total precipitation (mm/day) and evaporation (mm/day) simulated with REMO-EC4 and DMI Analyses for August 29th 1995. a: 30h (tot. prec.); b: 78h (tot. prec.); c: 30h (evap.); d: 78h (evap.).

2 REGIONAL STUDIES ON SHORT TIME SCALES

During the PIDCAP period observations were taken which can and will be used to validate model results on a timescale from days to 3.5 months. Two time periods were defined for model intercomparison studies, first the whole PIDCAP period of three months and second a 6 day period from 27.8.95 to the 2.9.95. REMO has been driven by analyses data provided by the German and Danish weather services as lateral boundary conditions. For each physical parameterization scheme two simulations have been performed, one with 50 km and a second one with 18 km resolution on the horizontal scale. Therefore it is possible to compare the different physical parameterization schemes against each other. The use of different boundary data sets gives some information about the influence of the driving fields onto the regional model results.

Six 30-h forecasts (the first 6 hours are not taken into account in order to avoid spin-up problems) and a 6-day forecast using REMO with ECHAM4-physics on 18 km resolution driven by analyses from DMI and DWD for the second period have been performed. Figure 1 shows the results using DMI analyses at the lateral boundaries. The different behaviour initiated through the length of the forecast can be seen in the precipitation (a and b) and the evaporation (c and d) for the third 30-h forecast, e.g. the 29th of August, 6 am, to the 30th of August, 6 am, (a and c) and the third day of the 6-day forecast (b and d). After 3 days a difference in the spatial distribution of precipitation (a and b) especially east of the Baltic Sea can be seen. The precipitation band seems to be shifted towards the east and it seems to be a bit wider. This is also clearly seen in the evaporation pattern (c and b).

The influence of the different analyses (DMI and DWD) can be seen in Figure 2. Therefore 30 hours and 78 hours forecasts have been performed using REMO with ECHAM4 physics on a 50 km horizontal resolution driven by DMI (a and c) and DWD (b and d) analyses. The ECHAM4 physics was chosen for these studies to avoid advantages by having the identical physical parameterization packages used to create the analyses and to do the REMO run. The lateral boundaries have been updated every 6 hours, a data assimilation scheme was not used. After 30 hours the first differences in the spatial distribution of the precipitation can be detected. The position of the center of precipitation has been shifted. However, after 78 hours the position of the precipitation along the front and the widths are different to the simulation using DWD analyses.

The intercomparison between model results and observations for the total precipitation of August 1995 in the Baltic Sea drainage basin shows that the spatial distribution of precipitation is very similar in all simulations and agrees well with the observations. Figure 3 shows the total precipitation for August 1995 simulated by REMO on the 50 km grid using DWD physics (a) and ECHAM4 physics (b). In particular, local phenomena like the relatively dry regions over south-east Sweden and northern Denmark and the increase of precipitation (close to the long term climatology) over Poland during August 1995 are realistically simulated. Much more details are resolved on 18 km resolution (Figure 3c) and the amount of precipitation is in better agreement with the observations (Figure 3d). A more detailed validation of REMO results for the 3-months period against observations is under way. Especially the intercomparison of the

vertically integrated water vapour content measured by a method using GPS data modelled by REMO is under investigation.

3 GLOBAL STUDIES ON LONG TIME SCALE

Investigations of the water and energy cycle of the Baltic Sea and its drainage basin include long time series to understand the interannual and decadal variabilities. Therefore climate model runs can provide information to study the water and energy budgets.
Two multi-year integrations with the global climate model ECHAM4 and a regional multi-year run using the HIRHAM regional climate model have been analysed. In detail, the water and energy budgets for the Baltic Sea catchment have been calculated. The surface conditions over sea were different for the three runs. A seven years long run using climatological sea surface temperatures, a 10-years long run using observed sea surface temperatures (both global runs with T106 resolution) and a 9-years long regional climate model simulation on 50 km resolution using sea surface temperature information from a coupled ocean-atmosphere run with T42 resolution, have been compared. The intercomparison includes of course many difficulties and insecurities, e.g. different integration length and the preliminary results should only be considered as hints. A more detailed investigation needs some more climate simulations which can be compared more seriously.

Figure 4 shows the water budget for the Baltic Sea drainage basin. The global budgets are very similar, but the regional model shows a much stronger cycle. Only the evaporation over the sea is very close. This is true due to the sea surface temperature (SST) from the coupled run. For summer the SST is about 3 degrees colder than observations.

The intercomparison of the energy cycles of the global model runs and the regional model run is shown in Figure 5. The fluxes over sea are very similar for all models, but are different over land between the regional and the two global models. The latent and sensible heat fluxes simulated with the regional model are stronger, and the solar and terrestrial radiation are reduced.
Overall it must be mentioned that the intercomparison is very difficult, since the regional model simulates a different climatic state due to the ocean - atmosphere coupling. It seems that especially over the area of interest, the Baltic Sea basin, the flow is too zonal.

4 LINK BETWEEN HYDROLOGICAL AND ATMOSPHERICAL PROCESSES

Since the problems of scale, sub-grid variability and macro-scaling have been identified as key issues in climate modelling, research is looking at the link of hydrological and atmospherical models. One research activity in GEWEX (Global Energy and Water Cycle Experiment) is the interaction and improvement of atmospheric and hydrological models at global and regional scales. Within BALTEX (Baltic Sea Experiment) - a continental scale experiment of GEWEX - links between hydrological and atmospheric climate models are established on the macro-scale. The conceptual HBV - hydrological model is applied to the Baltic basin and will be used for intercomparison and validation of the global and regional climate models. The objective for the development of a macro-scale hydrological model for the basin is the intercomparison between processes described in hydrological models and climate models and validation against runoff data. The HBV-model has been calibrated and validated using runoff data on a monthly basis for 12 years.

With the global climate model ECHAM4 a ten-years long integration on T106 resolution for present climate has been performed. The simulated precipitation and temperature data from ECHAM4 were used as driving fields (input) for the HBV-model. Both models calculated the hydrological components (e.g. runoff, soil moisture, snow depth and snowmelt) using identical meteorological driving fields.

Only a few subbasins have been intercompared up to now. Preliminary results show that there are major differences in the snow water equivalent, however, the soil moisture dynamics show great similarities. The differences concerning the snow variables seem to be related to different evapotranspiration parameterizations. A detailed investigation of the model results as well as the mentioned approach is under way.

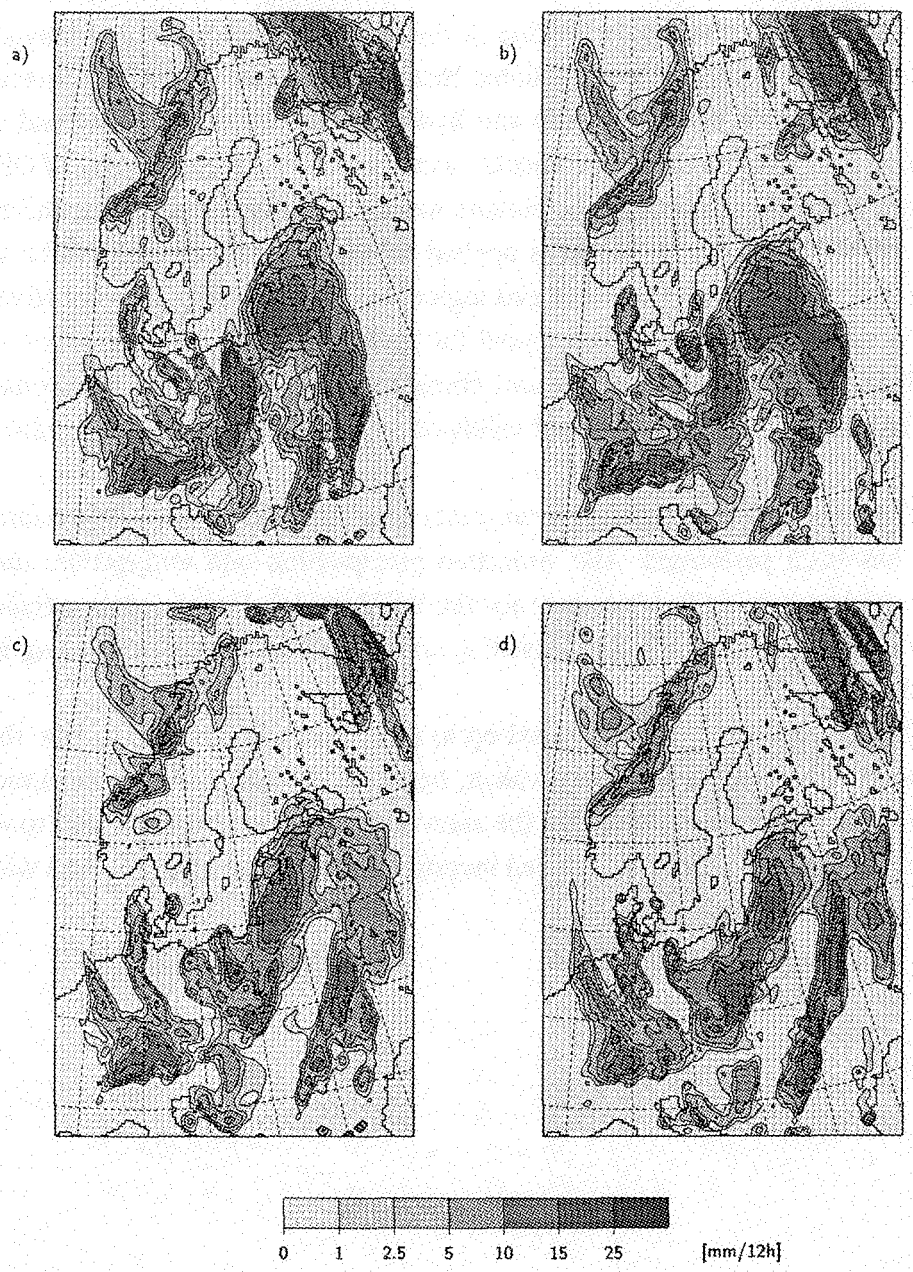

Figure 2: Total precipitation [mm/12h] for August 29th 1995 18h. a: 30h – DMI; b: 30h – DWD; c: 78h – DMI; d: 78 std – DWD.

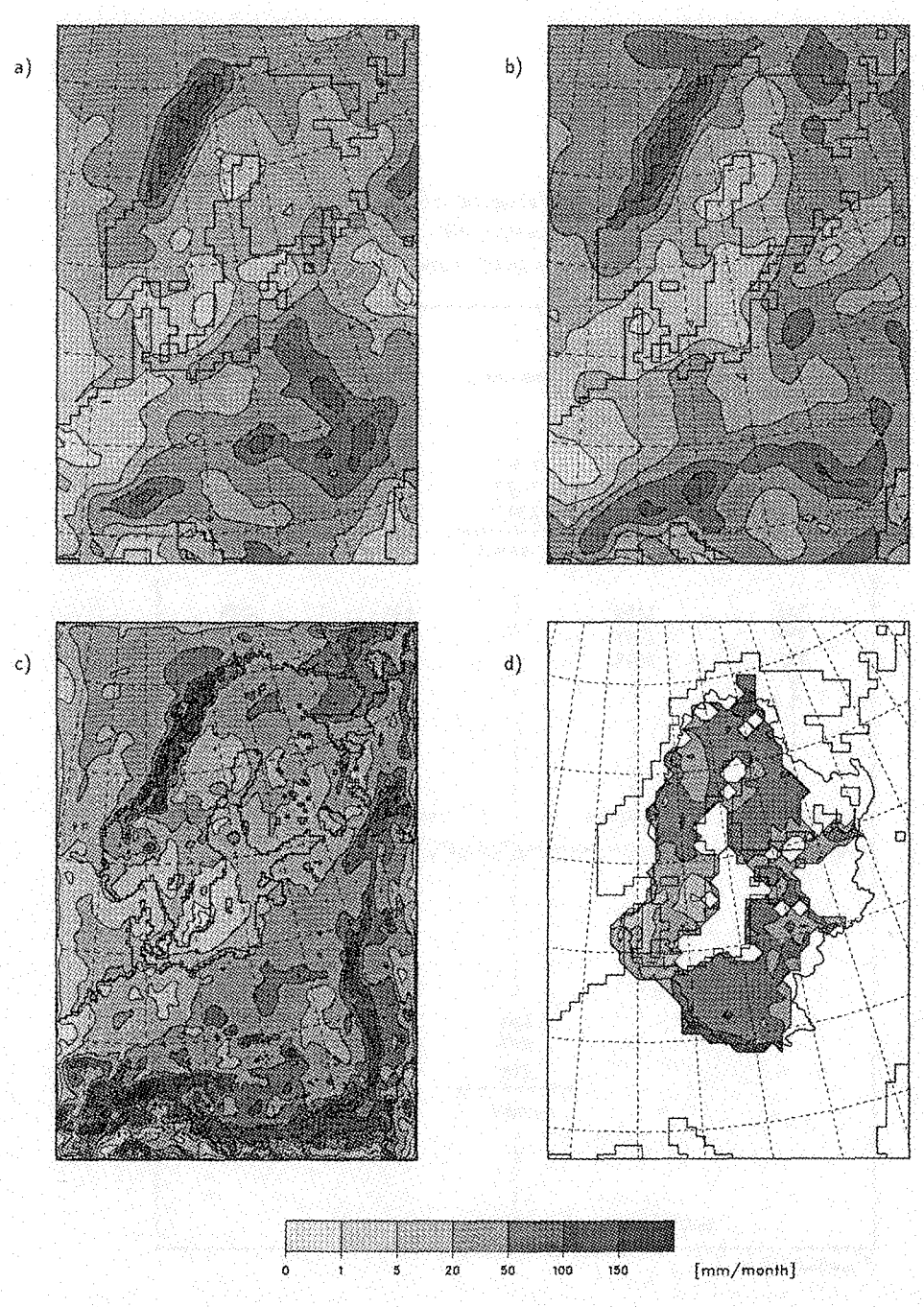

Figure 3: Total precipitation [mm/month] for August 1995. a: DWD–physics 0.5°; b: ECHAM4–physics 0.5°; c: DWD–physics 1/6°; d: observations.

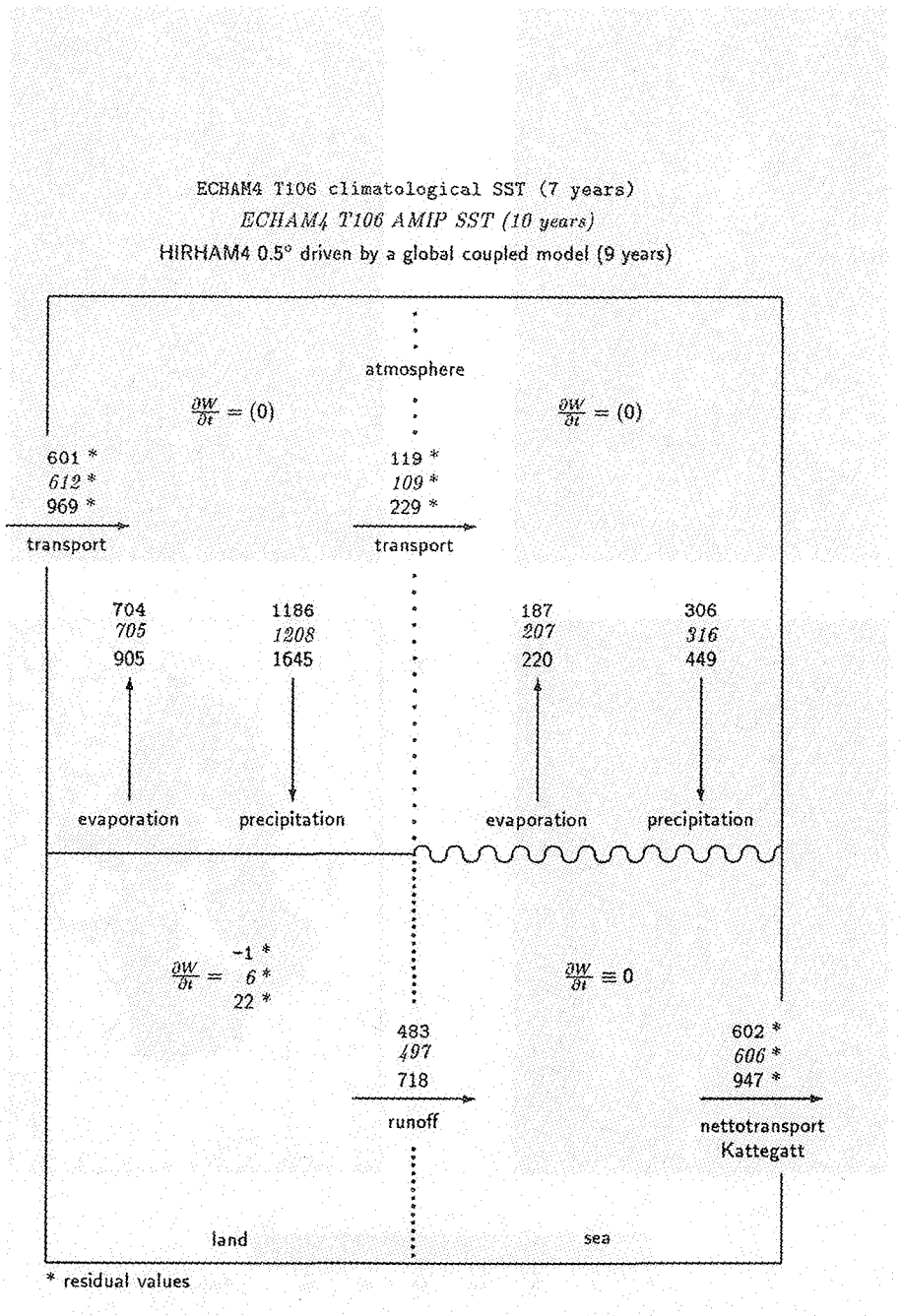

Figure 4: Water budget for Baltic Sea drainage basin [km^3/year]

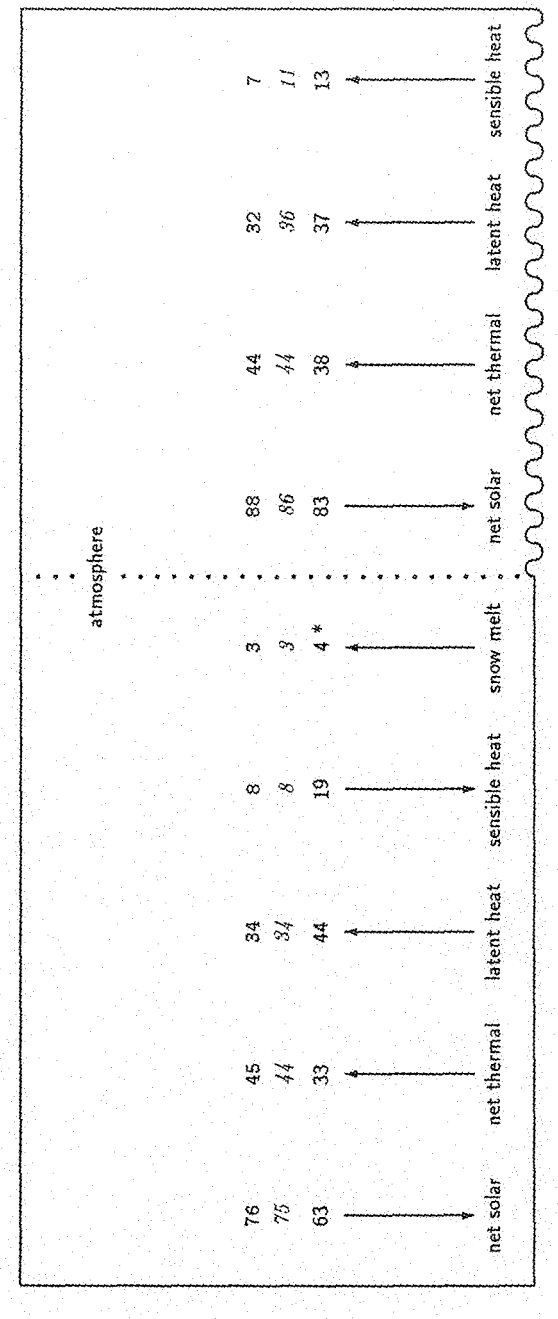

Figure 4: Energy budget for Baltic Sea drainage basin [W/m^2]

Figure 5: Energy budget for Baltic Sea drainage basin (Wm^{-2})

SNOV COVER SIMULATIONS IN THE BALTEX AREA USING A GLOBAL CLIMATE MODEL

Bettina Loth, Lennart Bengtsson, Daniela Jacob
Max-Planck-Institute for Meteorology, Bundesstrasse 55
D-20146 Hamburg

ABSTRACT

The simulation quality for snow has been analysed for the Hamburg climate model ECHAM4. This global model relatively well captures the snow properties in the BALTEX region. The differences to observations (up to 15 % for snow area, 10 % to 70 % for snow mass) are mainly smaller than the measuring uncertainties. Less than observed snow is calculated over the western part of the BALTEX area, whereas more than observed snow is simulated over the eastern part of this region.

The differences between the observed and simulated values mainly result from inaccuracies of the simulated circulation of the atmosphere. These uncertainties, which are partly determined by the differences in model and real topography, are connected with biases in near surface temperature and precipitation. An in-depth analysis of the causes as well as the question whether the changes due to the implementation of the multi-layer snow model are within the limits of climate variability are under investigation.

1 INTRODUCTION

The snow cover is an important component of the global and regional energy and water cycles. It leads to a temporal shift in the discharge as well as to a net cooling of atmosphere and surface on time scales ranging between hours and centuries (cf. Walsh, 1993).

In the BALTEX area, snow may influence the surface fluxes from late September to early June. The whole area may be snow covered for several weeks. Temporal snow conditions with stronger melting processes and embedded snow-free periods occur at the south boundary of the BALTEX area (50° N to 55° N), whereas in the north (65° N to 70° N) snow usually persists from the end of September to April/May. The deepest snow covers (monthly mean values between 80 cm and above 100 cm) occur over the north-western part of Sweden in February

This paper describes the simulation quality for snow in the BALTEX area using the climate model ECHAM4. Results are shown for integrations of the ECHAM4 standard version and the case that ECHAM4 is coupled to a multi-layer snow model. The estimated snow properties (snow area, mass, depth) are compared with observations. A summary is provided in the final section.

2 MODEL AND OBSERVED DATA DECRIPTION

2.1 Model and Experiments

The recent version of the atmospheric climate model ECHAM (ECHAM4, Roeckner et al., 1996) has been used with climatological values of sea ice coverage, a triangual truncation of T42 (about 2.8° x 2.8°) 19 vertical levels up to 10 hPa (30 km) and a time step of 24 minutes.

The simulation quality for snow has been analysed for three model performances:

- a 30-year run using climatological SST
- a 10-year integration using the observed SST from 1979 to 1988 (AMIP period)
- a 10-year integration using a multi-layer model for the snow cover (Loth et al., 1993) and climatological SST values.

We have focused on the verification of global simulations, since these integrations provide the boundary conditions in studies with regional climate models and some of the regional models (e.g. REMO) have a version in which the ECHAM4 physics is used.

2.2 Observed Data Sets

The simulated snow properties are compared with the values from two observed data sets: the snow depth climatology (revised version of Foster and Davy, 1988), which is based on ground measurements, and the passive micro-wave measurements of snow depth from 1978-87 (Foster et al., 1996), which nearly cover the AMIP period. A fixed value of 300 kg/m^3 is used to derived snow mass estimations from these observations. Since observed densities usually range between 10 kg/m^3 for newly fallen snow under calm conditions to 450 kg/m^3 for aged snow, taking this snow density leads to a potential overestimation of snow mass in autumn and early winter, whereas the snow mass is probably underestimated in spring and early summer.

The satellite data leads to generally smaller values of snow area and mass compared to the ground observations. The derived snow areas differ by 0.3 to 0.6 Mio. km^2 whereas the snow masses deviate by 16 $*10^{12}$ to 73$*$ 10^{12} kg. These differences mainly result from uncertainties in the satellite data (Foster et al., 1996).

3 RESULTS

3.1 Snow Area and Mass

The recent version of the global Hamburg Climate Model (ECHAM4) well captures the snow extent and the accumulated snow mass (Figure 1). Both snow properties are modelled with a relatively high accuracy. The differences between the snow area derived from the snow depth climatology and the simulated snow extent are less than 15 %. These differences are smaller than the measuring uncertainties, in particular in October and November. The snow mass differences are also rather small (less than 10 %) from October to February. They increase in March to May, when the simulated masses using the ECHAM4 standard version exceed the values derived from the snow depth climatology by about 20$*10^{12}$ kg to 40$*10^{12}$ kg (about 40 % to 70 %).

In comparison to the 30-year control run and the AMIP estimation, the 10-year integration with ECHAM4 coupled to the multi-layered snow model leads to smaller values of both snow area and snow mass. The largest changes in snow area (about 0.3 Mio. to 0.4 Mio. km^2) occur in October and May, when the snow coverage partially disappears in the area north of the Baltic Sea using ECHAM4 coupled to the multi-layer snow model. Whereas the smaller value of snow area in October ranges between the two observations and might be in a better agreement with the observations, the snow area in May seems to be underestimated using the multi-layer snow model. However, the simulation quality of the spring snow mass is significantly improved in this 10-year integration. The general overestimation of spring snow mass calculated by the ECHAM4 standard version disappears completely. Compared to the results of the ECHAM4 standard version the snow mass is reduced by about 20 to 50$*10^{12}$ kg from December to May.

The differences in snow using the ECHAM4 standard version and the ECHAM4 coupled to the multi-layer model mainly originate from three factors; i) changes in the accumulation rate, ii) changes in the simulated near-surface temperatures and iii) changes in the modelled surface fluxes and snow processes due to the new snow parameterization. In all simulations, the 30-year control run, the AMIP calculation as well as in the 10-year simulation using the multi-layer snow model, the winter precipitation exceeds the observed values (Legates and Willmott, 1990a) by

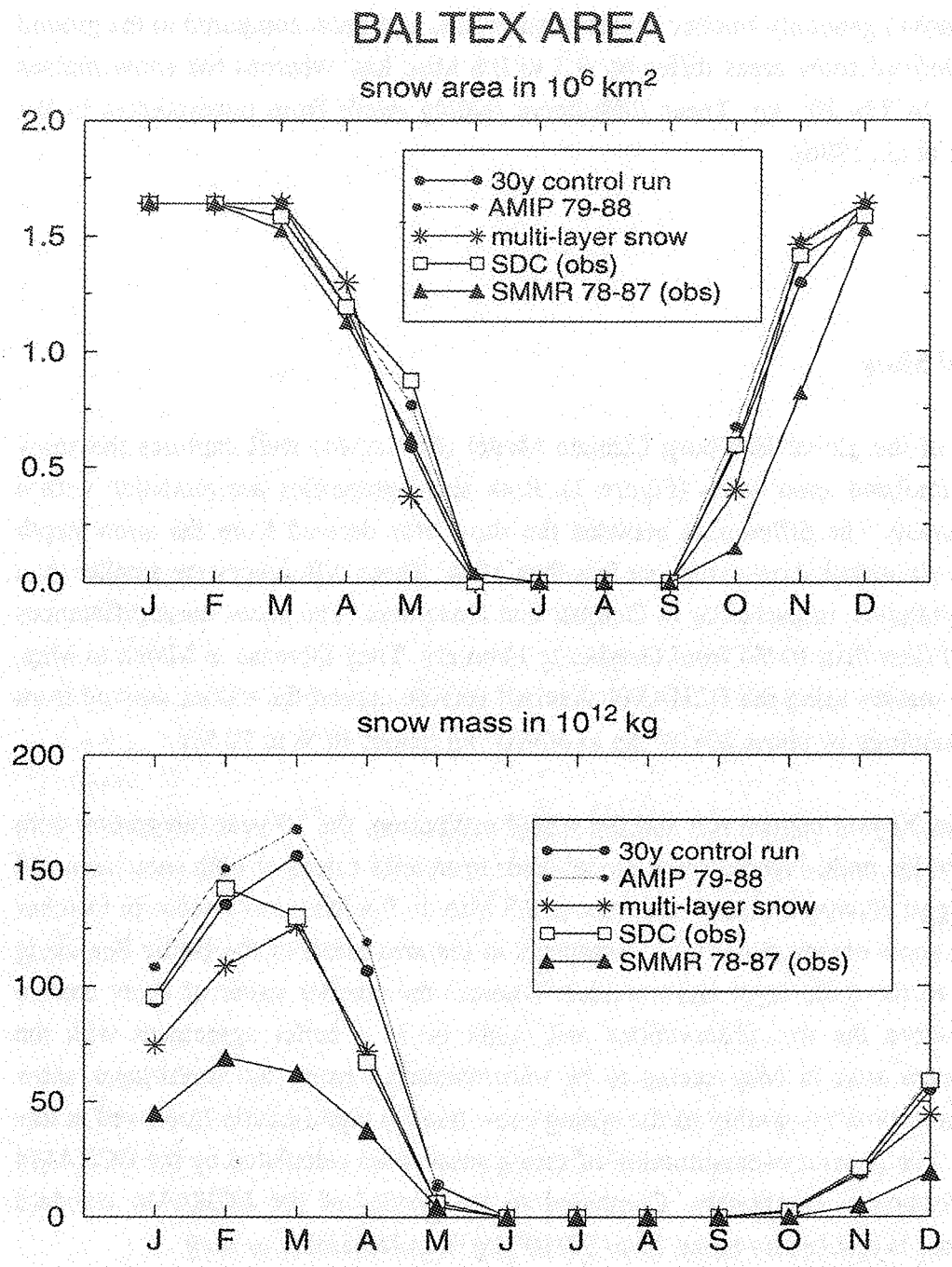

Fig.1: Mean annual cycle of snow area and mass derived from ECHAM4 climate simulations and observations. Simulation results are shown for the 30y control run, the AMIP period (1979-88) and the case that a multi-layer snow model was implemented into ECHAM4. The calculations are compared with values derived from ground observations (Snow Depth Climatology, revised version of Foster and Davy, 1988) and satellite data for 1978-87 (SMMR, Foster et al., 1996).

about 5 to 12 mm/month. That excludes the precipitation rate as the main factor of both the higher than observed spring snow mass using the standard ECHAM4 model (despite the precipitation bias) and the differences between the model simulations. The accumulation rate, however, is also determined by the snow-to-rain ratio, which is decreased in the simulations using the multi-layer snow model and thus leads to a lower snow accumulation. The probably too high snow percentage using the standard ECHAM4 as well as the simulated delay in the spring melting seems (at least partly) to result from the negative temperature bias of -1 K to -3 K lasting from January to April (compared to Legates and Willmott, 1990b). This bias reduces in winter and does not occur in March and April using the multi-layer snow model.

Since the three mentioned effects are mutually dependent and an increase in air temperature, for example, may have the same effect on the simulated melting processes as the better resolution of the processes in the model, it seems not easily possible to extract the direct effect of the new snow scheme.

3.2 Snow Depth

In general, the snow depth in the BALTEX area is also well captured by the ECHAM4 model. The annual cycle as well as the values of the single months are estimated with a relatively high accuracy. The maximum differences between the simulated and observed depths range between 10 cm and about 30 cm.

From October through May the simulations underestimate the observed values (snow depth climatology, revised version of Foster and Davy, 1988) in the western part of the BALTEX area, whereas the model results exceed the measurements in the eastern part of this region. Figure 2 shows the changes of the spatial extension and the amplification of these differences patterns throughout the winter season. In both simulations, the 10-year integration using the multi-layer snow model and the 30-year control run, the building up of the pattern starts in October with the appearance of the seasonal snow cover. Whereas in the 30-year control run the centres of the negative anomaly (-1 cm to -20 cm) are along the whole Norwegian-Swedish mountain chain, there are only two centres in the 10-year integration using the multi-layer snow model (South Norway and North-west Norway). About the same two centres show the highest changes in February (-20 cm to -30 cm) in the difference pattern of the 30-year control run, while for the 10-year integration using the multi-layer snow model larger differences (about -30 cm) occur over a relatively wide area of Norway. In May the negative part of the difference patterns is similar between the two integrations and similar to the autumn pattern of the ECHAM4 standard version. More than observed snow is simulated during the whole winter season over North-east Finland

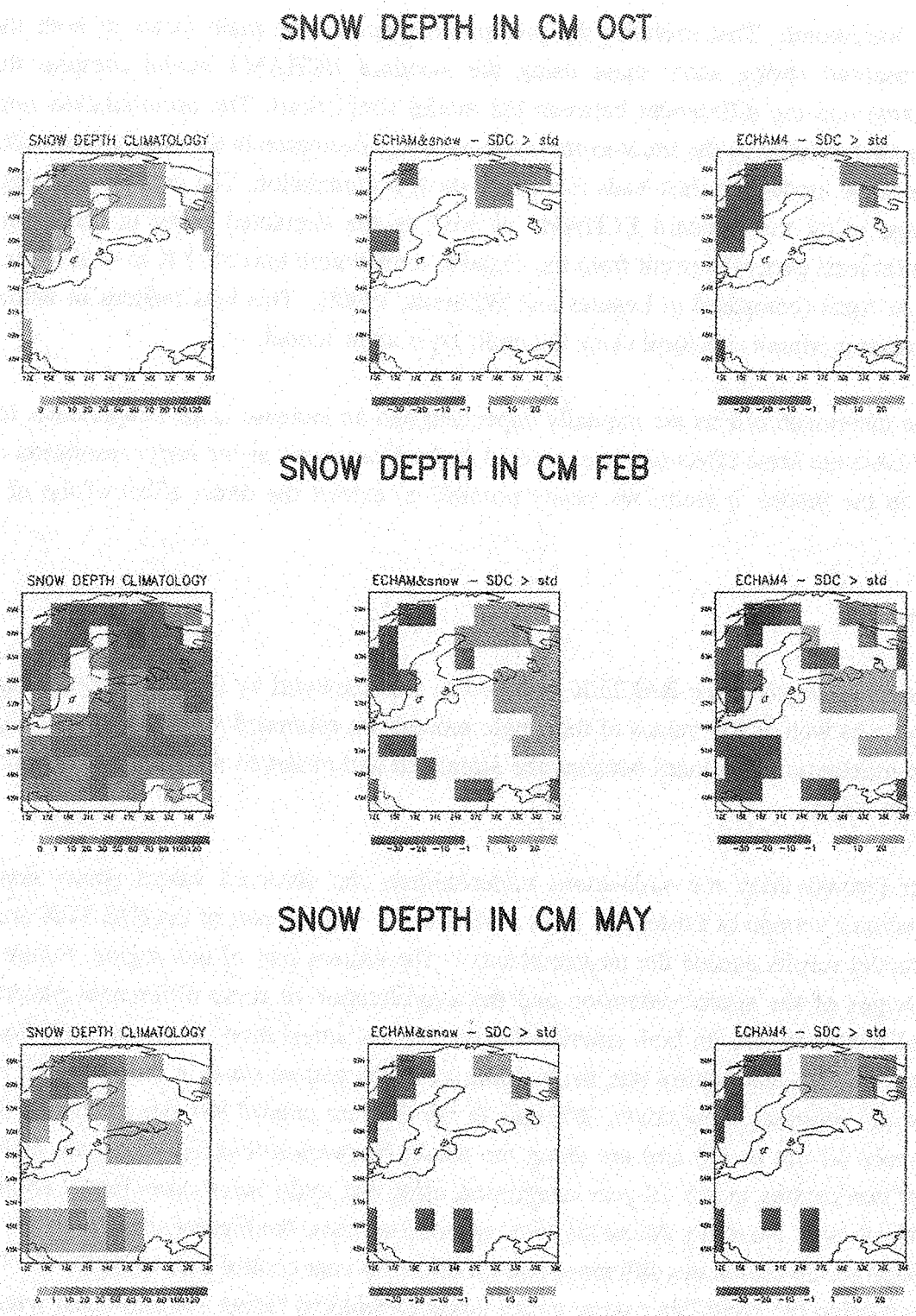

Fig. 2: Monthly mean values of observed snow depth and the differences to a 10y ECHAM4 integration using a multi-layer snow model and a 30y run of the ECHAM4 standard version. The drawn differences exceed one standard deviation of the simulations. The observed values are derived from the Snow Depth Climatology (revised version of Foster and Davy, 1988). Results are shown for the accumulation (October), ageing (February) and melting (May) periods.

and North-Carelia (+1 cm to +20 cm). In February both integrations also overestimate the snow depth over large parts of western and central Russia (+1 cm to +20 cm).

The changes in the simulation using the ECHAM4 standard version and ECHAM4 coupled to a multi-layer snow model mainly result from an increase in the air temperature and a lower snow-to-rain ratio when using the more sophisticated snow mass being transported to western Scandinavia and by the modification of the energy fluxes at snow surface due to the changed snow scheme. It could also be possible that the change in the surface parameterization directly has an impact on the simulated atmospheric circulation (track of cyclones, intensity and position of frontal zone) or that the changes are within the limit of natural climate variability.

One reason for the differences between the observed and simulated snow depths seems to be the deviation of real and model topography, which affects the atmospheric circulation as well as the precipitation rate and the air temperature. For the western part, for example, the model altitude is lower than the observed altitude. Consequently, the simulations potentially end up in a positive temperature bias and less than observed precipitation over this area. Further these differences can partly be caused by uncertainties in the observations. A part of the deficiency can probably result from the snow parameterization (e.g. sub-grid variability of the snow cover might not be adequately resolved).

3.3 Measuring Uncertainties

In order to get an insight into the quality of the observed snow data the global snow depth climatology (revised from Foster and Davy,1988) has been compared with the mean value of the measured snow depths over Sweden during the period of 1961-90. Both sets are based on ground observations and interpolated on a T42 grid (about 2.8° x 2.8°).

The observed snow depths differ between 1 cm and about 20 cm (locally even more). The snow depth climatology tends to smaller values than those derived from the 1961-90 period.

4 SUMMARY

The ECHAM4 model relatively well captures the snow properties (snow area, snow mass and monthly mean values of snow depth) in the BALTEX region. The differences between the values derived from the observations and the model performances (up to 15 % for snow area, about 10 % to 70 % for the integral snow mass) are mainly smaller than the measuring uncertainties. The snow depth deviations range between 1 cm and 30 cm. Less than observed snow is calculated for

the western part of the BALTEX area, whereas more than observed snow is simulated for the eastern part of this region.

Compared to the standard version of ECHAM4 the implementation of a multi-layer snow model leads to an improvement in the simulation of the ablation processes. Nearly the same difference patterns of observed and simulated values is calculated for both integrations.

The main causes for the differences between the observed and simulated values are probably uncertainties in the simulated circulation of the atmosphere, which are connected with biases in both near surface temperature and precipitation. The differences are further influenced by the uncertainties of the observed data (e.g. up to 20 cm in snow depth).

Using the synoptic data of the 1981-94 period we are going to analyse the differences between the observed and simulated values of surface pressure, air temperature at 2 m altitude, precipitation and snowfall rate. The goal is to find out the mechanisms behind the simulated uncertainties and to compare the variability of the simulated and observed atmospheric and snow parameters.

REFERENCES

Foster. D. J. and D. R., Davy, 1988: "Global Snow Depth Climatology", USAF Publication USAFETAC/TN-88/006, Scott Air Force Base Illinois, 48 pp.

Foster, J.; G. Liston, R. Koster., R. Essery, H. Behr, L. Dümenil, D. Verseghy, S. Thompson, D. Pollard and J. Cohen, 1996: "Snow Cover and Mass Intercomparisons of General Circulation Models and Remotely Sensed Data", J. Clim. **9(2)**, 409-426.

Legates, D.R. and C. J. Willmott, 1990a: "Mean seasonal and spatial variability in gauge corrected global precipitation", J. Climatol. **41**, 11-21.

Legates, D.R. and C. J. Willmott, 1990b: "Mean seasonal and spatial variability in global surface air temperature", Theor. Appl. Climatol. 111-127.

Loth, B.; H. F. Graf and J. M. Oberhuber, 1993: "A Snow-Cover Model for Global Climate Simulations", J. Geophys. Res., Vol. 98 20D6, **10**, 451-10,464.

Roeckner, E.; K. Arpe, L. Bengtsson, M. Christoph, M. Claussen, L. Dümenil, M. Esch, M. Giorgetta, U. Schlese, U. Schulzweida, 1996: "The atmospheric circulation model ECHAM-4: Model description and simulation of present-day climate", MPI-Rep. **218**, MPI für Meteorologie, Hamburg, 90 pp.

Walsh, J.E., 1993: "Observational and Modeling Studies of the Influence of Snow Anomalies on the Atmospheric Circulation", in Shukla, J."Predictions of the Interannual Climate Variations", NATO ASI Series **6**, 89-105.

Validation of numerical precipitation forecasts by in situ measurements at sea

Martin Grosskiaus, Lutz Hasse
Institut für Meereskunde, Düsternbrooker Weg 20, D-24105 Kiel, Germany
Daniela Jacob
Max- Planck- Institut für Meteorologie, Bundesstrasse 55, D-20146 Hamburg, Germany

1 INTRODUCTION

Precipitation at sea forms a strong branch of the Baltic Sea hydrological cycle. Yet, undisturbed precipitation measurements at sea, except from a few stations at small islands, are practically not existent. We hope that in future numerical weather forecast models and remote sensing methods will provide improved precipitation estimates. However, weather forecast models and remote sensing techniques (e.g. seaward looking radars) urgently need ground truth at sea.

This note deals with the results of a first model validation study that has been performed with aid of in situ precipitation measurements on the Baltic Sea.

2 INSTRUMENTATION

Conventional rain collecting instruments fail when used at buoys or ships. The problem stems from the often rather high flow velocities around rain gauges at ships that may result from addition of wind and ship velocities. Therefore we use ship rain gauges developed at the Kiel Institut für Meereskunde (Hasse et al., 1997). A sketch of the ship rain gauge is given in Figure 1.

In order to mitigate the flow distortion by the gauge itself the upper collector has a slender conical shape that roughly corresponds to the champagne bowl design recommended by Folland (1988). A unique feature of this instrument is its additional lateral collector. This does not measure rainfall, but the amount of rain-drops carried with the air. The catch (N) during the sampling period (T) is proportional to the local flow velocity (U) and to the cross-section of the surface (A). Hence the fraction $N / (A*U*T)$ directly yields the liquid water content (LWC) in a unit volume of air. This measurement is independent of inclinations of the local flow. The local wind speed has to be determined by an anemometer mounted nearby the rain gauge. From the liquid water content of the air one can estimate the rainrate (RR) assuming a relation between LWC and RR. We empirically deduced this relation from the analysis of long-term disdrometer measurements on board R/V 'Alkor':

$$RR = 24.6 \cdot LWC^{1.3}$$

This equation requires the liquid water content in units of grams per cubic meter and returns the rainrate in mm/h.

Both the measurements of the upper and the lateral collecting surface are affected by wind induced undercatch. This is being compensated by an algorithm that has been determined from simultaneous measurements with an optical disdrometer, which can be regarded as unbiased. At low wind speeds, where the rain falls nearly vertically, collection at the top gives a good measure of the rainrate with few correction needed, at the same time sampling at the side is unsatisfactory. At high velocities sampling at the side gives a rather good estimate of rainfall, while measurements at top would need extensive correction. Hence a final rainrate is determined by the upper collecting surface at low wind speeds and by the lateral surface at high wind speeds with a linear transition between 9 m/s and 11 m/s.

3 DATA

As a contribution to the BALTEX experiment we supplied five ferry ships with a ship rain gauge, an anemometer and a GPS (Global Positioning System) receiver. These ferries shuttle between Lübeck (Germany) and the Finnish harbors Helsinki, Kotka or Hankö. Two more ship rain gauges are installed on offshore masts at Darss sill and Östergarnsholm (east of Gotland). Finally there are one German and one Finnish research vessel (R/V 'Alkor' and R/V 'Aranda', resp.) equipped with each a precipitation measuring system. Common sampling interval for all these gauges was eight minutes.

Model data for the PIDCAP-period were available from the regional model 'REMO' (operated by the Max-Planck-Institut für Meteorologie, Hamburg) and the 'Europamodell' (Deutscher Wetterdienst). Both models have the same model physics implemented. The main difference lies in the mode of operation: The 'Europamodell' (EM) has been re-initialized for each day using current fields of analysis, while REMO was initialized only once for the whole PIDCAP-period but using analysed parameter fields as forcing at the borders of the model domain. The temporal resolution of the 'Europamodell' (EM)-data was 6 hours and 1 hour for the REMO. Both model data sets were given on the same 0.5 x 0.5 degree grid over the Baltic Sea.

4 METHOD

It is not possible to directly calculate daily or monthly sums of precipitation from the in situ measurements, because the grid boxes along the ship's track are not permanently occupied by a ship. Hence the calculation of a measured PIDCAP precipitation total would require considerable extrapolation. So the technique used for the intercomparison was to compare each ship measurement with the corresponding model prediction. This has been done applying the following steps:

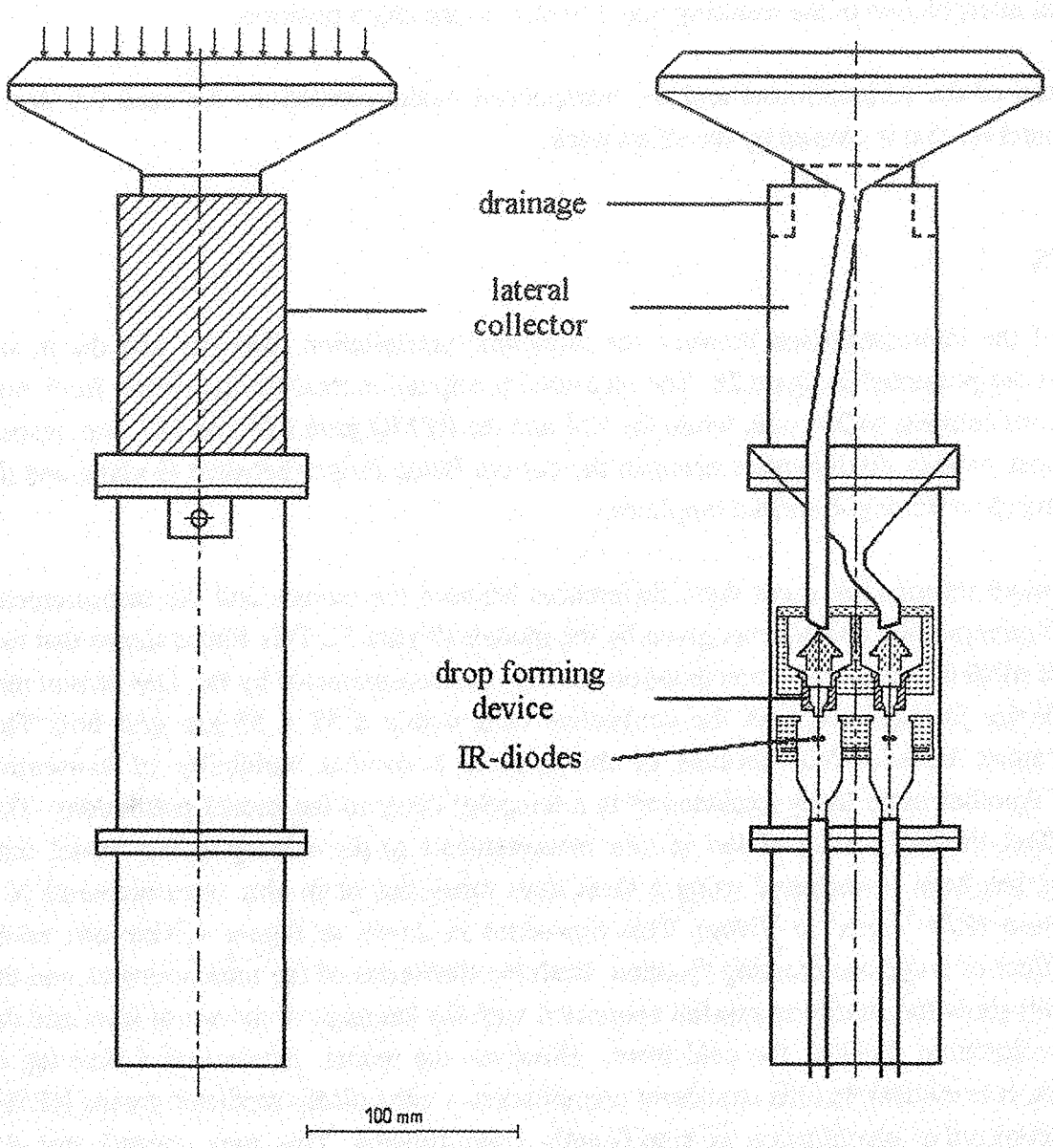

Figure 1: Side view (left) and cross-section (right) of the ship rain gauge. Rain is collected at the horizontal orifice (arrows) and at the lateral collector (shaded). There are 5 vertically running T-bars (not shown in the sketch) around the lateral collector that hinder the water drifting around the cylinder and be blown off in the lee. Total length is 48.5 cm and weight 4.0 kg.

i) Assignment of the in situ measurement to the corresponding model time interval and grid box.

ii) In order to artificially enhance the crude temporal resolution (especially of the EM-data) a timeseries was constructed by fitting a second order polynominal to the data of three subsequent time intervals (with the corresponding interval in the middle). This fit was also performed for the

eight surrounding grid boxes. These timeseries were used to calculate the rainrate at the time of the in situ measurement for the nine grid boxes concerned.
iii) Horizontal interpolation of the resulting nine rainrates to the ship's position.

iv) Cumulation of the measurements and the interpolated model predictions for each 0.5 degree longitudinal interval that is crossed by the ship's track.

5 RESULTS

The results of the intercomparison between the numerical precipitation forecasts and the in situ measurements are presented in figure 2b. The measured precipitation total for the period from Aug. 13th to Nov. 5th amounts to 297 mm, while the EM and the REMO gave 638 and 427 mm, respectively. The most striking discrepancies occur in the eastern Baltic Proper between Gotland and the Gulf of Finland (5 to 6.5 deg. E rotated longitude).

One can get more information about these differences between the models and the measurements looking at the precipitation components given by the models (Figure 3). This figure shows that east of Gotland the modelled convective precipitation exceeds the measurements by far. One reason may be that the ferries just did not meet the convective cells within a 55 x 55 km grid box. This assumption cannot be excluded, because of the extreme horizontal variability of convective precipitation. Another more likely explanation is a temporal delay in the model predictions. This delay may affect the assignment of the in situ measurements to the corresponding model time intervals. This has been investigated using a three days timeseries of in situ measurements at a constant position (R/V 'Alkor' in Visby). This timeseries is shown in Figure 4. One can easily identify the effect of a cyclone crossing Gotland. Both the timeseries of the measurements and the REMO (run 59) show the stratiform rainfall connected with the intercept of the warm front and the convective precipitation behind the cold front. However, the model data reveal a time lag of about 10 hours. It is evident that the stratiform precipitation is quite nicely predicted by the REMO whereas the convective precipitation is significantly overestimated. This may suggest that the discrepancies between the measured and modelled precipitation as shown in Figure 2b are mainly due to an overestimation of convective precipitation by the numerical models, although this cannot be verified by this example only.

6 CONCLUSIONS

Long-term operation of ship rain gauges showed the feasibility of precipitation measurements at moving ships. Calibration is obtained at sea by simultaneous measurements with an optical disdrometer. Ship rain gauges are successfully being used in BALTEX for the validation of numerical precipitation forecasts and remote sensing products. An intercomparison between in situ measurements of precipitation and numerical forecasts revealed a significant overestimation of rainfall by

the models for the PIDCAP-period. 1996 data showed a rather variable relation between precipitation measurements and EM-forecasts indicating that the results presented here are not a typical feature of the model forecasts. The international introduction of ship rain gauges to Voluntary Observing Ships will make it possible to extend studies like this to the world oceans.

Acknowledgement

We thank the Deutsche Forschungsgemeinschaft and the BMBF (German department of Science and Technology) for funding the development of the ship rain gauge as a contribution to WOCE (World Ocean Circulation Experiment). Poseidon Schiffahrt hosts five of our gauges on their route between Germany and Finland, we gratefully acknowledge their help. We thank the Deutscher Wetterdienst for making precipitation data available to us.

REFERENCES

Folland, C.K., 1988: Numerical models of the raingauge exposure problem, field experiments and an improved collector design. *Q.J.R. Meteorol. Soc.* **114**, 1485-1516.

Grossklaus, M., 1996: Niederschlagsmessung auf dem Ozean von fahrenden Schiffen (Precipitation measurement at sea from moving ship). *Berichte Inst. für Meereskunde Kiel*, **278**, 112 pp.

Hasse, L., M. Grossklaus and K. Uhlig, 1994: New ship rain gage. *Instruments and observing methods, report No 57.* World Meteorological Organisation, Geneva, WMO / TD-No **588**, 97-101.

Hasse, L., M. Grossklaus, K. Uhlig and P. Timm, 1997: A ship rain gage for use in high wind speeds. *J. Oceanic Atmos. Sci*, (revised).

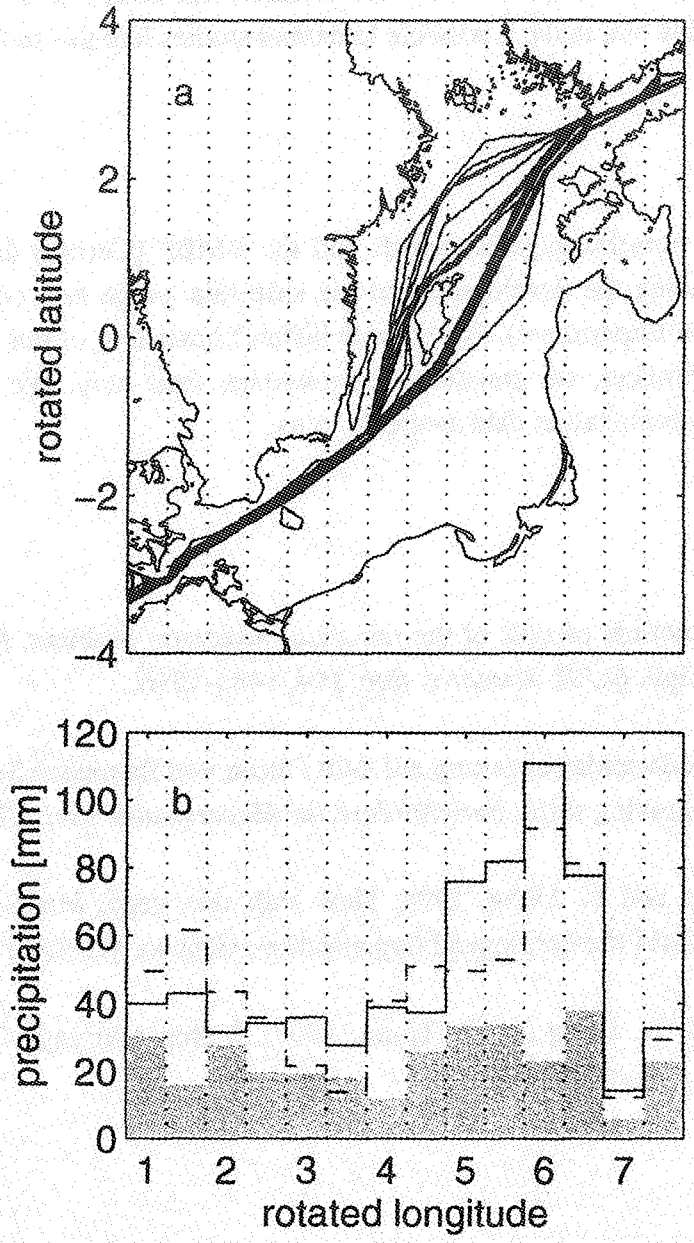

Figure 2 a): Track of the Baltic Sea ferries that are equipped with an ship rain gauge (PIDCAP- Period). This map is given using the rotated coordinate system of the models. The dotted vertical lines indicate 0.5 degree longitudinal intervals. b) Cumulated precipitation measured by the ferries (shaded columns) and the corresponding values of the EM (solid line) and the REMO, run 71 (dashed line).

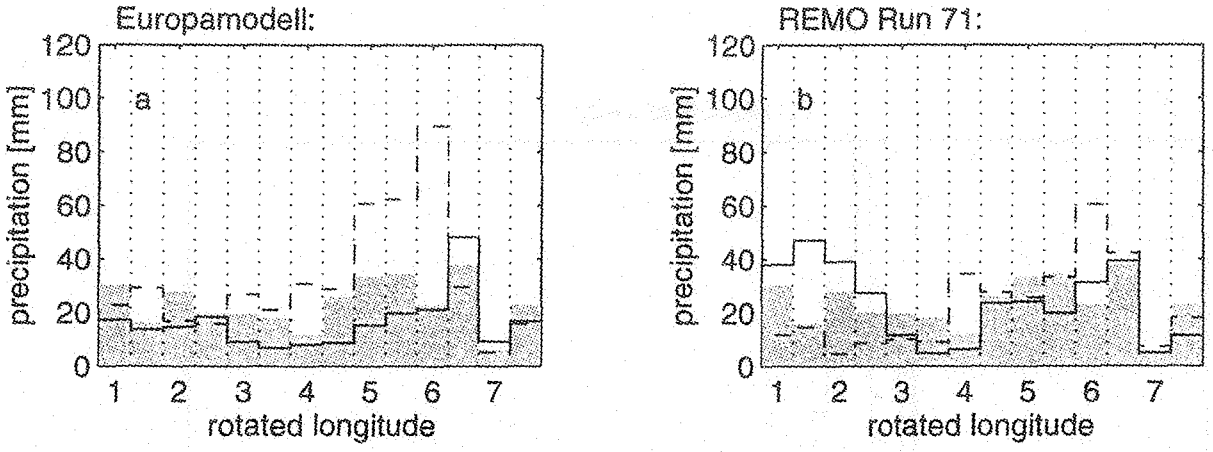

Figure 3: Cumulated precipitation along the ship's tracks. In situ measurements (shaded columns), convective portion (dashed line) and stratiform portion of modelled precipitation (solid line) are shown.

a) Components given by the EM;

b) Components given by the REMO (run 71).

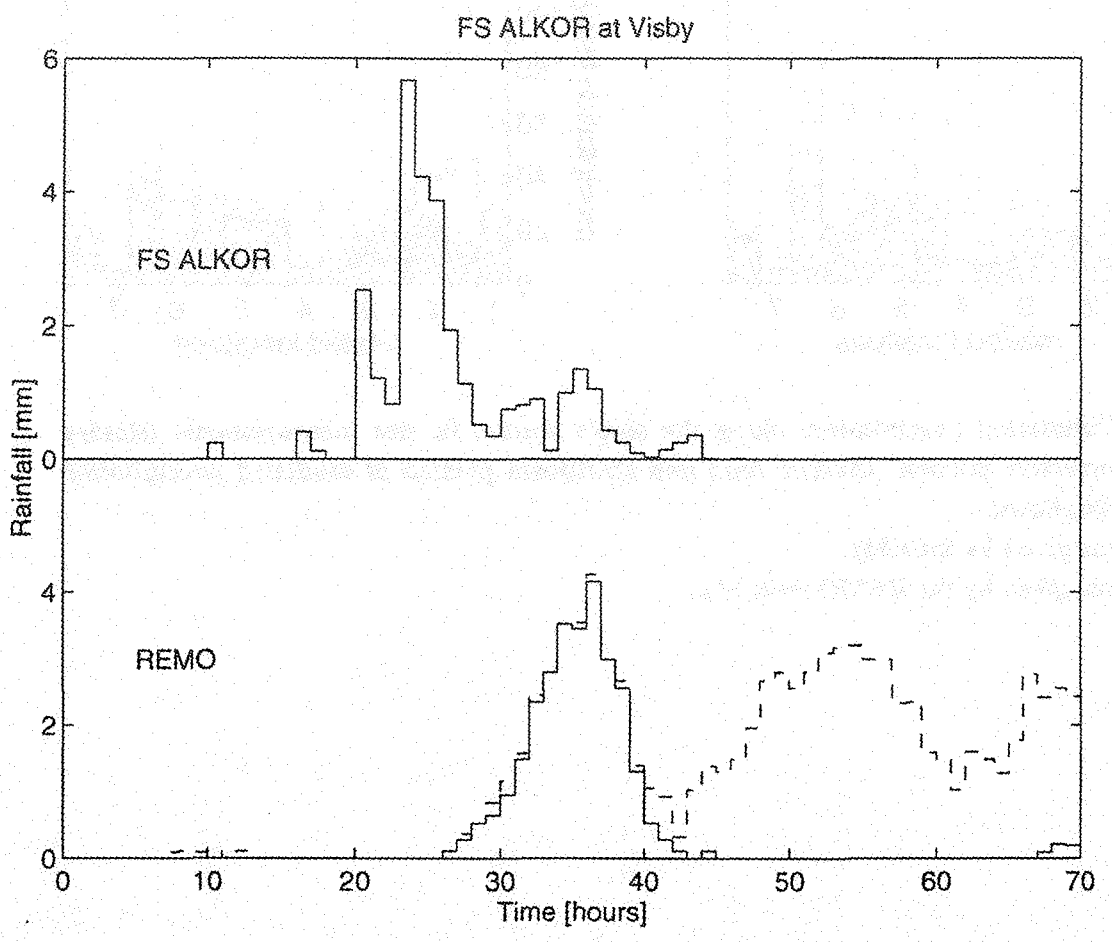

Figure 4: Timeseries of precipitation measured at R/V 'Alkor' (upper graph) and predicted by the REMO, run 59 (lower graph). Only for the model results the stratiform (convective) precipitation is marked by the solid (dashed) line. This timeseries covers the period from 8/29/95 2:00 UTC to 9/1/95 0:00 UTC. For this study we used the REMO 59 run, because at the time of publication these data were the latest available results with the high resolution of 18 x 18 km.

PIDCAP RE-ANALYSIS AND ATMOSPHERIC BUDGET DIAGNOSIS

Bent Hansen Sass and Xiaohua Yang
Danish Meteorological Institute
Copenhagen, Denmark

ABSTRACT

Data-assimilations have been made with the HIRLAM forecasting system for the PIDCAP period. The model set-up used for data-assimilations is briefly described, and problems related to an accurate determination of atmospheric moisture- and energy budgets are outlined. The temporal variation of the individual components of the atmospheric budgets of the Baltic catchment area is presented. This involves a distinction between the effect of dynamics and other processes such as radiation, condensation and turbulence. A preliminary comparison on a daily and monthly basis between model estimated precipitation and corresponding analysed precipitation gives good agreement for land areas where measurements with a relatively high density are available.

1 INTRODUCTION

The study of atmospheric humidity and energy budgets is of fundamental importance for the understanding of meteorological processes. A special feature of studies carried out for limited areas is the occurrence of fluxes of heat and moisture across the lateral boundaries. These types of studies have become increasingly important in recent years. Efforts are made to understand the complete hydrological cycle of the ocean-earth-atmosphere system of a specific region such as the Baltic Sea catchment area. A natural framework for numerical studies of the atmospheric parts of the budgets is given by a complete data-assimilation and forecasting system. The present study summarizes the results achieved with the HIRLAM forecasting system (Kallen 1996) when applied for the Baltic Sea and surrounding areas to study the atmospheric budgets during PIDCAP (Pilot Study for Intensive Data Collection and Analysis of Precipitation). This period is from August 1995 to November 1995. The HIRLAM forecasting system is developed in a collaborative project among the national weather services of Sweden, Norway, Iceland, Holland, Finland and Denmark. The system set-up is described in section 2. The results involving individual components of the humidity and energy cycle are described in section 3, and final remarks are given in section 4.

2 HIRLAM DATA ASSIMILATION SYSTEM

The goal of the system set-up for data-assimilation is to produce high resolution analyses and forecasts in a suitable area around the Baltic Sea. The HIRLAM 2.5 forecasting system is used (Kallen 1996).

The forecast model includes cloud water as a prognostic variable. The model has been upgraded with a non-local first order turbulence scheme used operationally at the Danish Meteorological Institute. The scheme is based on Holtslag and Boville (1993) and the development work during the HIRLAM collaboration. A double-nested system has been designed. The integration area of the coarse mesh model version (CSE) extends from Greenland and the Polar sea in the north to North Africa in the south. The eastern boundary goes through Russia, the Caspian Sea to the Red Sea. The western boundary goes through the central part of the North Atlantic Ocean. The model resolution is 0.4 degree in the horizontal and 24 levels in the vertical. The lateral boundary values are supplied by ECMWF- (European Centre for Medium Range Weather Forecasts) analysis fields with a horizontal resolution of 1.5 degree. The fine mesh model version (FIN) is run with a 0.2 degree horizontal resolution using 31 vertical levels. The integration area covers most of the European region, from the Polar sea in the north to the northernmost part of the Mediterranean region. The eastern boundary goes through Russia, the Black Sea and the western part of Turkey. The western boundary goes from the bay of Biscay trough Ireland to the Denmark Strait. Boundary values for this model version are supplied from the CSE model. The main reasons for choosing the double nested solution are the following: First, the available ECMWF analysis fields do not include 'cloud water' as a prognostic variable. By running the CSE version the cloud water field from that model can be supplied as lateral boundary values to the FIN model version. Second, the double-nested solution avoids potential numerical problems associated with a large change in horizontal resolution between a host model (ECMWF) and a high resolution internal model, in this case the FIN model version.

3 RESULTS AND DISCUSSION

a) Precipitation and evaporation

Table 1 summarizes monthly accumulated precipitation for the coarse mesh version CSE and the fine mesh version FIN. Also a separation between the BALTEX land area (catchment) and Baltic Sea is carried out. In general, the FIN model version gives slightly more precipitation than the CSE version. A preliminary comparison to the precipitation analyses for the period (Rubel 1996), which is based on raw rain-gauge data, indicates somewhat higher values diagnosed by the model (typically 10 - 20 percent). This is consistent with the corrections normally imposed on raw measurements in order to achieve the correct amounts. It is hard to prove that the precipitation amounts of FIN are more accurate than the corresponding results

from CSE. Table 1 reveals that the monthly differences in precipitation over the land area and the sea area are significant, although not dramatic, and may change sign from month to month. That is, in September the precipitation over Sea exceeds that over land while the reverse situation occurs in August. In October the differences are rather small and of a different sign in the two versions. Figure 1a shows the day to day values from August to November of the area averaged 24-hour precipitation for the entire Baltic catchment area. The corresponding computation valid for the Baltic Sea is shown in Figure 1b, which exhibits a significant day to day variability. On a smaller area the weather conditions may be dominated by either fair weather or rainy weather on a given day. This is consistent with the larger variability in Figure 1b over the Baltic Sea which is smaller than the catchment area. The maximum values exceed 10 mm in one day. Also the precipitation minus evaporation over the Baltic Sea have been computed (not shown). The results indicate that this parameter changes sign from month to month, being positive in September and October 1995, but negative in August and November 1995.

b) Moisture- and energy budgets

The computation of accurate energy and moisture budgets is not a trivial task. There are two principal problems. First, the computation of vertically integrated fluxes across the lateral boundaries requires very accurate wind components in order to reduce inaccuracies in the large fluxes involved. Second, the accuracy of the diagnosed processes such as precipitation is dependent on the uncertainties associated with the parameterized processes in the atmospheric model. Figure 2a shows individual components of the moisture budget over the entire Baltic catchment area. The values apply to changes over one day ($kg/(m^2\ day)$), and the individual terms represent evaporation, rain, snow, the total effect of physics, and the total effect of physics plus dynamics. The numbers in the legend apply to averages over the entire 4 months period. It is seen that the day to day variability is dominated by precipitation release and dynamic effects. In the case of significant low pressure systems entering the area these terms are often large opposing terms, e.g., in late August and in the beginning of September 1995. However, the results for late September (day 57 - 60) show that significant precipitation release may occur without strong net dynamic effects. In October and November 1995 snow events have been reported (e.g. Isemer 1996) which are reflected in the model. Figure 2b shows similarly the energy changes from day to day over the entire catchment area. The curves represent precipitation, solar radiation, long-wave radiation, surface sensible heat flux, total effect of physics, and total effect of physics plus dynamics.

Table 1: Statistics of Monthly Precipitation

Period	Model Resolution	Baltic Catchment Area (mm)	Baltic Sea (mm)	BALTEX Land Area (mm)
August	CSE	64.85	55.17	66.99
	FIN	72.57	61.08	75.30
September	CSE	75.34	92.24	71.58
	FIN	80.29	105.96	74.19
October	CSE	61,16	58.56	61.73
	FIN	65.41	67.28	64.97
August-October	CSE	201.34	205.98	200.30
	FIN	218.27	234.32	214.46

A number of characteristic features are apparent. The net long-wave cooling of the area is a dominating term and relatively constant throughout the PIDCAP period. The cooling is normally in the range between 150 and 200 Wm^{-2}. The solar heating rate is smaller and decreases as expected from about 80 Wm^{-2} in the first part of August to about 20 Wm^{-2} in the last part of November. The sensible heat flux is rather small, especially in October and in November where it changes sign between slightly positive and negative values. Latent energy fluxes are much more variable and exceeds values of 100 Wm^{-2}. Since the individual physical processes partly compensate one another the net effect of physics is often small in the first part of the PIDCAP period, and only rarely reaches positive values in the October and November 1995. It is seen that the daily variability from all processes including dynamic effects is very large in October and in November. The peak events up to about 600 W/m^2 on the positive side, and about -400 Wm^{-2} on the negative side are remarkable. They are synoptically associated with the passage of warm ridges and cold troughs, respectively, over deep layers.

4 FINAL REMARKS

A framework for atmospheric diagnostic studies for the PIDCAP period on a limited area has been briefly outlined above, and results of moisture and energy diagnostics over the Baltic Sea catchment area have been presented for the PIDCAP period. More diagnostics are produced in the modelling framework, e.g. the diagnosis of hourly variations and vertical profiles of temperature and humidity tendencies due to various processes. These additional features are

useful for detailed diagnostic studies on various time scales and also in the process of further improving the formulations of various meteorological processes in the model.

REFERENCES

Holtslag, A.A.M and B.A. Boville, 1993: Local versus Non-local Boundary Layer diffusion in a Global Climate Model. J.Climate, **6**, 1825-1842

Isemer, H.-J., 1996: Weather Patterns and Selected Precipitation Records in the PIDCAP period, August to November 1995. GKSS Report 96/E/55, Geesthacht, Germany.

Kallen, E. (editor), 1996: The HIRLAM system 2.5 Documentation Manual, June 1996, 178pp, [Available from SMHI, S-60176 Norrkoping, Sweden]

Rubel, F., 1996: PIDCAP Quick look Precipitation Atlas, Central Institute for Meteorology and Geo-dynamics, Vienna. Publ. no. 374

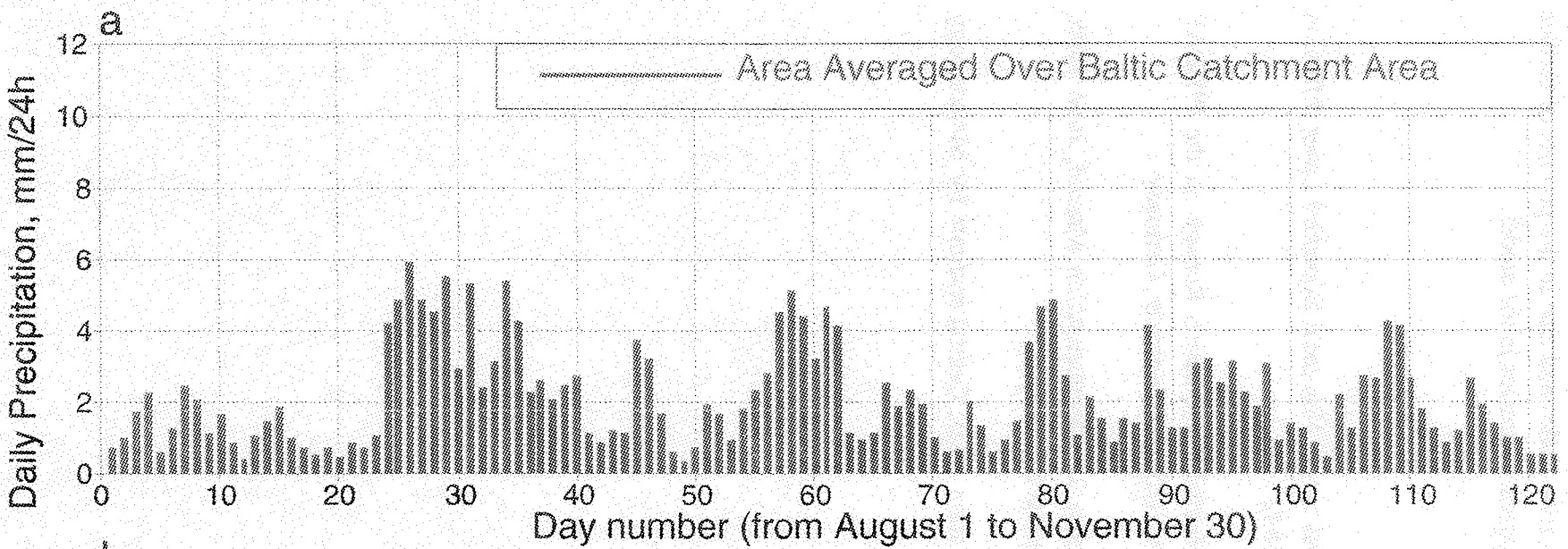

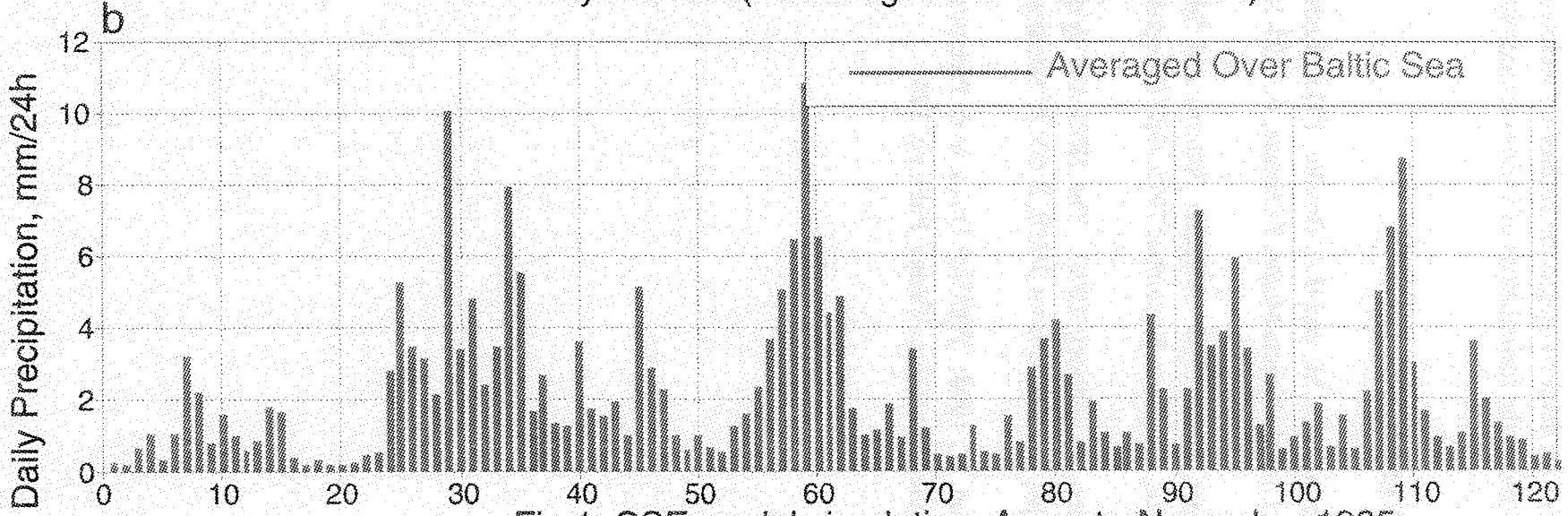

Fig 1. CSE model simulation, August - November 1995

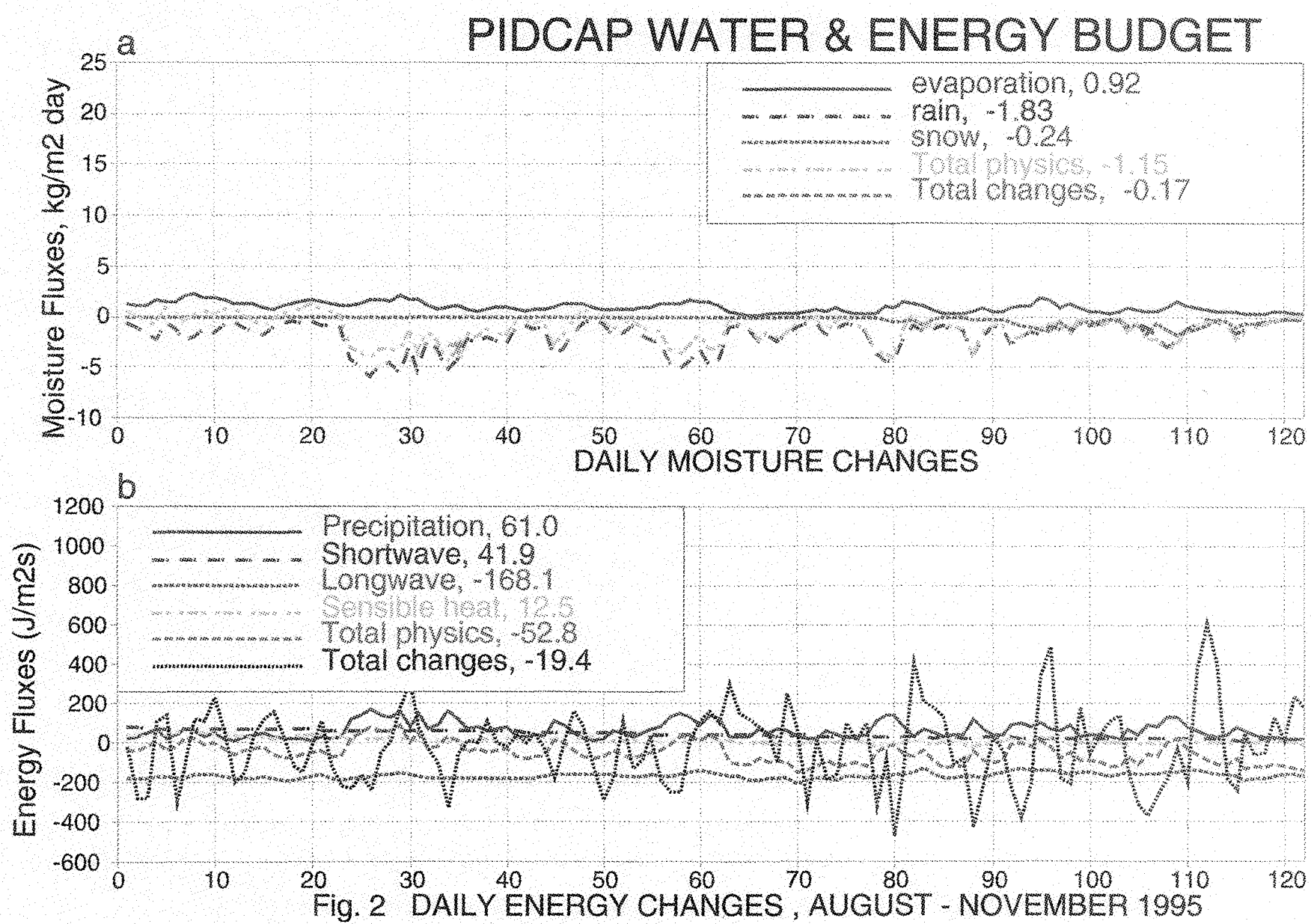

Fig. 2 DAILY ENERGY CHANGES , AUGUST - NOVEMBER 1995

ATMOSPHERE-ICE-OCEAN COUPLING IN THE BALTEX RE-ANALYSIS PERIOD 1986/87

A. Omstedt and N. Gustafsson,
Swedish Meteorological and Hydrological Institute
S-601 76 Norrköping, Sweden

The atmosphere, the ice and the ocean constitute a physical system with strong coupling. In shallow semi-enclosed seas, as the Baltic Sea, the changes of properties in the upper layers of the sea and in the sea ice are also often rapid. This is due to large variability in the meteorological forcing, large river inflows and the presence of coast lines and islands, which causes divergences in the upper layers of the sea. The development of high resolution weather forecasting models make it now possible to resolve many of the specific features of the Baltic Sea geometry as sub-basins and straits. This together with advanced ice-ocean models give us good possibilities to develop coupled models for the Baltic Sea. A coupled model system using the HIRLAM atmosphere and the BOBA ice-ocean model is now in operational use at SMHI and has also been applied in a BALTEX re-analysis study. The results are most promising but it is necessary to apply manual corrections or data assimilation for the sea surface temperature to avoid drift of the coupled model. The model system as well as results will be presented during the seminar. The development of coupled atmosphere-ice-ocean models within the BALTEX program will also be outlined.

REFERENCES

Gustafsson N., A. Omstedt. and L. Nyberg, 1997:
Coupling high resolution atmosphere and ocean models for the Baltic Sea. In manuscript.

First Steps Towards a Fully Coupled Baltic Sea Ocean - Atmosphere Model

Renate Hagedorn and Andreas Lehmann
Institut für Meereskunde, Kiel

Daniela Jacob
Max-Planck-Institut für Meteorologie, Hamburg

ABSTRACT

To explore and quantify the various processes which determine the space and time variability of the water and energy cycle of the Baltic Sea and its drainage basin, it is necessary to understand the coupled system of ocean and atmosphere. As a first step towards a fully coupled system, being composed of the regional atmospheric model REMO and the Kiel Baltic Sea model, some sensitivity studies have been done varying the SST. The simulations were performed for the PIDCAP period (August to October 1995), during that an intensive cyclonic development was observed which led to an extreme cooling of the oceanic mixed layer. Main differences in SSTs occur in the Bornholm and Gotland Basins. They influence mainly corresponding heat fluxes and at a lower level the dynamics of the atmospheric model. Thus, the resulting changes show the considerable impact of different SSTs of the Baltic Sea, used as lower boundary condition for the atmosphere.

1 INTRODUCTION

The importance of interactions between atmosphere and ocean on the global scale is shown by many coupled model studies. It is also known that on the regional scale the atmosphere influences the ocean. Simulations with the Kiel Baltic Sea model show, that the process of massive influx of saltwater from the North Sea into the Baltic Sea can only be modeled with correct atmospheric forcing. In contrast to that we know little about the fact how the Baltic Sea influences the atmosphere.

To explore interactions between atmosphere and ocean on the regional scale the regional atmospheric model (REMO) from MPIfM Hamburg and the Baltic Sea model (BSMO) from IfM Kiel will be coupled. Thus, we want to contribute to the quantification of the energy- and water cycle of the Baltic Sea and its catchment area.

2 MODELS

The 3-dimensional atmospheric model REMO is based on the operational forecast model of the German Weather Service (DWD). It is used in the so-called climate mode with the physical parameterizations which are implemented in the Europa-Model (Jacob et al., 1997). The horizontal resolution is 1/6 degree on the rotated longitude/latitude grid. This is equivalent to approximately 18 x 18 km^2.

The Kiel Baltic Sea Model is a 3-dimensional eddy-resolving baroclinic model with a horizontal resolution of approximately 5 x 5 km^2 (Lehmann, 1995). Until now, these two models have been run separately and both were forced with DWD analyses or forecasts, respectively.

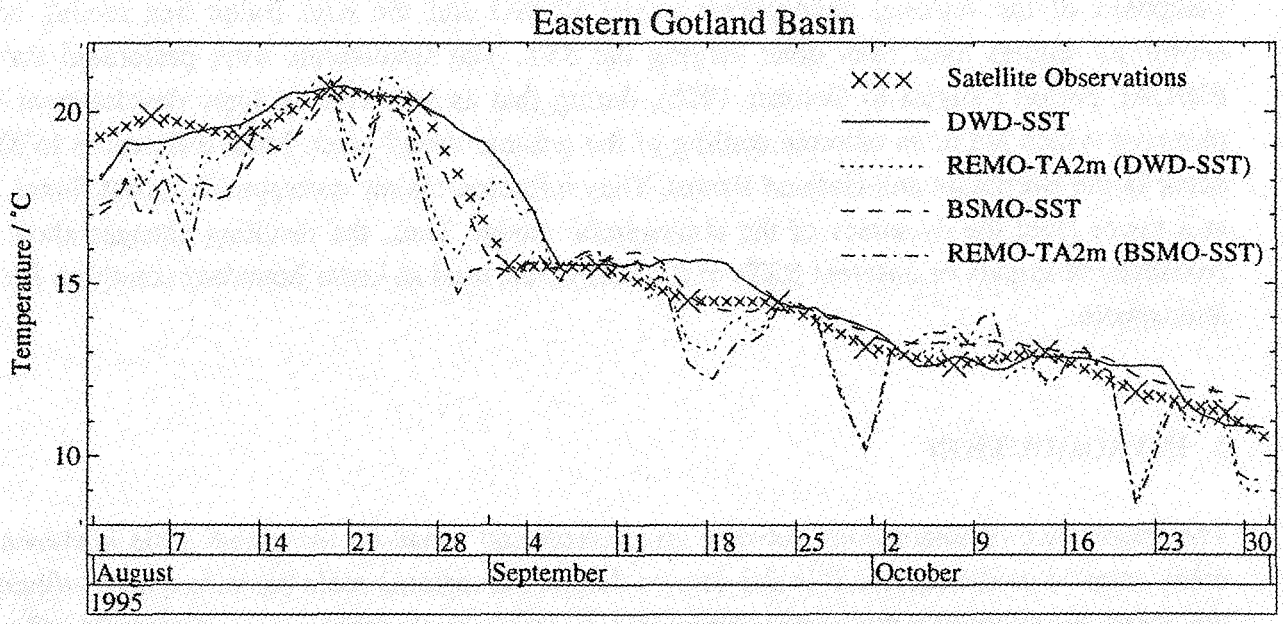

Figure 1: Sea Surface Temperatures (SST) and 2-m Air Temperatures (TA2m) averaged over the Eastern Gotland Basin. Crosses: SST from Infrared-Satellite Observations, solid line: SST from DWD analyses (0.5 degree EM), dotted line: TA2m from REMO with DWD-SSTs as boundary condition, dashed line: SST from BSMO driven with REMO-Results, dashed-dotted line: TA2m from REMO with BSMO-SSTs as boundary condition.

3 SENSITIVITY STUDIES

The first steps towards the coupling are sensitivity studies with different forcings for both models. Firstly, we performed a run of REMO with DWD analyses as boundary conditions. The results of this run were used as forcing for the Kiel Baltic Sea Model. SSTs, as a result of this run, were used as surface boundary condition for a new run of REMO. The simulations were performed for the PIDCAP-Period (Pilot Study for Intensive Data Collection and Analysis of Precipitation)

from August to October 1995. Differences up to 6 degree Celsius in single grid boxes appeared while comparing satellite observed SSTs with DWD-SSTs used in REMO so far. Also, there are large differences apparent in SSTs averaged over the Eastern Gotland Basin (Figure 1), especially during the period of rapid cooling of the oceanic mixed layer (08/26/95 - 09/02/95).

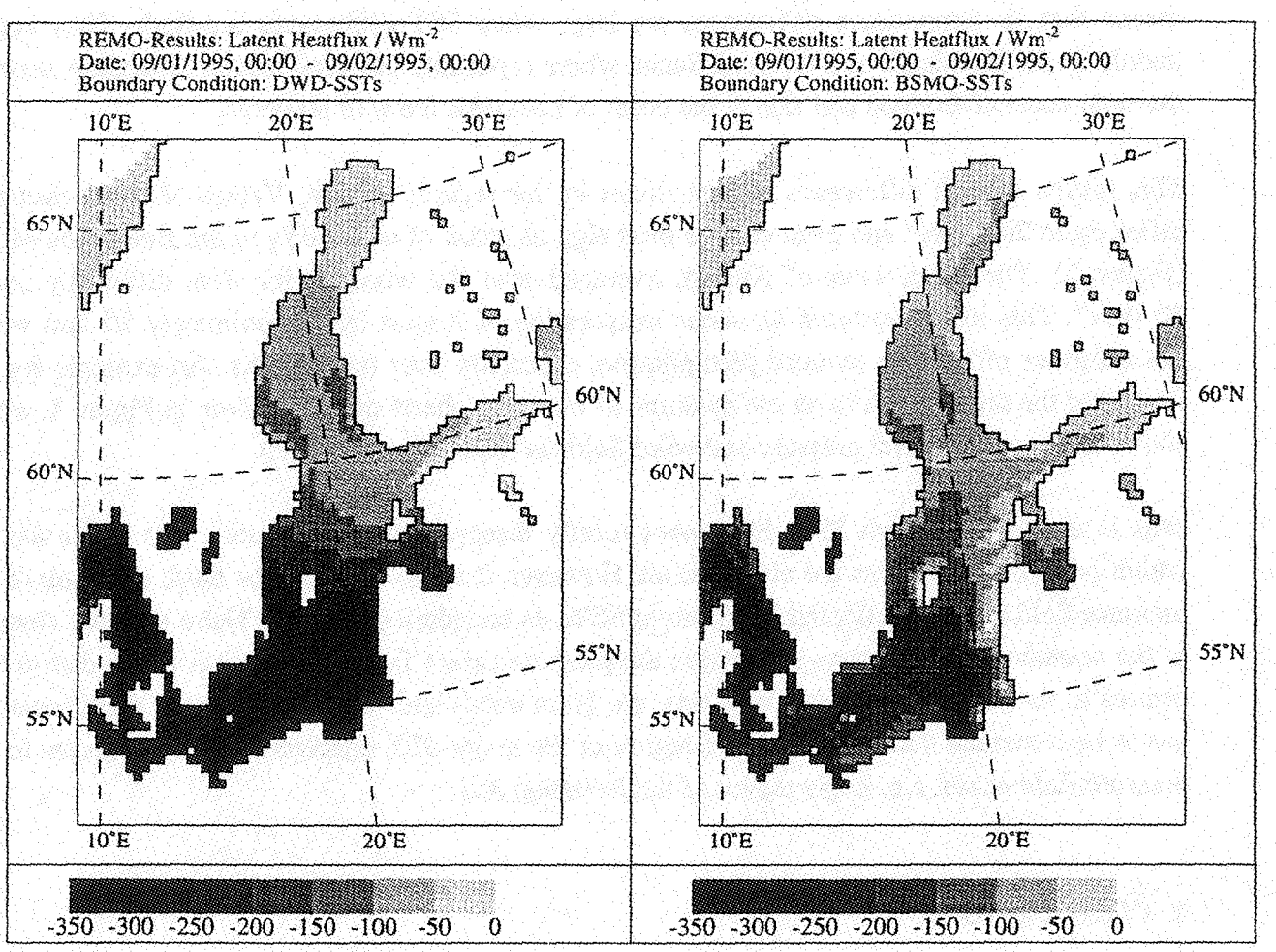

Figure 2: Mean latent heatflux, 09/01/1995, 00:00 - 09/02/1995, 00:00; left: SSTs from DWD analyses as boundary condition, right: SSTs from BSMO as boundary condition.

The rapid cooling was induced by strong cyclonic activities over the BALTEX region, which also caused an extensive outbreak of polar air masses over Europe. In the 2-m air temperatures of the first run of REMO, this cooling is evident as well, although - probably depending on DWD-SSTs which are too large - later relatively high air temperatures occur. Nevertheless we took these results for the forcing of the Baltic Sea model. At the beginning of the simulation, the BSMO-SSTs are too cold, which is due to the initialization. But, after 3 weeks the values reached the observed SSTs. After that, the behaviour of the BSMO-SSTs is better than the results of the

DWD-SSTs. Especially during the cooling period the BSMO-SSTs are closer to the observed SSTs, and later atmospheric cooling situations are reflected in the SSTs.

The comparison of 2-m air temperatures of both REMO simulations, forced with DWD-SSTs or BSMO-SSTs, shows that differences in air temperatures depend on differences in SSTs. This means that air temperature differences are large when SST differences are high. They appear mainly in the Bornholm and Gotland Basin, where especially the wind driven upwelling zones at the west coast of Gotland and also at the coast of Lithuania are well rendered.

This results in high differences of heat fluxes in this regions as well. Values of latent heat flux differ up to 200 Wm^{-2} and even change their sign as result of cold SSTs in the Baltic Sea Model (Figure 2). The mean value of August, averaged over the whole Baltic Sea, differs by nearly 30 Wm^{-2}. This in turn reduces the mean evaporation of August by approximately 20 mm which has a further effect of a reduced precipitation, especially over this regions. An example for the impact of the different SSTs on the dynamic of the atmospheric model is given in Figure 3, which shows the mean sea level pressure and wind fields at September 5th, 1995.

This is the date at which SST differences mostly disappeared, nevertheless, this is the date at which pressure differences are visible at all. However, it is obvious that the basic structure of the pressure field is hardly effected by different SSTs as boundary condition. There are only changes in the southern Baltic Sea region, where the pressure centre from the first run is divided in two centres in the second run. Induced by this, the 10-m wind fields are also different. Additionally it has to be remarked that apart from the region of the major SST differences, small changes in the pressure field occur, e.g. in the region of the Bothnian Sea.

4 CONCLUSIONS

The comparison of satellite observed SSTs and SSTs from DWD analyses showed relatively large differences, especially in situations were rapid changes in the mixed layer occurred. The sensitivity studies indicated that the atmospheric response to the different surface boundary conditions are not negligible. Above all, the changes in heat fluxes are very high, whereas the pressure field is less influenced by different SSTs. It is expected that the fully coupled model will give further information about the interaction between ocean and atmosphere in the BALTEX area.

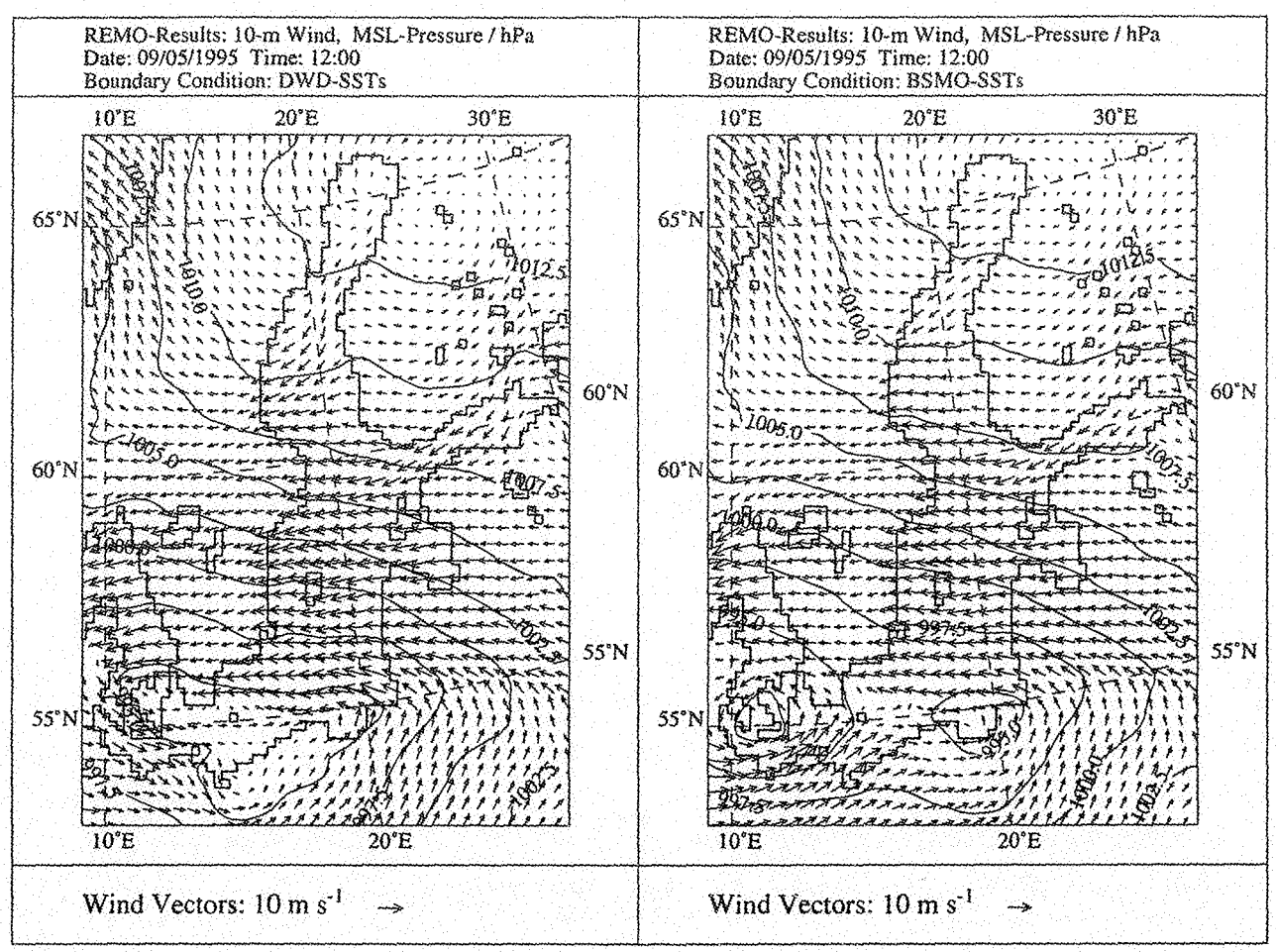

Figure 3: Mean sea level pressure field and 10-m wind field for 09/05/1995, 12:00; left: SSTs from DWD analysis as boundary condition, right: SSTs from BSMO as boundary condition.

REFERENCES

Jacob, D., R. Podzun, 1997: Sensitivity Studies with the Regional Climate Model REMO. Met. and Atm. Physics (accepted)

Lehmann, A., 1995: A three-dimensional baroclinic eddy-resolving model of the Baltic Sea. Tellus, **47A**, 1013 - 1031

ON THE WATER, HEAT AND SALT BALANCE OF THE BALTIC SEA

Andreas Lehmann
Institute of Marine Research, Kiel, Germany

ABSTRACT

Understanding the role of the Baltic Sea in energy and water cycles requires models for the relevant transport processes. Models must be capable of accurately representing the response of currents and sea level to direct forcing by the wind, and by wind-induced changes of sea level in the Kattegat leading to exchange flows through the Danish Straits. The models must further describe the response of the circulation to forcing by river runoff, precipitation/evaporation and by melting/freezing, with specific emphasis on freshwater budget and thermohaline circulation.

A coupled ice-ocean model is utilized to investigate the water, salt and heat budget of the Baltic Sea for the years 1992/1993. The oceanic component is a three-dimensional baroclinic model of the whole Baltic Sea, with a horizontal resolution of 5 km and 28 vertical levels specified. The ice model is based on the Hamburg Sea Ice Model, with the same horizontal resolution. The coupled system is driven by atmospheric data, mostly provided by the Europa-Model of the German weather service. River runoff is taken from a monthly mean data base. From the two-year model run, the different components of the water, heat and salt budget are identified, and analysed in view of the their contribution to the heat, salt and water cycle.

1 INTRODUCTION

The investigation of the energy and water budget of the Baltic Sea and its catchment area is one main aim of BALTEX. The understanding of the role of the Baltic Sea in energy and water cycles requires models for the relevant transport processes. The models must describe the response of the circulation to forcing by river runoff, precipitation/evaporation and by melting/freezing with specific emphasis on the freshwater budget and thermohaline circulation. Due to the strong interaction of atmosphere, ice and ocean a quantification of the fluxes between the components requires the utilization of coupled numerical systems.

As a first step towards a fully coupled atmosphere-ice-ocean model a coupled ice-ocean model was utilized to investigate the water, salt and heat budget for the years 1992/93. The oceanic

component is a three-dimensional baroclinic model of the whole Baltic Sea, with a horizontal resolution of 5 km and 28 vertical levels specified (Lehmann, 1995). A dynamic-thermodynamic ice model which is based on the Hamburg Sea Ice model (Hibler, 1979; Stössel and Owens, 1992) is coupled to the ocean model. There is no mixed layer model between the components, thus the models are directly interacting via the fluxes of heat, salt and momentum. External forcing is provided by the Europa-Model of the German weather service (Majewski, 1991) and by river runoff taken from Bergström and Carlsson (1994). The initial conditions for the three-dimensional fields of temperature, salinity and currents and for the two-dimensional field of surface elevation were taken from a previous model run. The initial fields are representing a typical winter distribution for the Baltic Sea.
From the two-year model run, analysis data files of the model variables: temperature, salinity, currents and sea surface elevation were extracted for every 6 hours. This data set is the basis of the following analysis.

2 MEAN SEA SURFACE TOPOGRAPHY

The mean inclination of the Baltic Sea surface is a consequence of the mean density stratification which is dominated by the salinity distribution. Due to high river runoff (470 km^3/year) and a more-or-less continuous inflow of haline water through the Danish Straits a permanent inclined halocline is maintained. As the vertical average of salinity of the Baltic decreases from west to north and east, the sea surface elevation increases. The height difference between the inner part of the Gulf of Bothnia and the Skagerrak amounts to 34 - 40 cm (Figure 1). There is a steep sea level gradient in the border zone between Kattegat and Skagerrak, reaching 2 cm per 10 km. This reflects the salinity front there, separating the brackish Baltic Sea water from the saline North Sea water, and the associated Baltic current. The annual average of the sea surface elevation calculated from the oceanographic model is in good agreement with the mean surface topography calculated geodetically from long-term sea level stations (Ekman and Mäkinen, 1996). Thus, the mean density stratification of the 1992/93-model run is in good agreement with observations.

3 MEAN CIRCULATION AND VOLUME TRANSPORT

Due to the ephemeral nature of the meteorological forcing, there is no evidence of a permanent current system in the Baltic Sea. In spring and early summer wind forcing is weak, thus the circulation is mostly determined by the baroclinic field. In autumn and winter strong westerly winds are prevailing, thus the circulation is determined by Ekman dynamics and the basin-like bottom topography superimposing the baroclinic signal. The annual mean of the barotropic circulation for the years 1992 and 1993 shows only minor deviations. There is a cyclonic circulation

which comprises the Bornholm and Gotland Basin, with water entering this circulation by a branch from the Gulf of Finland and through the Aaland Sea (Figure 2). Through the Bornholm Gat, water is leaving this circulation with a further flow through the Arkona Sea and the Danish Straits feeding the Baltic current. Within the subbasins, there are cyclonic circulation patterns with the net transport between the basins is determined by the river runoff into the subbasin, each.

The internal barotropic circulation between Gotland and Bornholm Basin (1000-2000 km^3/year) is about an order of magnitude higher compared with the total river runoff to the Baltic Sea (470 km^3/year). On the annual average, the water volume which is supplied by the river runoff leaves the Baltic Sea through the Danish Straits. Thus the net volume flow from the Baltic Sea into the North Sea corresponds to the river runoff modified by the net effect of precipitation minus evaporation. The rates of evaporation and precipitation for the year 1993 are displayed in Figure 3.

The precipitation rates were prescribed from monthly mean values (Dahlström, 1986), whereas, the evaporation was diagnostically calculated from atmospheric parameters and from the simulated sea surface temperatures. The simulated mixed layer temperatures were verified against SST's observed from satellite. The evolution of the mixed layer temperature was satisfactorily simulated by the model.
However, during spring and summer modeled sea surface temperatures lay 1-2° C below the observations. Thus, the calculated evaporation rates underestimate the real conditions. The total annual volume flow out of the Baltic Sea for 1993 amounts to ~ 495 km^3 including 22 km^3 from the precipitation surplus.

4 WATER AND SALT BUDGET

On the basis of the total water and salt budget deficiencies of the Baltic Sea model will be discussed. The accumulated volume transport and the total salt content of the Baltic Sea for 1993 are displayed in Figure 4. At the beginning of the year, there is a strong inflow in January of about 220 km^3, and a second inflow in March. Until the end of the year, outflow dominates the transport through the Danish Straits resulting in a total flow out of the Baltic Sea of about 440 km^3 which is approximately the volume input supplied by river runoff. During the major Baltic inflow, in January 1993, a water volume of 220 km^3 penetrates into the Baltic Sea.

In comparison with observations the model underestimates the inflow by about 80 km^3. Correspondingly, the increase of the salt content is also underestimated during this event (2 Gt model; 4.5 Gt observations).

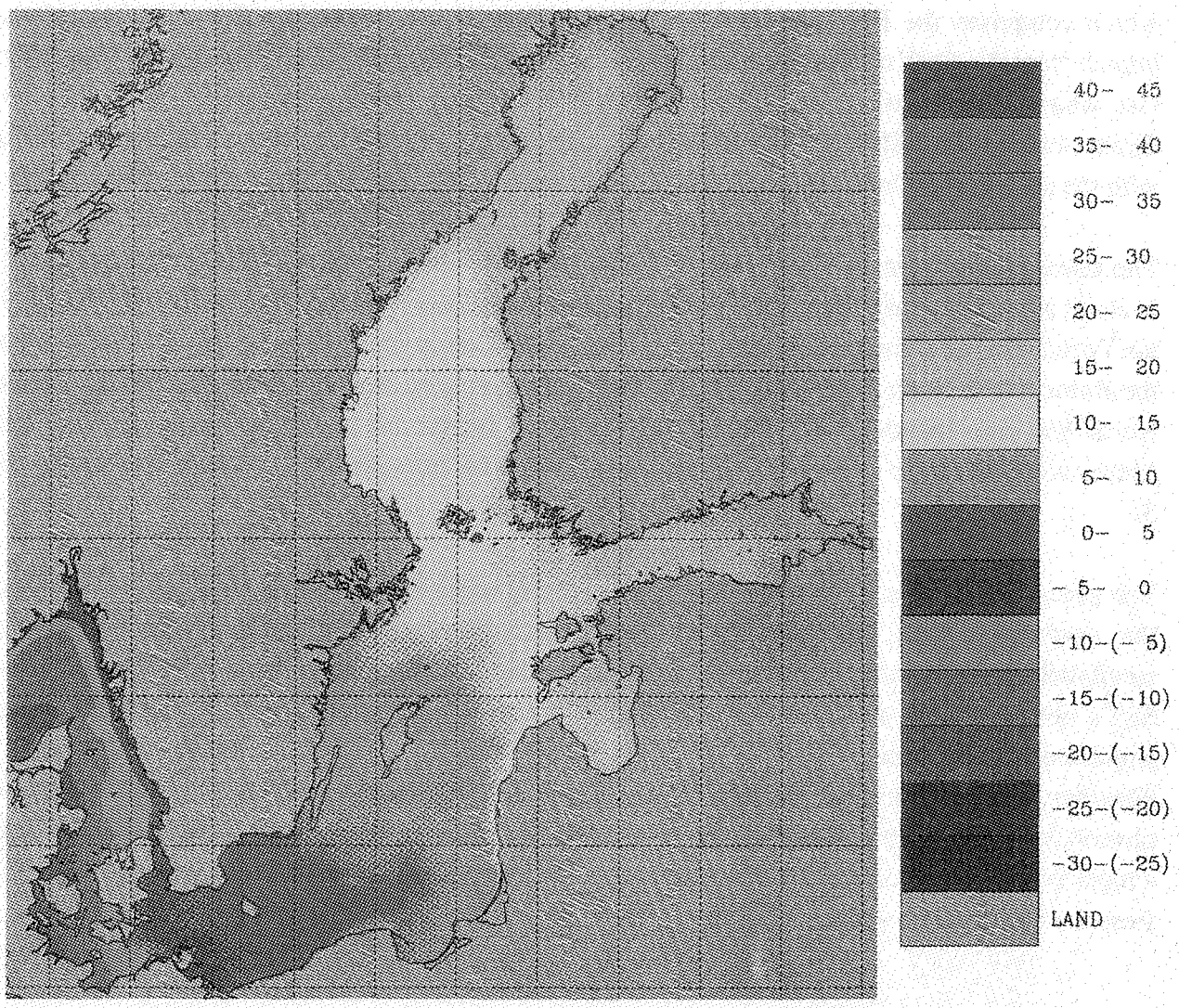

Figure 1: Annual average of the simulated sea surface elevation [cm] for 1992.

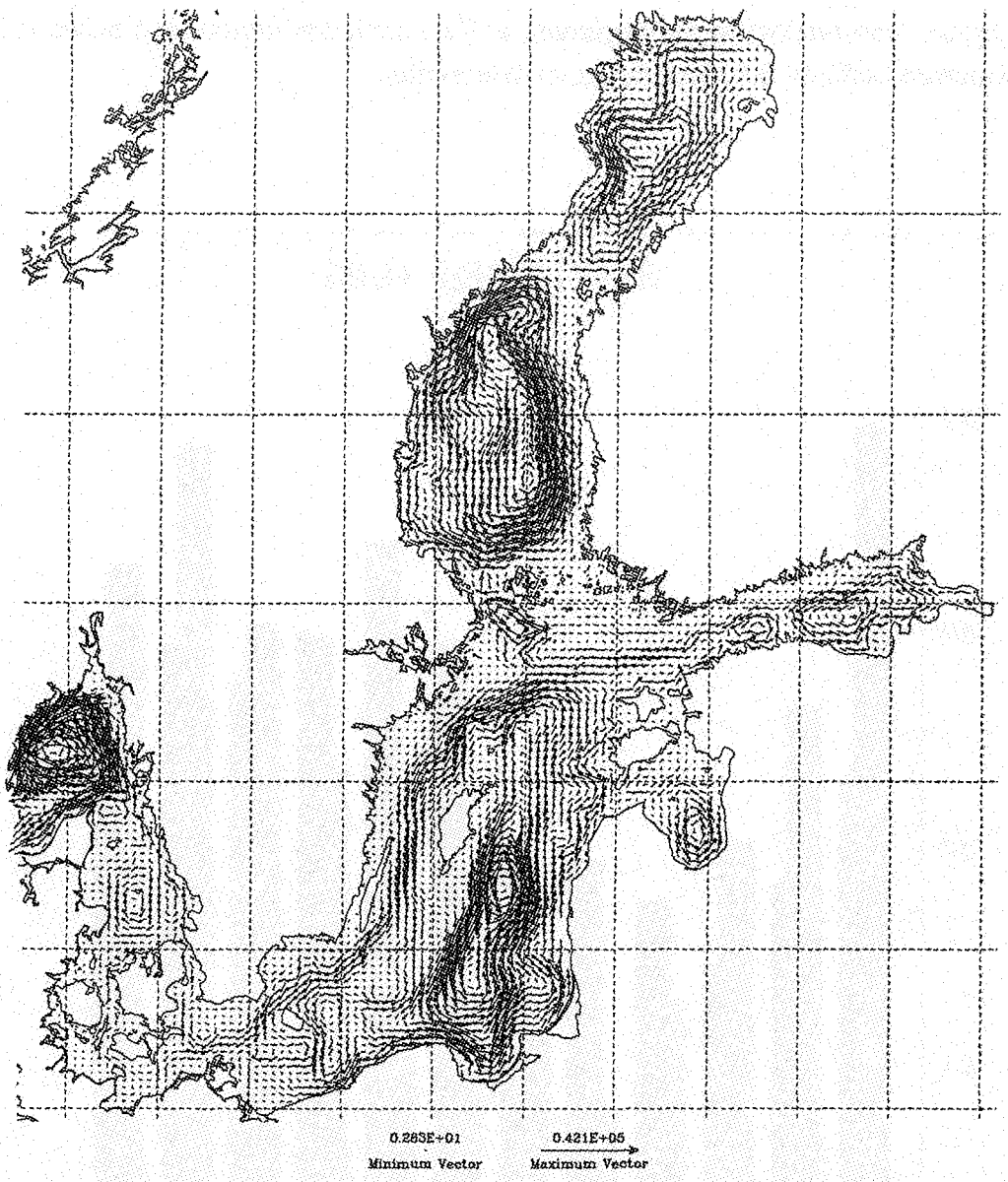

Figure 2: Annual average of the barotropic circulation [m^3/s] for 1992.

There are mainly three reasons responsible for the underestimation of the volume and salt transport. Firstly, there are uncertainties in the atmospheric forcing provided by the Europa-Model which may lead to erroneous sea surface elevations in the Kattegat and western Baltic and hence will lead to an underestimation of the transports through the Danish Straits. Secondly, due to the western boundary condition (Lehmann, 1995), under strong wind events from western directions the piling up of water in the Kattegat is not satisfactorily simulated. Thirdly, the position of the Belt Sea front and the vertical distribution of salinity in the Belt Sea was not

verified against observations at the beginning of the simulation period, and hence it is unlikely that the simulated salinity field hits the actual distribution.

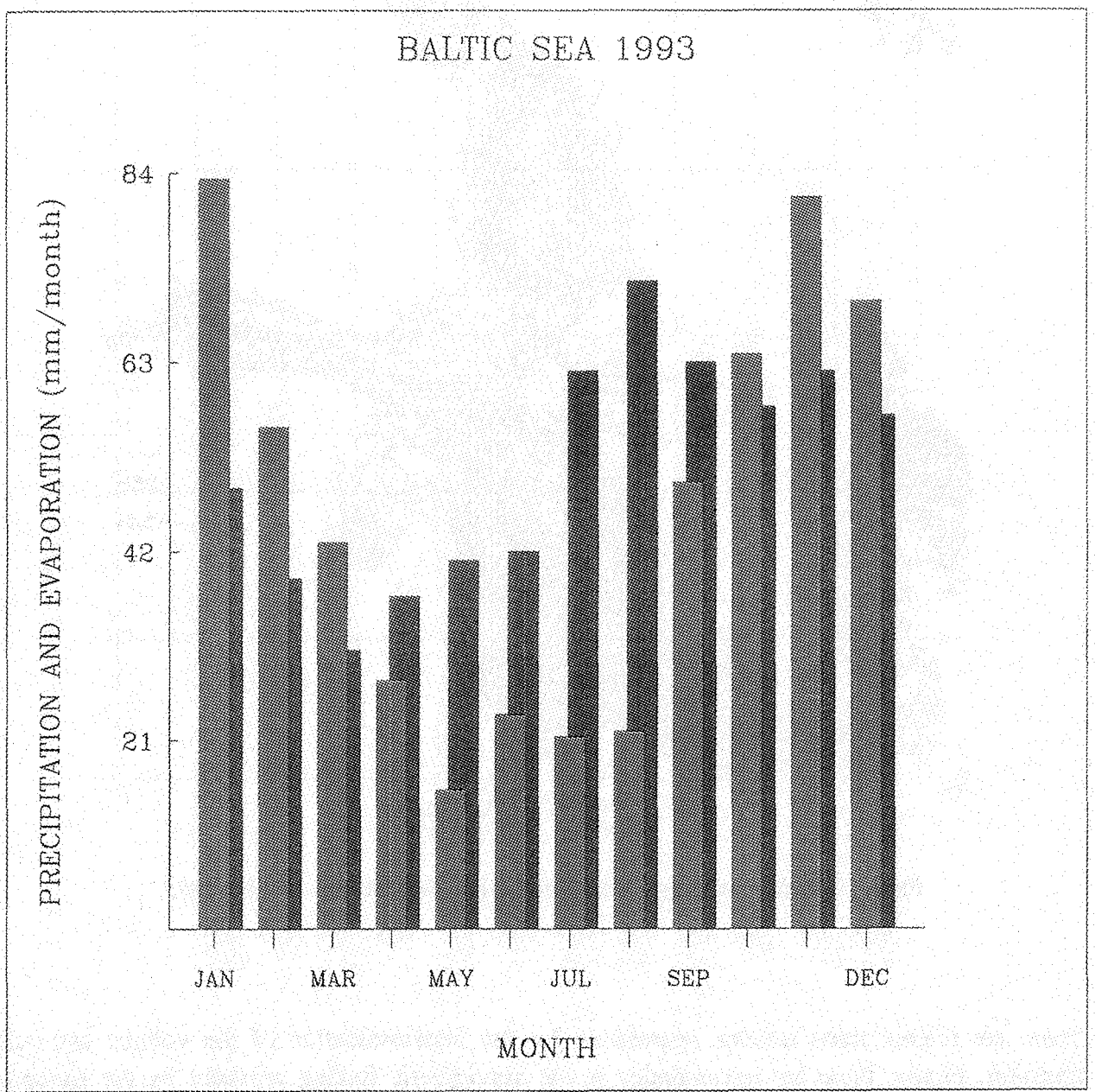

Figure 3: Rates of precipitation (blue) and evaporation (red) [mm/month] of the total Baltic Sea for 1993. Precipitation rates are taken from Dahlström, 1986.

5 CONCLUSIONS

Estimates of the water, heat and salt budgets for the years 1992/93 are calculated by utilizing a coupled ice-ocean model of the Baltic Sea. However, the effect of sea ice is not considered in this analysis. The main components which determine the salt and water budget are realized by the model.

Currents and stratification are simulated in response to atmospheric forcing and fresh water input by river runoff. The storage of water in the Baltic Sea and its variability as well as the evolution of the mixed layer temperature is in reasonable agreement with observations. From the two-year simulation a quantification of the water budget of the Baltic Sea is possible.

The accumulated volume transport through the Danish Straits is determined by river runoff superimposed by highly fluctuating in- and outflow events controlled by the meteorological forcing. For the year 1993, the fresh water input due to precipitation minus evaporation amounts to ~5% of the total river runoff. However, there are several aspects which limit the confidence of this estimation. Firstly, some of the atmospheric parameters (precipitation and cloud cover) and the river runoff were taken from monthly mean data. Secondly, the comparison of the transports through the Danish Straits with observations reveals deficiencies in the simulation which are partly due to uncertainties in the atmospheric forcing and the choice of the western boundary condition. To remedy these deficiencies, a better representation of the atmospheric parameters is necessary which may be achieved by coupled atmosphere-ice-ocean models, and additionally, the western boundary condition must be improved to simulate the inflow of haline water more realistically.

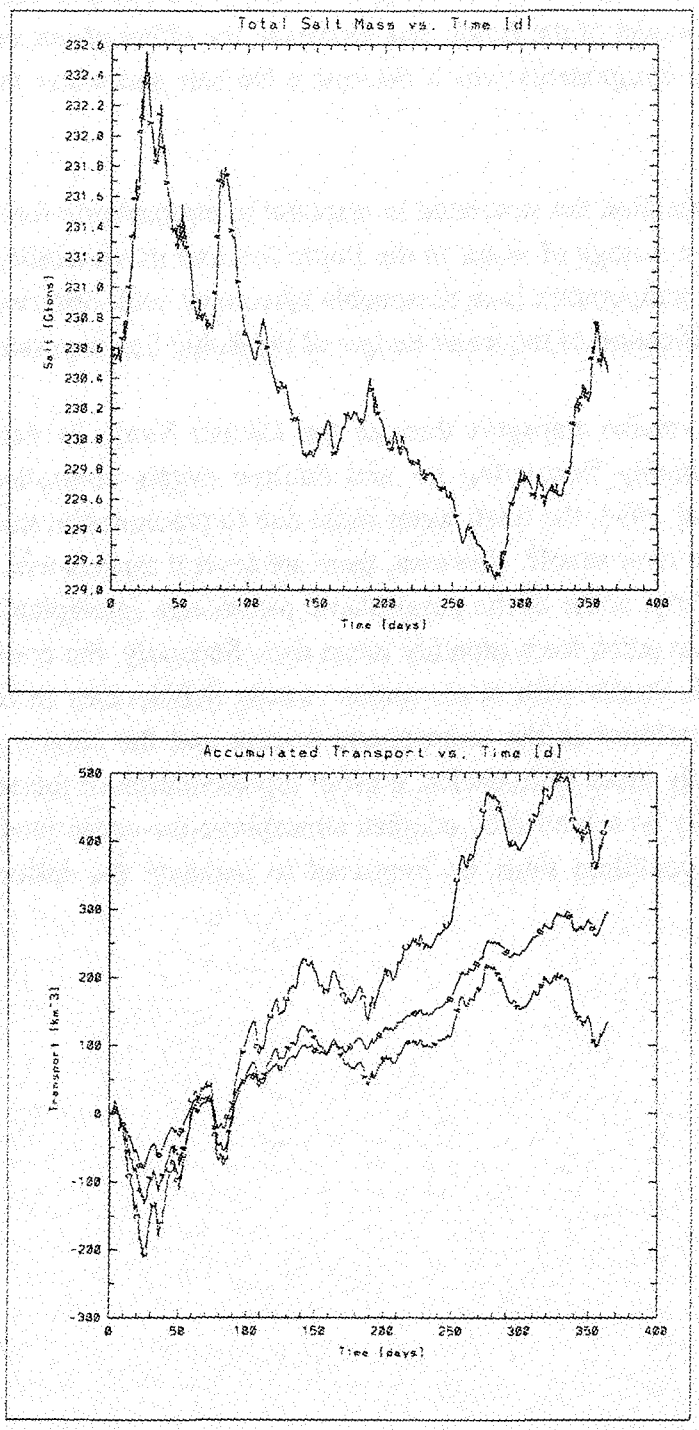

Figure 4: Accumulated volume transport and total salt content of the Baltic Sea for 1993, lower panel: A, B and C denote the transport through Sound, Great Belt and Belt Sea (sum of A and B), respectively.

REFERENCES

Bergström S. and B. Carlsson, 1994: River runoff to the Baltic Sea: 1950-1990, Ambio **23** (nos.4-5), 280-287.

Dahlström, B., 1986: Determination of areal precipitation for the Baltic Sea. In Baltic Sea Environment Proceedings No. **16**, 174pp.

Ekman, M. and J. Mäkinen, 1996: Mean sea surface topography in the Baltic Sea and it's transition to the North Sea. A geodetic solution and comparison with oceanographic models. J. Geophys. Res., **101**, C5, 11993-1999.

Hibler III., W.D., 1979: A dynamic thermodynamic sea ice model. J. Phys. Oceanogr., **9**, 815-846.

Lehmann, A., 1995: A three-dimensional baroclinic eddy-resolving model of the Baltic Sea. Tellus, **47**, 1013-1031.

Majewski, D., 1991: The Europa-Modell of the Deutscher Wetterdienst. ECMWF Seminar on numerical methods in atmospheric models. **2**, 147-191.

Stössel A. and W.B. Owens, 1992: The Hamburg sea-ice model. DKRZ Techn. Report No. 3.

Variational Soil Moisture Analysis by Assimilating Screen-Level Atmospheric Observations

Fred Kucharski, Andreas Rhodin, Ulrich Callies and Dieter P. Eppel
Institute of Hydrophysics, GKSS Research Centre
D-21502 Geesthacht

ABSTRACT

A variational analysis scheme for soil moisture in the domain of the operational regional weather forecast model (DM) of the Deutscher Wetterdienst (DWD) is investigated using analyzed fields of screen level atmospheric temperatures and relative humidities in a five-day period in March 1994. Retrieved soil moisture values turn out to be considerably lower than in the operational reference run. The improved quality of the resulting sensible and latent heat fluxes can be assessed on the basis of better forecasts they imply. The analyzed soil moistures themselves are consistently very low and can be doubted to be realistic for this time of the year. They should be considered as being mere effective parameters to be tuned with respect to the specific soil model in order to provide correct lower boundary conditions for the atmosphere.

1 INTRODUCTION

For a given radiative forcing the partitioning of surface energy fluxes into sensible and latent heat fluxes strongly depends on the moisture available in the upper layers of the soil. Since soil moisture content evolves on time scales of several days or even weeks - except for the uppermost few centimeters - it cannot adapt to fast changing atmospheric situations. Its incorrect specification in weather forecast models may distort model energy and moisture fluxes which, by influencing the atmospheric boundary layer, ultimately leads to persisting low-quality forecasts.

Since soil moisture distributions over the solution domains of weather forecast models cannot be measured directly for the time being, estimation procedures for initial fields of moisture usable for forecast simulations are needed. Mahfouf (1991) showed the feasibility of inferring soil moistures from atmospheric data of the lower boundary layer. In his study he used data from an intensive phase of the HAPEX-MOBILHY campaign (Andre et al., 1986) together with a one-dimensional boundary-layer model coupled to a soil module. Two strategies were investigated: a sequential update technique based on optimal interpolation and a variational approach. Numerical experiments were conducted during clear-sky conditions when the atmosphere-soil coupling is strongest. One conclusion was that the variational assimilation generally yielded superior results.

In the variational approach no statistical correlations between soil-moisture misspecification and the forecast errors of screen-level temperature and humidity need be collected whereas in the optimal interpolation approach these correlations have to be determined for a large number of different atmospheric conditions and soil-surface characteristics. This is feasible only for a small number of cases which are supposed to be representative. The variational approach is more flexible because it uses the forecast model itself in order to account for the different situations. However, it was the sequential approach, and not the variational assimilation, that was later on implemented into a mesoscale model (Bouttier, 1993a, Bouttier, 1993b). The variational technique was considered to be too involved because, in principle, an adjoint of the full forecast code would be needed in a routine forecast environment.

Callies et al. (1997) could show that soil moisture can be retrieved from routine atmospheric data by variational techniques. In this study, the one-gridpoint investigation of Callies et al. (1997) is extended to the whole solution domain of the forecast model "Deutschland Modell" (DM) of the German Weather Service. The aim of this study is to demonstrate that on the scale of operational forecast models the technique applied to one grid point can directly be transferred to treating whole fields. The variational problem of simultaneously retrieving soil moisture at a large number of grid points is reduced to a large number of independent problems. A variational algorithm based on a perturbation method using the coupled soil and boundary-layer model independently in each column is applied to the whole solution domain. This allows to use the method in an operational environment without the need for an adjoint code of the full prediction model. The method is applied to a five-days episode in spring 1994 during which low level conditions were predicted generally too cold and too moist. The overall results show that the method works even under non-ideal conditions (partial cloud cover).

2 VARIATIONAL ASSIMILATION PROCEDURE AND SOIL MOISTURE RETRIEVAL

In variational data assimilation a cost function J is minimized which measures the discrepancies between observations and their model counterparts over a certain time span. The initial soil moisture values in two model layers are to be retrieved for all grid points eventually leading to the best forecast of atmospheric temperature and relative humidity at screen-level height (2 m). In this application, analyses of temperatures and relative humidities at 12 and 15 UTC (13 and 16 h local time) on the grid of the DM are used. These data are routinely available in the operational environment. This describes one minimization problem with two control variables at every grid point. For the DM this amounts to 2 X 11881 unknowns.

A sample period of five days (March 3-7, 1994) is chosen during which the large errors of predicted screen-level temperatures over Central Europe occurred. Following a cold period at the

end of February, these were the first mild days with temperatures above 10 degrees. The workstation version of the DM is used as a quasi-operational environment. The assimilation-forecast cycles comprise 48 hours starting each night at 0 UTC with the first 24 hours for data assimilation. The DM is driven by analyzed boundary data from the Europa Model of the DWD every 6 hours. During a DM run the fields required for driving the simplified model (temperature, rel. humidity and wind at the lowest atmospheric levels, as well as incoming radiation and precipitation at the ground) are stored in 30 minutes intervals. They are interpolated later in the soil moisture assimilation process to obtain the forcing and residue data for each time step.

According to the parameterizations of the soil model, bare ground evaporates with potential evaporation when the actual soil moisture equals or exceeds field capacity. In the operational forecast the soil is almost saturated in large areas (Figure 1 a)). Because in early spring the vegetation cover in the model is very small (values less than 20 percent) the model's evaporation takes place at its potential rate almost everywhere.

Figure 1 b) shows the forecasts with unchanged initial soil moisture for March 5: deviations (forecast - analysis) of 2 m temperature (left panel) and relative humidity (central panel) averaged at 12:00 and 15:00 UTC on each day. During the whole period the model shows the tendency to be significantly colder and wetter than observations in most areas of the domain towards too high soil moistures used in the model. In the assimilation runs, each day analyzed atmospheric 2 m temperatures and relative humidities at 12:00 and 15:00 UTC are used to retrieve upper layer soil moistures at 6:00 UTC by minimizing the cost function. This time span covers the whole period of strong radiative forcing in order to assess the full impact of soil moisture on the evolution of the atmospheric boundary layer.

By minimizing the cost function J the deviations between model results and observations (Figure 1 b)) were largely reduced. Figure 1 c) (left panel) shows the retrieved soil moisture in the upper layer on March 5. The overall changes relative to the operational forecast (Figure 1 a), right panel) confirm that soil moisture was too high during the whole period. This result is consistent with the forecast errors presented in Figure 1 b).

3 FORECAST WITH RETRIEVED SOIL MOISTURE

The goal of soil moisture retrieval is the improvement of a subsequent forecast. Thus, from the 4th to the 7th of March each day a DM run was started at 0:00 UTC with initial soil moisture replaced by the retrieved soil moisture the previous day. Using the retrieved soil moisture generally improves the forecast with only small areas of weak deterioration. The reduction in mismatch between forecast and analysis is presented in Figure 1 d) for March 6. Again the

patterns in the temperature (left column) and relative humidity (right column) fields are highly correlated.

Deterioration of the forecast occurred only in those areas where the operational forecast was already very good or where forecast errors exhibit a strong spatial small-scale inhomogeneity.

4 ANALYSIS OF THE WATER AND ENERGY BALANCE AT THE SURFACE

Figure 2 shows the evolution of the mean sensible and latent heat fluxes in the DM model domain during the 5-days period. The fluxes obtained with the retrieved soil moisture differ considerably from the original ones (the Bowen ratio changes by a factor of 3). They are presumably much closer to reality than the latter because their modeled effect on the low level atmosphere leads to the observed screen level parameters.

One can consider the present procedure as an attempt to analyze the daily cycles of sensible and latent heat fluxes, respectively, by tuning the single parameter soil humidity. The reliability of analyzed fluxes may be expected to be higher than the reliability of the soil moisture values themselves. The reason is that to retrieve the fluxes from observed atmospheric near-surface temperatures and humidities, only the atmospheric boundary model is needed. On the other hand, to retrieve soil moisture from the above observable variables, in addition the soil model has to be applied. If we presume modeling of soil processes being less sound and less accurate than modeling of the atmosphere, an inverse analysis method will necessarily tend to produce soil moistures being less realistic than the related surface fluxes.

5 CONCLUSIONS

In a preceding paper (Callies et al., 1997) we studied variational soil moisture analysis on the basis of atmospheric screen level observations for the specific conditions near Braunschweig (Northern Germany) at March 5, 1994. In the present study we applied the same analysis algorithm (based on a reduced 1-column stand-alone model version being extracted from the operational regional forecast model of the German Weather Service) at all grid points of the regional model considering the extended period March 3 to March 7, 1994.

Utilization of the retrieved soil moisture improves the subsequent forecast of screen level temperature and humidity considerably.

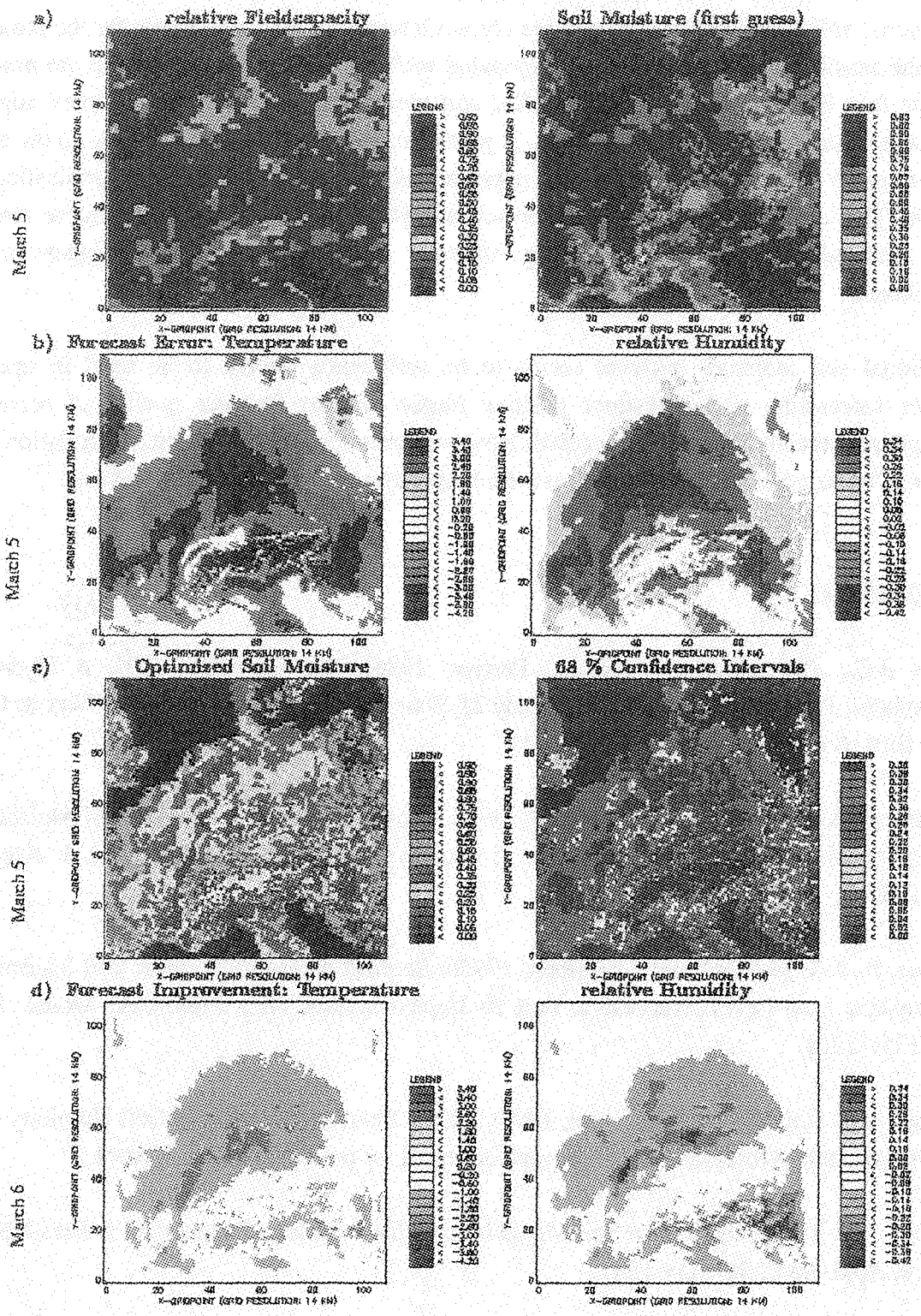

Figure 1: Experiment performed on March 5 and March 6,1994.

The retrieved values are consistently very low and can be doubted to be realistic for this time of the year. They should be considered as being mere effective parameters to be used with respect to the specific soil model in order to provide correct lower boundary conditions for the atmosphere. Thus the sensible and latent heat fluxes modeled with the retrieved soil moisture are much more realistic than those derived with unmodified soil moisture and thus should be more appropriate for instance for water budget calculations. A promising approach could be to pick up the analyzed surface energy fluxes and to use them as upper boundary conditions for a more sophisticated soil module. This could produce soil moisture values, which are considered either more realistic or better adapted (in the sense of being effective parameters) to a hydrological modeling environment.

Variational soil moisture retrieval seems to be sufficiently robust to be used in operational weather forecasting and a distinct positive impact on the forecast quality of screen level atmospheric parameters can be expected. However some parameters of the assimilation scheme remain to be tuned based on experiences with longer episodes and different seasons.

REFERENCES

Andre, J.C., J.P. Goutorbe and A. Perrier, 1986: HAPEX-MOBILHY, a Hydrological Atmospheric Pilot Experiment for the Study of Water Budget and Evaporation Flux at Climatic Scale. Bull. Amer. Meteorol. Soc., 138-144.

Bouttier, F., J.-F Mahfouf and J. Noilhan, 993a: Sequential Assimilation of Soil Moisture from Atmospheric Low-Level Parameters. Part I: Sensitivity and Calibration Studies. J. Appl. Met., 1335-1350.

Bouttier, F., J.-F Mahfouf and J. Noilhan, 1993b: Sequential Assimilation of Soil Moisture from Atmospheric Low-Level Parameters. Part II: Implementation in a Mesoscale Model. J. Appl.. Met., 1351-1364.

Callies, U., A. Rhodin and D.P. Eppel, 1997: A Case Study on Variational Soil Humidity analysis from Atmospheric Observations. Tech. rept. accepted for publication in J. Hydrol.

Mahfouf, J.-F. 1991: Analysis of Soil Moisture from Near-Surface Parameters: A Feasibility Study. J. Appl. Met., **30** 1534-1547.

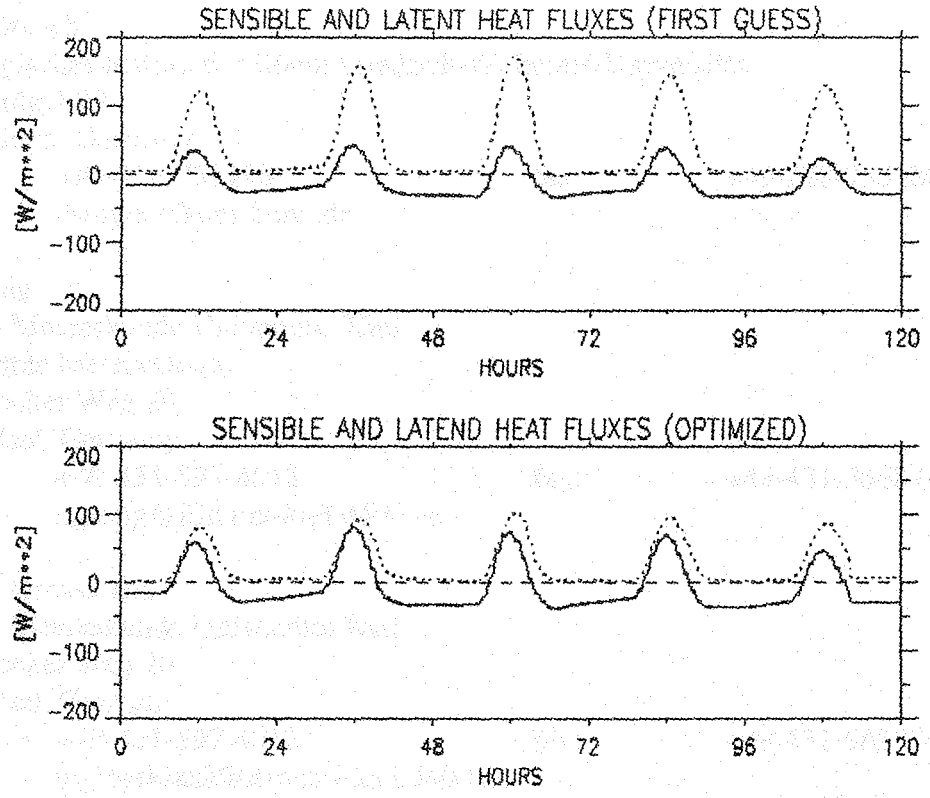

Figure 2: Mean sensible (straight line) and latent (dashed line) heat fluxes in the DM model domain (land points only) during the period March 3 to March 7, 1994, with unchanged (upper row) and retrieved soil moisture (lower row).

Addresses of the leading authors

Dr. Franz H. Berger
Institut für Hydrologie und Meteorologie
Technische Universität Dresden
Pienner Str. 9
D-01737 Tharandt, Germany
phone: +49-35203-381345 +37331 fax: +49-35203-381302 +37495
e-mail: berger@forst.tu-dresden.de

Matthias Drusch
Meteorologisches Institut der Rhein.Friedrich-Wilhelms-Universität
Auf dem Hügel 20
D-53121 Bonn, Germany
phone: +49-228-735198 fax: +49-228-735188
e-mail: csimmer@uni-bonn.de

Holger Gäng
Institut für Meereskunde Universität Kiel
Abt. Maritime Meteorologie
Düsternbrooker Weg 20
D-24105 Kiel, Germany
phone: +49-431-597-4012 fax: +49-431-565876
e-mail: hgaeng@ifm.uni-kiel.d400.de

Dr. Martin Grossklaus
Institut für Meereskunde Universität Kiel
Düsternbrooker Weg 20
D-24105 Kiel, Germany
phone: +49-431-597-4012 fax: +49-431-565876
e-mail: mgrossklaus@ifm.uni-kiel.d400.de

Renate Hagedorn
Institut für Meereskunde Universität Kiel
Düsternbrooker Weg 20
D-24105 Kiel, Germany
phone: +49-431-5973974 fax: +49-431-565876
e-mail: rhagedorn@ifm.uni-kiel.de

Dr. Felix Hamelbeck
Universität Wien
Institut für Meteorologie und Geophysik
Hohe Warte 38
A-1190 Wien, Austria
phone: +43-1-36026-3004 fax: +43-1-3685612
e-mail: hamelbeck@zamg.ac.at

Dr. Daniela Jacob
Max-Planck-Institut für Meteorologie
Bundesstraße 55
D-20146 Hamburg, Germany
phone: +49-40-41173-313 fax: +49-40-41173-298
e-mail: jacob@dkrz.de

Fred Kucharski
GKSS Forschungszentrum GmbH
GMV - Modellverfahren
Max-Planck-Straße
D-21502 Geesthacht, Germany
phone: +49-4152-87-1521 fax: +49-4152-87-1565
e-mail: kucharski@gkss.de

Prof. Dr. Jouko Launiainen
Finnish Institute of Marine Research - FIMR -
B.O. Box 33
FIN-00931 Helsinki, Finland
phone: +358-9-613 941 fax: +358-9-331 025 +358961394494
e-mail: jouko.launi@fimr.fi

Dr. Andreas Lehmann
Institut für Meereskunde Universität Kiel
Düsternbrooker Weg 20
D-24105 Kiel, Germany
phone: +49-431-5974013 fax: +49-431-565876
e-mail: alehmann@ifm.uni-kiel.de

Dr. Ralf Lindau
Institut für Meereskunde an der Universität Kiel
Düsternbrooker Weg 20
D-24105 Kiel, Germany
phone: +49-431-5973988 fax: +49-431-565876
e-mail: rlindau@ifm.uni-kiel.de

Manfred Lobmeyr
GKSS Forschungszentrum GmbH
Institut für Atmosphärenphysik
Postfach 1160
D-21494 Geesthacht, Germany
phone: +49-4152-87 1542 fax: +49-4152-87 2020
e-mail: lobmeyr@gkss.de

Dr. Dag Lohmann
Princeton University
Department of Civil Engineering and Operations Research
Princeton, New Jersey 08544, USA
phone: +1-609-258-6383 fax: +1-609-258-2799
e-mail: lohmann@earth.princeton.edu

Dr. Bettina Loth
Max-Planck-Institut für Meteorologie
Bundesstraße 55
D-20146 Hamburg, Germany
phone: +49-40-41173-378 fax: +49-40-441751
e-mail: loth@dkrz.de

Dr. Heinz-Theo Mengelkamp
GKSS Forschungszentrum GmbH
Institut für Atmosphärenphysik
Postfach 1160
D-21494 Geesthacht, Germany
phone: +49-4152-87-1558 fax: +49-4152-87-2020
e-mail: mengelkamp@gkss.de

Gisela Müller
Meteorologisches Institut der
Rhein. Friedrich-Wilhelms-Universität
Auf dem Hügel 20
D-53121 Bonn, Germany
phone: +49-228-735108 fax: +49-228-735188
e-mail: UZS868@IBM.RHRZ.uni-bonn.de

Prof. Dr. Anders Omstedt
Swedish Meteorological and Hydrological Institute
S-60176 Norrköping, Sweden
phone: +46-11158284 fax: +46-11170207 +46 11170208
e-mail: aomstedt@smhi.se

Dr. Anna Rozwadowska
Polish Academy of Sciences
Institute of Oceanology
Powstanców Warszawy 55
PL-81712 Sopot, Poland
phone: +48-58-517281 fax: +48-58-512130
e-mail: a.rozwadowska@iopan.gda.pl

Anna Rutgersson
Swedish Meteorological and Hydrological Institute
S-60176 Norrk^ping, Sweden
phone: +46-11-158595 fax: +46-11-170208
e-mail: arutgers@smhi.se

Dr. Bent Hansen Sass
Danish Meteorological Institute
Meteorological and Oceanographic Research Division
Lyngbyvej 100
DK-2100 Copenhagen, Denmark
phone: +45-39157436 fax: +45-39157460
e-mail: bhs@dmi.min.dk

International BALTEX Secretariat Publication Series

No. 1 : Minutes of First Meeting of the BALTEX Science Steering Group
at GKSS Research Center in Geesthacht, Germany, May 16-17, 1994.
August 1994.

No. 2 : Baltic Sea Experiment BALTEX - Initial Implementation Plan.
March 1995, 84 pages.

No. 3 : First Study Conference on BALTEX, Visby, Sweden, August 28 - September 1, 1995.
Conference Proceedings. Editor: A.Omstedt, SMHI Norrköping, Sweden.
August 1995, 190 pages.

No. 4 : Minutes of Second Meeting of the BALTEX Science Steering Group
at Finnish Institute of Marine Research in Helsinki, Finland, January 25-27, 1995.
October 1995.

No. 5 : Minutes of Third Meeting of the BALTEX Science Steering Group
at Strand Hotel in Visby, Sweden, September 2, 1995.
March 1996.

No. 6 : BALTEX Radar Research - A Plan for Future Action.
October 1996, 46 pages.

No. 7 : Minutes of Fourth Meeting of the BALTEX Science Steering Group
at Institute of Oceanology PAS in Sopot, Poland, June 3-5, 1996.
February 1997.

No. 8: *Hydrological, Oceanic and Atmospheric Experience from BALTEX.*
Extended Abstracts of the XXII EGS Assembly, Vienna, Austria, April 21-25, 1997.
Editors: M. Alestalo and H.-J. Isemer. August 1997, 172 pages.

Copies are available upon request at the International BALTEX Secretariat.